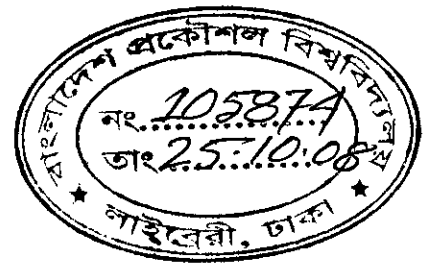


MAXIMUM HEAT FLUX AND WETTING DELAY DURING QUENCHING OF HIGH TEMPERATURE CARBON STEEL BLOCK

A Thesis

submitted in partial fulfillment of the requirements for
the Degree of Master of Science
in
Mechanical Engineering



by


Mousumi Ahmed



Department of Mechanical Engineering
Bangladesh University of Engineering and Technology (BUET)
Dhaka, Bangladesh
July, 2008

RECOMMENDATION OF THE BOARD OF EXAMINERS

The thesis titled "Maximum heat flux and wetting delay during quenching of high temperature carbon steel block", submitted by Mousumi Ahmed, Student No. 100510005P, Session: October, 2005, has been accepted as satisfactory in partial fulfillment of the requirements for the degree of Master of Science in Mechanical Engineering on July 19, 2008.


29/7/08

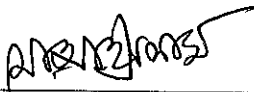
Dr. Alope Kumar Mozumder
Assistant Professor
Department of ME
BUET, Dhaka

Chairman (Supervisor)



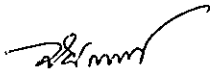
Dr. Abu Rayhan Md. Ali
Professor and Head
Department of ME
BUET, Dhaka

Member (Ex-Officio)



Dr. Md. Ashraful Islam
Professor
Department of ME
BUET, Dhaka

Member



Dr. Md. Shafiqul Islam
Senior Scientific Officer
Reactor Operation and Maintenance Unit
Atomic Energy Research Establishment
Bangladesh Atomic Energy Commission, Dhaka

Member (External)

CERTIFICATE OF RESEARCH

This is to certify that the work presented in this thesis is carried out by the author under the supervision of Dr. Alope Kumar Mozumder, Assistant Professor, Dept. of Mechanical Engineering, Bangladesh University of Engineering and Technology (BUET), Dhaka, Bangladesh.

@Alope
29/7/08

Dr. Alope Kumar Mozumder

Mousumi

Mousumi Ahmed

DECLARATION

No portion of the work contained in this thesis has been submitted in support of an application for another degree or qualification of this or any other university of Institution of learning.



Mousumi Ahmed

Author

ACKNOWLEDGEMENT

It gives me great pleasure to thank all the people who helped me during my thesis work at BUET.

I would like to express my thanks with deep sense of gratitude to my supervisor Dr. Alope Kumar Mozumder, Assistant Professor, Dept. of Mechanical Engineering, BUET for helping, guiding and encouraging me to complete this thesis work. Without his numerous suggestions and immense knowledge, it would have not been possible for me to bring this work into its present form.

I would like to thank other members of my broad of examiners Prof. Abu Rayhan Md. Ali, Department of Mechanical Engineering, BUET, Prof. Md. Ashraful Islam, Department of Mechanical Engineering, BUET and Dr. Md. Shafiqul Islam, Bangladesh Atomic Energy Commission for their critical reviewing of this thesis work.

I would also like to thank Saga University for their available experimental facilities of this research work. Without using the experimental data of this experiment, which was performed by Mozumder [16] at Saga University, it would have not been possible to continue this research work.

I would like to thank my family for supporting me throughout my study in BUET. I would also like to thank my friends for helping me out during my study in BUET.

ABSTRACT

Jet impingement quenching shows promising potential of achieving high heat flux today. Most recent studies investigated thermodynamic behaviors during quenching of copper, brass and steel blocks by jet impingement and determined the effects of dominating parameters on the maximum heat flux and wetting delay. Generalized correlations for predicting maximum heat flux and wetting delay were also developed. These correlations can predict the experimental data very well for both of copper and brass blocks. Experimental data for steel block have different character and can not be predicted by the above correlations. Therefore, the present study has been focused to investigate separately to explore the characteristics of these two phenomena for the steel block that has been experimented recently in Saga University, Japan. These two phenomena have been analyzed under various test conditions which included the jet velocities of 3-15 m/s, jet subcoolings of 5-80K and initial block temperatures of 250-600 °C.

The surface temperature and surface heat flux was estimated by an inverse heat conduction technique using the measured temperatures at two depths of 2.1mm and 5.0 mm from the surface. The surface temperature decreased very slowly with time just after the jet impingement. After a certain time delay, the surface temperature decreased at a faster rate. The digitized images of flow movement were also analyzed in the present study. It was found that the liquid didn't wet the entire surface just after the jet impingement. After a certain time period, the wetting front started to move in the radial direction.

The effects of experimental parameters on the maximum heat flux and wetting delay were also observed in the present study. The characteristics of maximum heat flux and wetting delay are strongly influenced by the jet velocity and liquid jet subcooling. The maximum heat flux increases with the jet velocity and also with liquid subcooling. For higher jet velocity and higher jet subcooling, the wetting delay is decreased. Both the maximum heat flux and wetting delay are found to be almost independent of block initial temperature. Finally, for the two regions of radial positions (10-20mm and 20-35mm) correlations of maximum heat flux together with the dominating parameters are developed. The proposed correlations show the accuracy of maximum heat flux within $\pm 25\%$ and $\pm 30\%$ respectively for the block initial temperatures of 250-400°C.

TABLE OF CONTENTS

	Page
ACKNOWLEDGEMENT.....	a
ABSTRACT.....	b
TABLE OF CONTENTS.....	c-e
LIST OF FIGURES AND TABLES.....	g-j
NOMENCLATURE.....	k-l
CHAPTER 1.	
INTRODUCTION.....	1-5
1.1 Jet Impingement Quenching, 1	
1.2 Boiling Phenomena, 1	
1.3 Maximum heat flux during quenching, 3	
1.4 Wetting delay / Resident time during quenching, 4	
1.5 Objectives of this study, 4	
CHAPTER 2.	
LITERATURE SURVEY.....	6-8
CHAPTER 3.	
EXPERIMENT.....	9-10
3.1 General, 9	
3.2 Experiment, 9	
3.3 Test Conditions, 10	
CHAPTER 4.	
DATA ANALYSIS.....	11-14
4.1 General, 11	
4.2 Analysis of temperature data, 11	
4.2 Analysis of digitized images, 14	

CHAPTER 5.

WETTING DELAY AND MAXIMUM HEAT FLUX..... 15-22

- 5.1 Importance of Wetting Delay during quenching, 15
- 5.2 Regimes of Wetting Delay, 16
- 5.3 Importance of Maximum Heat flux during quenching, 17
- 5.4 Maximum Heat Flux in Boiling Curve, 18
- 5.5 Surface temperature and surface heat flux distribution, 19
 - 5.5.1 Surface temperature and surface heat flux distribution with time, 20
 - 5.5.2 Surface temperature and surface heat flux distribution with time, 21
- 5.6 Visual Observations during quenching, 22

CHAPTER 6.

RESULTS AND DISCUSSIONS..... 23-36

- 6.1 Determination of wetting delay, 23
- 6.2 Effect of parameters on wetting delay, 24
 - 6.2.1 Effect of jet velocity
 - 6.2.2 Effect of jet subcooling
 - 6.2.3 Effect of Initial Block Temperature
- 6.3 Effect of parameters on Maximum heat flux, 25
 - 6.3.1 Effect of Radial Position on Maximum Heat Flux, 25
 - 6.3.2 Effect of Jet Velocity on Maximum Heat Flux, 26
 - 6.3.3 Effect of Sub-cooling on Maximum Heat Flux, 27
 - 6.3.4 Effect of initial block temperature on maximum heat flux, 28
 - 6.3.4 Effect of block material on maximum heat flux, 28
- 6.4 Correlation for Maximum Heat Flux, 29

CHAPTER 7.

CONCLUSIONS AND RECOMMENDATIONS..... 37-38

REFERENCES..... 39-41

APPENDIX A Experimental set up and procedures, 42

A.1 Experimental set up, 42

A.1.1 Heated Block, 43

A.1.2 Data Acquisition System, 44

A.1.3 Visual Observation, 44

A.1.4 Audible Observation, 45

A.2 Experimental Procedure, 45

APPENDIX B Inverse Solution, 46

APPENDIX C Thermo-physical properties of materials, 48

APPENDIX D Surface temperature and Surface heat flux distribution, 49

B.1 Surface temperature distribution with time, 49

B.2 Surface temperature distribution with radial position, 53

B.3 Surface heat flux distribution with time, 55

B.4 Surface heat flux distribution with radial position, 59

APPENDIX E Determination of wetting delay in different test conditions, 61

APPENDIX F Effect of different parameters on maximum surface heat flux, 63

F.1 Maximum heat flux with radial position, 63

F.2 Effect of jet velocity on maximum heat flux, 69

F.3 Maximum heat flux with liquid subcooling, 74

3

LIST OF FIGURES AND TABLES

- Fig. 1.2 Typical pool boiling curve for water at one atmosphere, 2
- Fig 1.4 Cooling curve during quenching, 4
- Fig.4.1 Successive analysis of temperature data, 12
- Fig. 5.1 Regimes of resident time [cooling curve and heat flux during quenching], 16
- (a) St, $T_b = 350\text{ }^\circ\text{C}$, $\Delta T_{\text{sub}} = 50\text{ K}$, $u = 3\text{ m/s}$
 - (b) Cu, $T_b = 350\text{ }^\circ\text{C}$, $\Delta T_{\text{sub}} = 50\text{ K}$, $u = 3\text{ m/s}$
 - (c) Cu, $T_b = 350\text{ }^\circ\text{C}$, $\Delta T_{\text{sub}} = 5\text{ K}$, $u = 3\text{ m/s}$
- Fig. 5.4 Regimes of boiling and maximum heat flux during wetting front propagation,
($T_b=400^\circ\text{C}$, $\Delta T_{\text{sub}}=50\text{K}$, $u=3\text{m/s}$, $t=4.3\text{ s}$), 18
- Fig 5.5.1.1 Surface temperature vs. time curve ($T_b=400^\circ\text{C}$, $\Delta T_{\text{sub}}=20\text{K}$, $u=03\text{m/s}$), 20
- Fig 5.5.1.2 Surface heat flux vs. time curve ($T_b=400^\circ\text{C}$, $\Delta T_{\text{sub}}=20\text{K}$, $u=03\text{m/s}$), 20
- Fig. 5.5.2.1 Variation of surface temperature with radial position
($T_b=400^\circ\text{C}$, $\Delta T_{\text{sub}}=20\text{K}$, $u=03\text{m/s}$), 21
- Fig. 5.5.2.1 Surface heat flux distribution with radial position
($T_b=400^\circ\text{C}$, $\Delta T_{\text{sub}}=20\text{K}$, $u=03\text{m/s}$), 21
- Fig 5.6 Wetting front propagation during quenching, 22
(for $T_b=550\text{C}$, $T_{\text{sub}}=50\text{K}$, $u=05\text{ m/s}$)
- Fig. 6.1.1 Surface temperature vs. time curve (for $T_b=300^\circ\text{C}$ $\Delta T_{\text{sub}}=50\text{K}$, $u=15\text{ m/s}$), 23
- Fig. 6.1.2 Surface temperature vs. time curve (for $T_b=400^\circ\text{C}$ $\Delta T_{\text{sub}}=20\text{K}$, $u=03\text{ m/s}$), 24
- Fig. 6.1.3 Surface temperature vs. time curve (for $T_b=550^\circ\text{C}$ $\Delta T_{\text{sub}}=80\text{K}$, $u=03\text{ m/s}$), 24
- Fig 6.3.1 Variation of maximum surface heat flux with radial position
(for $T_b=300^\circ\text{C}$, $\Delta T_{\text{sub}}=20\text{K}$), 26
- Fig. 6.3.2 Effect of jet velocity on maximum heat flux (for $T_b=400^\circ\text{C}$, $\Delta T_{\text{sub}}=20\text{K}$), 27
- Fig 6.3.3 Variation of Maximum surface heat Flux with liquid subcooling
(for $T_b=400^\circ\text{C}$, $u=10\text{m/s}$), 27
- Fig. 6.3.4 Effect of initial block temperature on maximum heat flux
($\Delta T_{\text{sub}} = 05\text{K}$, $u=03\text{m/s}$), 28
- Fig. 6.3.6.1 Comparison of q_{max} data for copper and brass with the proposed correlation
(for region II (11-25 mm)) [18], 30
- Fig. 6.3.6.2 Comparison of q_{max} data for copper and brass with the proposed correlation
(for region II (11-25 mm)) [18], 31

- Fig 6.3.6.3 Comparison of experimental data of Q_{max} for initial temperature of 250- 400°C with the proposed correlation (for region I), 33
- Fig 6.3.6.4 Comparison of experimental data of Q_{max} for initial temperature of 250-400°C with the proposed correlation (for region II), 34
- Fig 6.3.6.5 Comparison of experimental data of Q_{max} for initial temperature of 450-600°C with the proposed correlation (for region II), 35
- Fig 6.3.6.6 Comparison of experimental data of Q_{max} for initial temperature of 450-600°C with the proposed correlation (for region II), 36
- Fig. A.1 Schematic diagram of the experimental set-up, 42
- Fig. A.1.1.1 Schematic diagram of the test section and heating element, 43
- Fig. A.1.1.2 Thermocouple locations in the test block, 44
- Fig D.1.1 Surface temperature vs. time curve ($T_b=250^\circ\text{C}$, $\Delta T_{sub}=50\text{K}$, $u=5\text{m/s}$), 49
- Fig. D.1.2 Surface temperature vs. time curve ($T_b=250^\circ\text{C}$, $\Delta T_{sub}=80\text{K}$, $u=10\text{m/s}$), 49
- Fig D.1.3 Surface temperature vs. time curve ($T_b=350^\circ\text{C}$, $\Delta T_{sub}=05\text{K}$, $u=05\text{m/s}$), 50
- Fig D.1.4 Surface temperature vs. time curve ($T_b=350^\circ\text{C}$, $\Delta T_{sub}=80\text{K}$, $u=10\text{m/s}$), 50
- Fig D.1.5 Surface temperature vs. time curve ($T_b=500^\circ\text{C}$, $\Delta T_{sub}=50\text{K}$, $u=05\text{m/s}$), 51
- Fig D.1.6 Surface temperature vs. time curve ($T_b=550^\circ\text{C}$, $\Delta T_{sub}=80\text{K}$, $u=03\text{m/s}$), 51
- Fig D.1.7 Surface temperature vs. time curve ($T_b=600^\circ\text{C}$, $\Delta T_{sub}=05\text{K}$, $u=05\text{m/s}$), 52
- Fig D.1.8 Surface temperature vs. time curve ($T_b=600^\circ\text{C}$, $\Delta T_{sub}=80\text{K}$, $u=05\text{m/s}$), 52
- Fig. D.2.1 Variation of surface temperature with radial position ($T_b=250^\circ\text{C}$, $\Delta T_{sub}=50\text{K}$, $u=5\text{m/s}$), 53
- Fig. D.2.2 Variation of surface temperature with radial position ($T_b=250^\circ\text{C}$, $\Delta T_{sub}=80\text{K}$, $u=10\text{m/s}$), 53
- Fig. D.2.3 Variation of surface temperature with radial position ($T_b=500^\circ\text{C}$, $\Delta T_{sub}=50\text{K}$, $u=05\text{m/s}$), 54
- Fig. D.2.4 Variation of surface temperature with radial position ($T_b=550^\circ\text{C}$, $\Delta T_{sub}=80\text{K}$, $u=03\text{m/s}$), 54
- Fig. D.2.5 Variation of surface temperature with radial position ($T_b=600^\circ\text{C}$, $\Delta T_{sub}=05\text{K}$, $u=05\text{m/s}$), 55
- Fig. D.3.1 Surface heat flux vs. time curve ($T_b=250^\circ\text{C}$, $\Delta T_{sub}=50\text{K}$, $u=05\text{m/s}$), 55
- Fig. D.3.2 Surface heat flux vs. time curve ($T_b=250^\circ\text{C}$, $\Delta T_{sub}=80\text{K}$, $u=10\text{m/s}$), 56
- Fig. D.3.3 Surface heat flux vs. time curve ($T_b=300^\circ\text{C}$, $\Delta T_{sub}=50\text{K}$, $u=15\text{m/s}$), 56
- Fig. D.3.4 Surface heat flux vs. time curve ($T_b=350^\circ\text{C}$, $\Delta T_{sub}=05\text{K}$, $u=05\text{m/s}$), 57
- Fig. D.3.5 Surface heat flux vs. time curve ($T_b=350^\circ\text{C}$, $\Delta T_{sub}=80\text{K}$, $u=10\text{m/s}$), 57

- Fig. F.1.13 Variation of maximum surface heat flux with radial position
(for $T_b=600^\circ\text{C}$, $\Delta T_{\text{sub}}=50\text{K}$), 69
- Fig. F.2.1 Variation of maximum heat flux with jet velocity
(for $T_b=250^\circ\text{C}$, $\Delta T_{\text{sub}}=20\text{K}$), 69
- Fig. F.2.2 Variation of maximum heat flux with jet velocity
(for $T_b=250^\circ\text{C}$, $\Delta T_{\text{sub}}=50\text{K}$), 70
- Fig. F.2.3 Variation of maximum heat flux with jet velocity
(for $T_b=300^\circ\text{C}$, $\Delta T_{\text{sub}}=05\text{K}$), 70
- Fig. F.2.4 Variation of maximum heat flux with jet velocity
(for $T_b=350^\circ\text{C}$, $\Delta T_{\text{sub}}=80\text{K}$), 71
- Fig. F.2.5 Variation of maximum heat flux with jet velocity
(for $T_b=350^\circ\text{C}$, $\Delta T_{\text{sub}}=50\text{K}$), 71
- Fig. F.2.6 Variation of maximum heat flux with jet velocity
(for $T_b=400^\circ\text{C}$, $\Delta T_{\text{sub}}=05\text{K}$), 72
- Fig. F.2.7 Variation of maximum heat flux with jet velocity
(for $T_b=450^\circ\text{C}$, $\Delta T_{\text{sub}}=50\text{K}$), 72
- Fig. F.2.8 Variation of maximum heat flux with jet velocity
(for $T_b=500^\circ\text{C}$, $\Delta T_{\text{sub}}=50\text{K}$), 73
- Fig. F.2.9 Variation of maximum heat flux with jet velocity
(for $T_b=550^\circ\text{C}$, $\Delta T_{\text{sub}}=50\text{K}$), 73
- Fig. F.2.10 Variation of maximum heat flux with jet velocity
(for $T_b=600^\circ\text{C}$, $\Delta T_{\text{sub}}=50\text{K}$), 74
- Fig. F.3.1 Variation of Maximum surface heat Flux with liquid subcooling
(for $T_b=250^\circ\text{C}$, $u=03\text{ m/s}$), 74
- Fig. F.3.2 Variation of Maximum surface heat Flux with liquid subcooling
(for $T_b=250^\circ\text{C}$, $u=05\text{ m/s}$), 75
- Fig. F.3.3 Variation of Maximum surface heat Flux with liquid subcooling
(for $T_b=250^\circ\text{C}$, $u=10\text{m/s}$), 75
- Fig. F.3.4 Variation of Maximum surface heat Flux with liquid subcooling
(for $T_b=300^\circ\text{C}$, $u=15\text{m/s}$), 76
- Fig. F.3.5 Variation of Maximum surface heat Flux with liquid subcooling
(for $T_b=350^\circ\text{C}$, $u=05\text{m/s}$), 76
- Fig. F.3.6 Variation of Maximum surface heat Flux with liquid subcooling
(for $T_b=350^\circ\text{C}$, $u=15\text{m/s}$), 77

- Fig. D.3.6 Surface heat flux vs. time curve ($T_b=500^\circ\text{C}$, $\Delta T_{\text{sub}}=50\text{K}$, $u=05\text{m/s}$), 58
- Fig. D.3.7 Surface heat flux vs. time curve ($T_b=600^\circ\text{C}$, $\Delta T_{\text{sub}}=05\text{K}$, $u=05\text{m/s}$), 58
- Fig. D.4.1 Surface heat flux distribution with radial position
($T_b=250^\circ\text{C}$, $\Delta T_{\text{sub}}=50\text{K}$, $u=5\text{m/s}$), 59
- Fig. D.4.2 Surface heat flux distribution with radial position
($T_b=250^\circ\text{C}$, $\Delta T_{\text{sub}}=80\text{K}$, $u=10\text{m/s}$), 59
- Fig. D.4.3 Surface heat flux distribution with radial position
($T_b=350^\circ\text{C}$, $\Delta T_{\text{sub}}=80\text{K}$, $u=10\text{m/s}$), 60
- Fig. D.4.4 Surface heat flux distribution with radial position
($T_b=500^\circ\text{C}$, $\Delta T_{\text{sub}}=50\text{K}$, $u=05\text{m/s}$), 60
- Fig. F.1.1 Variation of maximum surface heat flux with radial position
(for $T_b=250^\circ\text{C}$, $\Delta T_{\text{sub}}=80\text{K}$), 63
- Fig. F.1.2 Variation of maximum surface heat flux with radial position
(for $T_b=250^\circ\text{C}$, $\Delta T_{\text{sub}}=20\text{K}$), 63
- Fig. F.1.3 Variation of maximum surface heat flux with radial position
(for $T_b=300^\circ\text{C}$, $\Delta T_{\text{sub}}=80\text{K}$), 64
- Fig. F.1.4 Variation of maximum surface heat flux with radial position
(for $T_b=300^\circ\text{C}$, $\Delta T_{\text{sub}}=20\text{K}$), 64
- Fig. F.1.5 Variation of maximum surface heat flux with radial position
(for $T_b=350^\circ\text{C}$, $\Delta T_{\text{sub}}=50\text{K}$), 65
- Fig. F.1.6 Variation of maximum surface heat flux with radial position
(for $T_b=400^\circ\text{C}$, $\Delta T_{\text{sub}}=80\text{K}$), 65
- Fig. F.1.7 Variation of maximum surface heat flux with radial position
(for $T_b=450^\circ\text{C}$, $\Delta T_{\text{sub}}=20\text{K}$), 66
- Fig. F.1.8 Variation of maximum surface heat flux with radial position
(for $T_b=450^\circ\text{C}$, $\Delta T_{\text{sub}}=80\text{K}$), 66
- Fig. F.1.9 Variation of maximum surface heat flux with radial position
(for $T_b=500^\circ\text{C}$, $\Delta T_{\text{sub}}=20\text{K}$), 67
- Fig. F.1.10 Variation of maximum surface heat flux with radial position
(for $T_b=500^\circ\text{C}$, $\Delta T_{\text{sub}}=05\text{K}$), 67
- Fig. F.1.11 Variation of maximum surface heat flux with radial position
(for $T_b=550^\circ\text{C}$, $\Delta T_{\text{sub}}=80\text{K}$), 68
- Fig. F.1.12 Variation of maximum surface heat flux with radial position
(for $T_b=550^\circ\text{C}$, $\Delta T_{\text{sub}}=50\text{K}$), 68

- Fig. F.3.7 Variation of Maximum surface heat Flux with liquid subcooling
(for $T_b=400^\circ\text{C}$, $u=15\text{m/s}$), 77
- Fig. F.3.8 Variation of Maximum surface heat Flux with liquid subcooling
(for $T_b=450^\circ\text{C}$, $u=03\text{m/s}$), 78
- Fig. F.3.9 Variation of Maximum surface heat flux with liquid subcooling
(for $T_b=450^\circ\text{C}$, $u=10\text{m/s}$), 78
- Fig. F.3.10 Variation of Maximum surface heat Flux with liquid subcooling
(for $T_b=500^\circ\text{C}$, $u=05\text{m/s}$), 79
- Fig. F.3.11 Variation of Maximum surface heat Flux with liquid subcooling
(for $T_b=550^\circ\text{C}$, $u=03\text{ m/s}$), 79
- Fig. F.3.12 Variation of Maximum surface heat Flux with liquid subcooling
(for $T_b=550^\circ\text{C}$, $u=15\text{ m/s}$), 80
- Fig. F.3.13 Variation of Maximum surface heat Flux with liquid subcooling
(for $T_b=600^\circ\text{C}$, $u=03\text{m/s}$), 80

Table 3.2 Test conditions of the experiment, 10

Table 4.1 Input temperature data to the inverse solution program, 13

Table 4.2 Output data file for surface temperature from the inverse solution program, 13

Table 4.3 Output data file for surface heat flux from the inverse solution program, 14

Table 4.4 Output data file for maximum surface heat flux from the inverse solution
program, 14

Table A.1 Thermo-physical properties of water, 48

Table A.2 Thermo-physical properties of steel material, 48

Table E.1 Resident time or wetting delay for all experimental conditions, 61

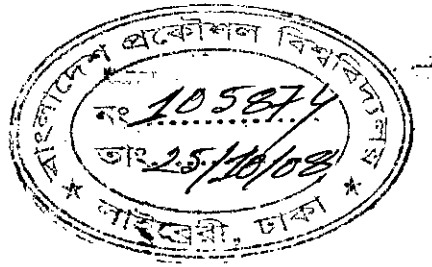
NOMENCLATURE

d	jet diameter (mm)
D	Diameter of the heated surface (mm)
Q_w	Surface heat flux (MW/m ²)
CHF, q_c	critical heat flux
r	Position in the radial direction of the block (mm)
r^*	Radial position of wetting front at the wetting delay (mm)
r_q	Radial position at maximum heat flux point (mm)
t	time (counted from the impingement of jet) (s)
t^*	resident time (s)
T	measured temperature (°C)
T_b	Initial block temperature (°C)
T_{liq}	Liquid temperature (°C)
T_{sat}	Saturated liquid temperature (°C)
T_w	Surface temperature (°C)
ΔT_{sub}	Liquid subcooling, ($T_{sat} - T_{liq}$) (K)
T^*	solid–liquid interface temperature (°C)
u	Jet velocity(m/s)
a	thermal diffusivity (m/s ²)
c	specific heat (kJ/kg K)
λ	Thermal conductivity (W/m ² K)
ρ	Density (kg/m ³)
σ	Surface tension (N/m)
Θ_w	non-dimensional surface temperature [T/T_b]
Φ_w	non-dimensional surface heat flux
$f(\tau, \lambda, \xi)$	function for depicting temperature variation on plane $\xi = \xi_n$ beneath the surface
τ	non-dimensional time= $\frac{at}{l^2 r}$
τ^*	non-dimensional time lag
$P_{j,k}^{(n)}$	coefficient derived from measured temperature variation

$G_{j,l}^{(m,n)}$	Coefficients in Eq. (3.2)
$H_{j,l}^{(m,n)}$	Coefficients in Eq. (3.3)
m_j	eigenvalue [root of $J_1(m_j) = 0$]
J_0	Bessel function
l_r	length in r direction of a cylindrical coordinate (mm)
l_z	length in z direction of a cylindrical coordinate (mm)
ζ_z	non-dimensional distance in z direction (z/l_z)
γ	non-dimensional distance in r direction (r/l_r)

Subscripts

l	liquid
s	solid



CHAPTER 1

INTRODUCTION

1.1 Jet Impingement Quenching

Quenching is a high heat removal technique which removes heat from hot surfaces at a sufficiently high rate by means of sudden contact with a low temperature fluid. This method is widely employed in heat treatment of metal parts to achieve desired hardness and mechanical properties. The rate of cooling also plays a dominant role to control internal alloy microstructure in case of alloy metal parts to ensure uniform as well as superior mechanical properties.

Among the various quenching techniques, jet impingement quenching have proven to be an effective cooling option over the past few years due to its capability of enhancing heat transfer rates. The wide applications of jet impingement cooling or quenching have been found in different manufacturing processes such as annealing of metals, tempering of glass, casting, extrusion, grinding etc. in order to improve product performance by improving their metallurgical and mechanical characteristics. This method is also used in cooling of high powered electronic components to maintain relatively low temperatures. This method also shows a promising application in Emergency Core Cooling (EMC) of water cooled nuclear reactors. In such emergency cases, cooling of the fuel element is immediately needed to remove the decay heat still within it even after the reactor is shutdown.

1.2 Boiling Phenomena

The jet impingement on the hot surfaces entails boiling heat transfer in its way. The complex mechanism of jet impingement boiling heat transfer is not fully understood yet. Wolf et. al [1] studied on jet impingement boiling and identified the existence of three basic modes of boiling heat transfer: nucleate boiling, transition boiling and film boiling. Inclusive analysis of various regimes of pool boiling may be needed for understanding the intricate mechanisms of jet impingement quenching.

Figure 1.2 shows the typical pool boiling curve for water at one atmospheric pressure. There are four regimes in the boiling curve. In the single phase convection regime, the rate of

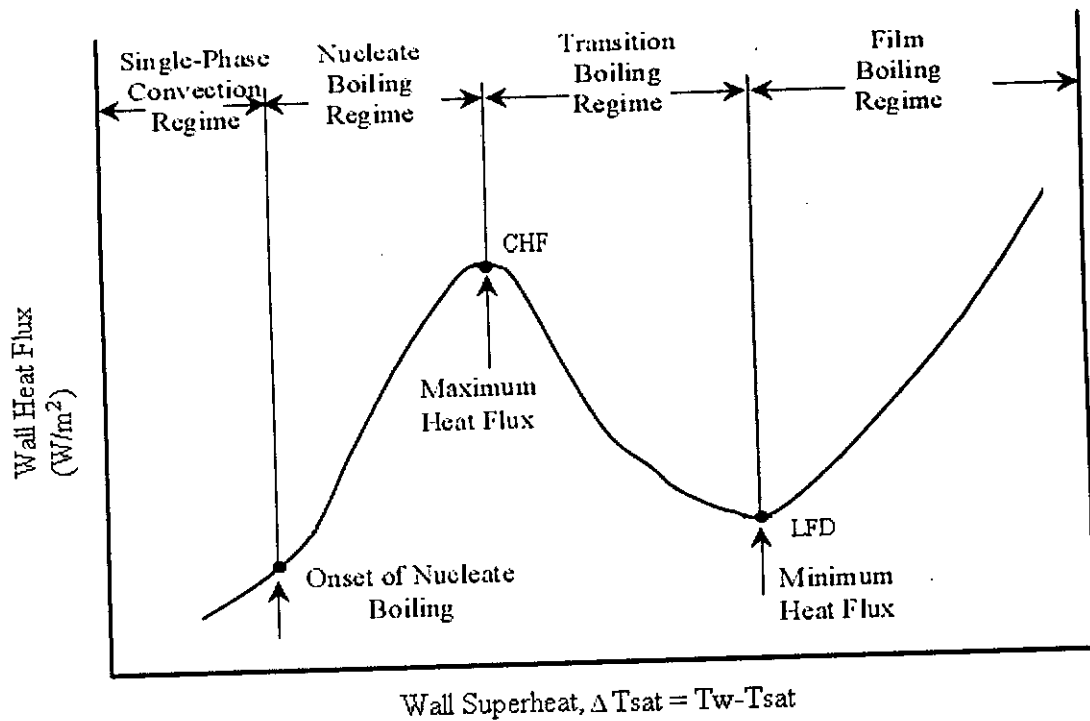


Fig. 1.2: Typical pool boiling curve for water at one atmosphere

heat transfer is dominated by the gravitational effects. At the point of onset of nucleate boiling vapor bubbles appear on the heated surface. The bubble releases from the active sites of the heated surface and increases with the wall superheat. The vapor escapes as jets or columns for the higher value of wall superheat which subsequently forms slugs of vapor over the heated surface. The heat flux reaches its maximum value which is known as critical heat flux.

After the CHF point a vapor film or blanket begins to form on the surface. The transition boiling is the mixed boiling mode of film boiling and nucleate boiling which is very unstable. Since the surface covered by the vapor film is increased with the wall superheat, the wall heat flux is reduced significantly. If the wall superheat is further increased, the surface is fully covered by the vapor blanket. Therefore, stable film boiling occurs in this region and the liquid does not come into contact with the heated surface. The transition point between the transition boiling and the film boiling is known as the Leidenfrost point (LFD) or the point of minimum heat flux which may be thought of as the transition where the stable film is collapsed or the stable film is started to form. This LFD point is very important during jet impingement quenching which is still incompletely understood by the scientific community.

Many researchers and scientists have been focusing their efforts to investigate Leidenfrost temperature in jet impingement boiling heat transfer. A new milestone in thermal science will be opened when this phenomenon will be completely depicted.

1.3 Maximum Heat flux during Quenching

Maximum heat flux is the maximum value of heat flux which is transferred within the safe limit of heat transfer equipment. The involved mechanism of maximum heat flux during quenching is not clearly stated yet though many analytical and experimental works have been done by many researchers. In the present study we are concerning about the transient maximum heat flux of the heated surface which is to be quenched by impinging jet. The maximum heat flux is estimated from the solid side which cannot be measured directly. Researchers [18-20] developed the inverse heat conduction technique to estimate the surface maximum heat flux.

Some researchers have studied the maximum heat flux on the surface from the liquid side which is defined as critical heat flux, CHF or steady critical heat flux. The critical heat flux condition we have observed in the pool boiling curve as shown in Fig. 1.1 where CHF point is considered as the transition point between the nucleate boiling and the transition boiling region. The nucleate boiling goes through a flow regime transition to film boiling with a continuous vapor film separating the heater and the liquid. At critical heat flux condition, the vapor generated by nucleate boiling becomes so large that it prevents the liquid from reaching and rewetting the surface.

Ueda et al. [3] reported that the critical heat flux matched with the maximum transient heat flux during transient cooling of copper test piece. Mitsutake et al. [9] noticed the agreement between the critical heat flux, CHF and maximum transient heat flux, q_{\max} for copper block, while the disagreement for brass. Ueda and Inoue [8] found that the maximum heat flux shows a somewhat higher value than the critical heat flux. Mozumder [15] observed the dissimilarity between these two values. The thermal properties of solid material have a significant influence on the transient maximum heat flux during quenching. They found that the critical heat flux was closer to maximum heat flux for material with high thermal conductivity.

1.4 Wetting Delay during Quenching

When the liquid jet is first impinged on the heated surface it does not immediately wet the entire surface. The liquid immediately covers a small region of the entire surface and it remains stagnant in that region for a certain period of time which is termed as the wetting delay. This time period varies from fraction of second to a few minutes which depends on the experimental conditions. After this wetting delay period the wetting front starts moving and the surface temperature falls rapidly with time. This wetting delay is also known as the resident time, t^* . Before the resident time, the surface temperature decreases slowly almost at a constant rate. Due to transient effects, there is sudden drop of temperature at the very beginning of jet impingement.

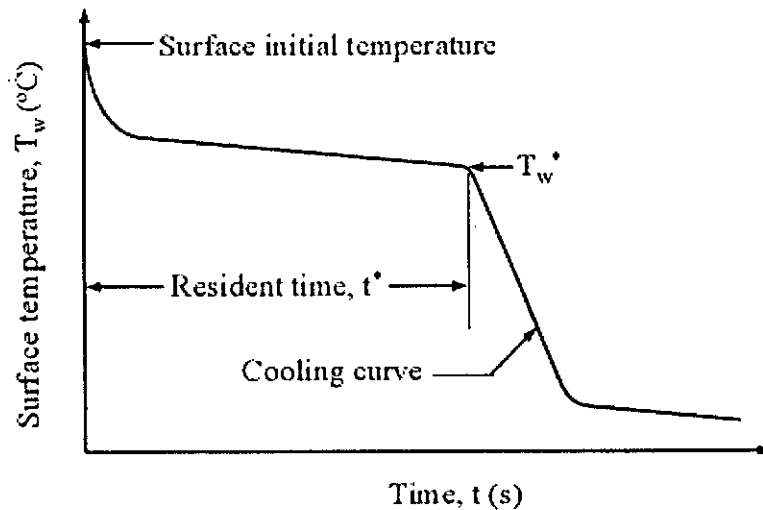


Fig 1.4 Cooling curve during quenching

1.5 Objectives of this study

The investigations on the maximum heat flux and wetting delay of jet impingement quenching for copper and brass block have been carried out in previous works [16-18]. The aim of the present study is to analyze the obtained experimental data from the experiment [16] for steel materials. The previous work observed the similar phenomena during quenching of copper and brass material but for steel block which were somewhat different. The correlation for maximum heat flux which was proposed in the previous work [18] was well matched for copper and brass block. The same correlation did not fit with the experimental data for the

steel material. In reality, the steel has been extensively used in manufacturing industries from the very beginning of the industrial development. Rapid cooling has been utilized in steel making processes to produce different grades of steels and associated metallic products by providing desired structural changes. It is necessary to control accurate temperature during its manufacturing operations in order to produce higher quality products. Though jet impingement quenching is thought to be of high heat flux removal process in steel industries, the phenomena that occur during quenching is less investigated until now. It is, therefore, essential to focus on heat transfer behaviors during jet impingement quenching of steel materials.

The specific objectives of the present research work are as follows:

- (a) To observe the wetting delay and maximum heat flux phenomena.
- (b) To investigate the parameters which control the maximum heat flux.
- (c) To investigate the parameters which control wetting delay and the temperature at the wetting front at the wetting delay time.
- (d) To develop a correlation for the maximum surface heat flux by incorporating the important non-dimensional numbers.
- (e) To investigate the parameters that control the position of maximum heat flux.

CHAPTER 2

LITERATURE SURVEY

Many experimental and analytical works on quenching phenomena have been studied during the last few decades. The quenching process has been defined by researchers in many ways. Nelson [2] defined quenching as the rewetting process for establishing direct liquid-solid contact where the surface initial temperature exceeds the rewetting temperature. Dua and Tien [4] carried out an experimental work that involved a falling film of liquid nitrogen to rewet a copper surface initially at room temperature. The rewetting temperature was represented by the Leidenfrost temperature of liquid nitrogen on the copper surface. Chan et al. [5] defined the rewetting as the re-establishment of continuous liquid contact with a hot dry surface. They found that rewetting always occur when the temperature of the hot surface is below a certain value generally referred as the rewetting, sputtering or Leidenfrost temperature.

Iloje et al. [6] defined the rewetting as the onset of transition or unstable boiling in going from stable film boiling to nucleate boiling, and found that it corresponded to the minimum film boiling heat flux on the standard boiling curve. Carbajo [7] reported that rewetting or quenching of a hot surface occurred when the coolant reestablished contact with the dry surface. Furthermore, this phenomenon takes place when the temperature of the surface cools down enough to allow a change in heat transfer region from film boiling to transition or nucleate boiling.

The quenching by water jet impingement is revealed as a rapid cooling process for high temperature surfaces. The heat transfer rate is significantly greater than other conventional cooling methods. Wolf et al. [1] reported that for single phase convection, the heat transfer coefficient for water jet impingement cooling exceeds 10kW/m^2 . For this reason, the cooling by impinging jets is preferred in many industrial applications.

Some studies [10-12] performed experimental investigations and emphasized on heat flux, temperature and the flow field by flow visualization during jet impingement boiling. Woodfield et al. [13] have focused on the phenomena that occurred during quenching of a hot surface. Kumagai et al. [14] carried out experimental investigations of transient

cooling of a hot thick copper plate by water jet impingement. They observed a time delay of approximately 100 seconds before the movement of wetting front where the jet velocity was 3.5 m/s and initial temperature of solid was 400°C. Many researchers have focused to investigate the complex phenomena of the wetting delay in jet impingement quenching.

Hammad [15] reported the resident times for three different materials with initial temperatures of 250 °C and 300 °C. A correlation for the resident time was developed which is function of initial temperature of solid, jet velocity, temperature of liquid, solid and liquid properties. He also observed the movements of both wetting front and transition boiling region over the heated block surface. He determined the maximum heat flux, the surface temperature, the positions and the time at which this value is occurred. It was found that the position of maximum heat flux was neither in the wetting front, nor in the transition boiling region rather it appeared in fully wetted region.

Some investigations [10, 12] conducted to explore the complex processes which direct the wetting front over the heated surface during jet impingement quenching. The flow pattern was observed before and after the movement of wetting front. The explosive flow pattern was observed for block temperature of higher than 300°C and the conical liquid sheet pattern was observed for lower temperature. It was also observed that the flow pattern changed from the explosive pattern to sheet pattern within the resident time in case of gradual cooling of high temperature surface.

Filipovic et al. [19] conducted transient boiling experiments where a large preheated specimen was quenched by a water wall jet on its top surface. They observed the propagation of the quench front in the direction of flow along the surface. They reported that the nucleate boiling or single phase convection was present in the upstream of the quench front while the film boiling was occurred in the downstream of the front. The quench front itself was in the leading edge of transition film boiling region. They also observed that the location of maximum heat flux moved along with the quench front and the value of maximum heat flux decreased with increasing time.

Ochi et al. [20] performed quenching experiment of a large flat plate which was exposed to a circular water jet. They observed that position of maximum heat flux is at the stagnation point and its value decreased with radial position. The value of maximum

heat flux was strongly affected by the water subcooling and jet velocity in the stagnation zone. It was also observed that the rewetting front velocity increased with the nozzle diameter, jet velocity and water subcooling.

Mozumder et al. [16-18] conducted the experimental investigations during quenching of three different cylindrical blocks i.e. steel, brass and cast iron using a subcooled water jet. They observed that the wetting front becomes stagnant for a certain period of time in a small central region before wetting the entire surface and defined this time as the resident time. They extensively studied the dominating parameters that control the movement of the wetting front towards the circumference of the hot surface and correlated important experimental parameters with the resident time and the surface temperature at the resident time for brass and copper hot block. They also showed that the position of the maximum heat flux also moves once the wetting front moves and the strong influence of jet velocity and the thermal properties of block material is found to the propagation of maximum heat flux and finally developed a correlation of the maximum heat flux for brass and copper block. These correlations of resident time and maximum heat flux have not been well predicted for the steel block. Research on heat transfer behaviors during quenching of steel materials is still less investigated. Hall et al. [11] observed an experimental study of boiling heat transfer during quenching of cylindrical copper disk by a subcooled, circular, free surface water jet. They correlated the radial distribution of maximum heat flux data with relations developed by other researchers from the steady state experiments for radial flow region.

CHAPTER 3

EXPERIMENT

3.1 General

In this present work, the experimental data have been taken from the experiment which was actually performed by Mozumder [16]. An overview of the experiment has been discussed in this chapter. The details of the main component parts of experimental set up and procedures have been described in Appendix A.

3.2 Experiment

The experiment [16] was conducted individually for three different materials of copper, brass and steel. In the previous work, the experimental investigations were carried out for these three materials where the similar behaviors were found for copper and brass block while some dissimilarities were found for steel materials. In this research work, the experimental data which were taken from the experiment where a hot cylindrical steel block was quenched by water jet impingement. A water jet of 2 mm was stroked at the center of the heated surface. The temperature readings of the thermocouples which were recorded by the data acquisition system were used to get the surface parameters i.e. surface temperature and surface heat flux of the heated block. A high speed video camera was used to capture the flow phenomena during quenching. Some video images were available to observe these flow phenomena for this study.

The extensive analysis of wetting delay and maximum heat flux phenomena for copper and brass materials already carried out in the previous works [16-18]. These phenomena for steel block are poorly understood yet. Therefore, comprehensive analysis for steel materials is still needed to explore the characteristics of these two phenomena. The present research work has been focused to investigate the wetting delay and maximum heat flux phenomena during quenching of carbon steel block under the same experimental conditions as for copper and brass block. The experimental data has been taken from the previously performed experiment as shown in Appendix A.

3.3 Test Conditions

The experiment has been conducted under various test conditions for the purpose of clear understanding of the heat transfer characteristics during jet impingement quenching of hot carbon steel block. The jet velocity and the jet sub cooling were varied for each initial temperature of the steel block as shown in Table 3.3.

Table 3.3 Test conditions of the experiment

Initial Temperature of Steel Block, $T_b(^{\circ}\text{C})$	Jet Diameter, d (mm)	Jet Subcooling temperature, $\Delta T_{\text{sub}}(\text{K})$	Jet velocity, u (m/s)
250,300,350,400,450,500,550,600 ($\pm 2^{\circ}\text{C}$ deviation)	2	05, 20, 50,80	3, 5, 10, 15 (± 0.1 m/s deviation)

CHAPTER 4

DATA ANALYSIS

4.1 General

The procedures to analyze the obtained experimental data from the experiment [16] for getting the surface history during jet impingement quenching of steel block have been discussed in this chapter. A very brief procedure to get the surface temperature and heat flux from the obtained temperature data (which is inverse solution) has been also introduced in this chapter.

4.2 Analysis of temperature data

During quenching of hot surfaces the direct measurement of surface heat flux and temperature is very difficult. It is impossible to get the thermal history directly just from the surface at which the jet is impinged without greatly disturbing the flow and boiling phenomena. An inverse heat conduction technique is proved to be useful to get the surface heat flux and temperature from knowing the surface temperatures inside the hot solid surface.

The temperature data from sixteen thermocouples at two depths of 2.1 mm and 5 mm from the surface which were recorded by the data acquisition system during the experiment [16] have directly used in this work. The temperature data were taken at 0.05s interval for different radial positions from the point of jet impingement over the heated surface. These temperature data have been used in an inverse heat conduction program that was developed by Monde et. al. [21] to determine the surface temperature and surface heat flux. The temperature data which were saved .txt file during the experiment have been used as input data to the inverse program, coded in FOTRAN computer language. The surface temperature and surface heat flux with time for each particular radial position have been estimated directly by using this program. The equations which were used in this inverse solution to estimate the surface parameters have mentioned in Appendix B. The maximum surface heat flux for each particular radial position to the corresponding time was also tabulated in a .txt file in this program. Samples of input data

file to the program and output data file from the program have shown in Table 4.1-Table 4.4.

The material properties of tested steel block have been considered at the initial temperature of 250°C in this program. The changes of temperatures within the range of 250-600°C have least significant effect on important material properties of the test specimen. The material properties for initial temperatures of 250-400°C are tabulated in Appendix C.

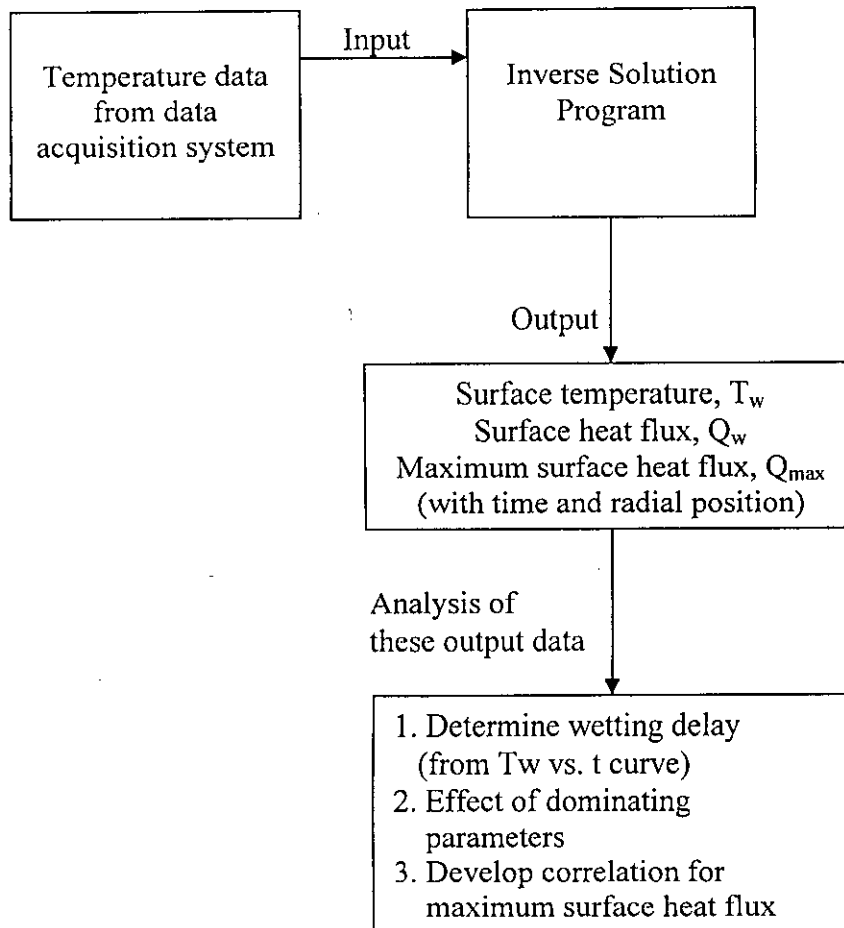


Fig.4.1 Successive analysis of temperature data

Then the output data files of surface temperature and surface heat flux from the inverse solution have been analyzed to get the heat transfer characteristics during quenching of carbon steel materials. This analysis has been carried for each experimental

condition. Though the experimental investigations of this work have already been carried out by Mozumder [16], the present research have also analyzed the effects of all experimental parameters which have influence on wetting delay and maximum heat flux phenomena. This research work has been emphasized to predict the behaviors of these two phenomena especially, during quenching of carbon steel block.

Table 4.1 Input temperature data to the inverse solution program

TS4002003.txt ()

time (s) ↓	Thermocouple position →				
0	400.62	399.85	400.51	400.49	400.91
0.05	400.51	399.83	400.41	400.45	400.91
0.1	400.65	398.57	400.47	400.46	400.95
0.15	400.62	392.91	400.54	399.94	400.96
0.2	400.59	383.87	400.58	397.45	400.94
0.25	400.2	373.3	400.45	391.78	400.95
0.3	399.15	362.14	400.06	383.58	400.9
0.35	397.58	351.05	399.25	373.94	400.79
0.4	395.36	340.16	398.06	363.71	400.49
0.45	392.54	329.57	396.36	353.39	399.92
0.5	389.28	319.48	394.24	343.22	399.01
0.55	385.65	309.8	391.78	333.41	397.64
0.6	381.64	300.56	388.97	323.96	395.92

Table 4.2 Output data file for surface temperature from the inverse solution program

time (s) ↓	radial positions (mm) →				
0	0	1	2	3	4
0.05	616.2351	623.9266	631.8753	639.1794	645.3648
0.1	476.3962	487.4754	500.0414	513.4271	527.6295
0.15	398.8613	410.4818	423.9794	438.8509	455.3122
0.2	346.4415	357.8252	371.1973	386.1686	403.072
0.25	307.6733	318.5322	331.3686	345.876	362.4516
0.3	277.4301	287.6552	299.7871	313.5816	329.4692
0.35	253.0967	262.6558	274.021	286.995	302.0223
0.4	233.0868	241.9879	252.5797	264.701	278.7981
0.45	216.3404	224.6111	234.4518	245.7286	258.8817
0.5	202.2067	209.884	219.0096	229.4708	241.696

Table 4.3 Output data file for surface heat flux from the inverse solution program
(for $T_b=400^\circ\text{C}$, $T_{liq}=20^\circ\text{C}$, $u=15\text{m/s}$)

time (s) ↓	radial position (mm) →				
0	0	1	2	3	4
0.05	0	0	0	0	0
0.1	1.03069	0.79868	0.52168	0.20459	0
0.15	2.06988	1.83162	1.54801	1.22313	0.84496
0.2	2.7934	2.57109	2.30611	2.00099	1.64273
0.25	3.28227	3.08196	2.84309	2.5669	2.24012
0.3	3.60651	3.42898	3.21758	2.97256	2.68088
0.35	3.81266	3.65676	3.47175	3.25722	3.00064
0.4	3.93358	3.79739	3.63666	3.45057	3.22728
0.45	3.99306	3.87441	3.7355	3.57527	3.38262
0.5	4.0066	3.90337	3.78379	3.64669	3.48178
0.55	3.98671	3.89687	3.79421	3.67755	3.53738

Table 4.4 Output data file for maximum surface heat flux from the inverse solution program

radial position (mm) ↓	Time (s) ↓	maximum heat flux (MW/m^2) ↓
0.00E+00	0.5	4.006600977
1	0.5	3.903366645
2	0.55	3.794212738
3	0.55	3.677552008
4	0.6	3.559031467
5	0.65	3.423806953
6	0.75	3.283732741
7	0.8	3.153841329

4.3 Analysis of digitized images

In the present study, quenching of the steel block by jet impingement also has been analyzed from the captured digitized images of high speed video camera. Some video images were available to visualize the actual fluid flow phenomena in quenching process.

CHAPTER 5

WETTING DELAY AND MAXIMUM HEAT FLUX

5.1 Importance of Wetting Delay

Wetting delay is the critical key parameter in jet impingement boiling heat transfer. This wetting delay defined as the resident time that is the time from the start of jet striking onto the hot surface to the start of wetting front moving. Stable film boiling occurs when the jet first strikes the heated surface where convective and radiative heat transfer locally removes the heat. This film becomes unstable after a certain time which is termed as the resident time and a wet patch is initiated. This wet patch spreads and results in the formation of a stable quenching front. Once the wetting front starts moving it takes little time to cover the entire heated surface [16].

Therefore, the wetting delay is an important control parameter that controls the total time needed to quench a heated surface. The longer resident time indicates the more time needed to quench the block that can lead to excessive cladding temperature even in some cases that may cause severe system failure. The dominating parameters which contribute to the movement of wetting front have not been elucidated yet.

Hammad et al. [24] reported that the heat flux reached its maximum value just after the wetting front started to move. So the resident time also gives an indication of the time required to reach the maximum heat flux point. Therefore, it is to be needed to look at first into the resident time as well as to investigate the dominating parameters which control the resident time and surface temperature at the wetting front at that time. In the present study, the wetting delay phenomenon was observed for different test conditions. This observation is thought to be helpful in defining the characteristics of jet impingement boiling heat transfer.

5.2 Regimes of Wetting Delay

Mozumder et al. [17] examined the resident times for each condition of experiment and classified the resident times into three regimes: (a) quick cooling, (b) moderate cooling and (c) slow cooling. He observed that the resident times for steel were very short while the resident times for copper were comparatively large. In this case of steel material, it took only a fraction of a second for the wetting front to start movement and the surface temperature cooled very rapidly immediately after the jet struck the surface. The thermal

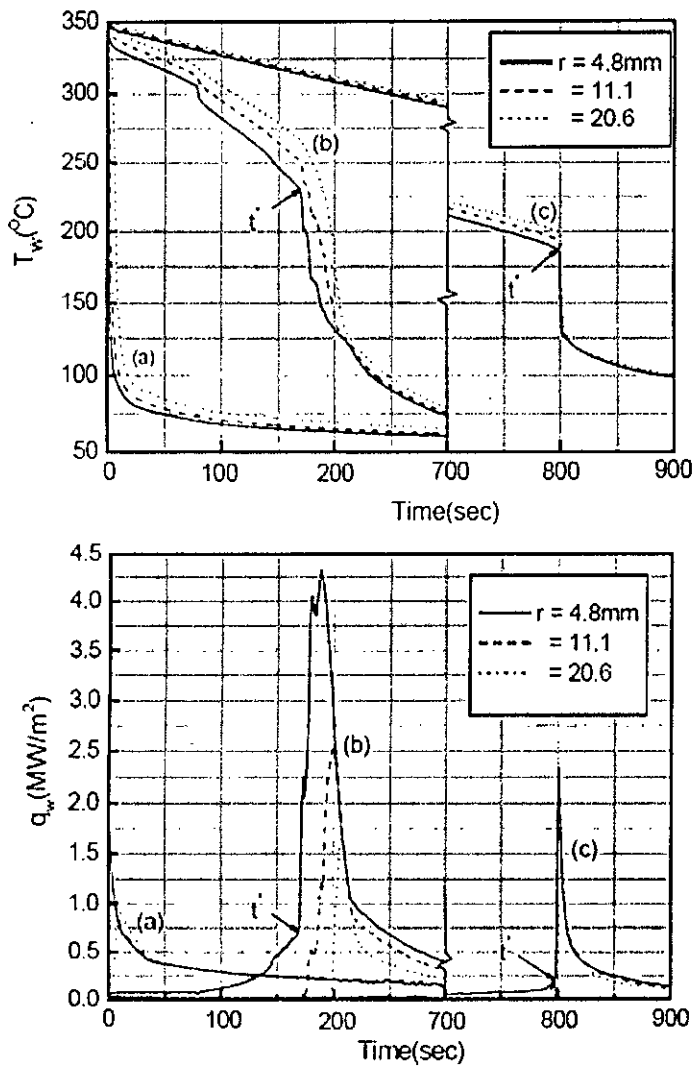


Fig. 5.2 Regimes of resident time [cooling curve and heat flux during quenching]

(a) St, $T_b = 350$ °C, $\Delta T_{sub} = 50$ K, $u = 3$ m/s (b) Cu, $T_b = 350$ °C, $\Delta T_{sub} = 50$ K, $u = 3$ m/s

(c) Cu, $T_b = 350$ °C, $\Delta T_{sub} = 5$ K, $u = 3$ m/s [17]

conductivity of carbon steel is about one tenth of copper material i.e. the ability of the carbon steel material to supply heat to the region of surface where the liquid contacts the surface is much less than that of copper. As a result the surface cools immediately just after striking the jet. For copper the thermal conductivity is high so that heat can be supplied easily to balance the heat flux demanded by the jet and maintain a high surface temperature.

The spatial temperature gradient at the resident time and during propagation of the wetting front is also different for three regimes. For shorter resident time regime, the radial temperature gradient is quite large at and after the resident time. In contrast, for regime (c) the solid surface temperature is much more uniform. The temperature gradient in the radial direction is small and the radial propagation of the wetting front is faster for larger resident times. Inversely, it is observed that a higher temperature gradient in the radial direction corresponds to slower wetting front velocity for quick cooling conditions. It is also found that the period of time between when the wetting front starts moving until the maximum heat flux condition is generally greater in the moderate cooling regime than the slow cooling regimes.

5.3 Importance of Maximum Heat Flux

The heat flux is very important parameter along with the wetting delay when the quenching is done for controlling the temperature of hot surfaces. It is the direct indication of cooling rate which is to be obtained during cooling process. Therefore knowledge of maximum heat flux from the solid side is essential for complete understanding the quenching phenomena. The present study has considered the experimental parameters such as initial block temperature, jet velocity, liquid subcooling and block material properties which contribute to the value of maximum heat flux and its position along with the movement of wetting front. Much work has been done on the critical flux in case of steady state experiments but fewer publications are available for insight into the maximum heat flux during transient quenching. Therefore, emphasis to explore the maximum heat flux phenomena during transient quenching experiments is reasonably needed.

5.4 Maximum Heat Flux in Boiling Curve

The surface temperature and the surface heat flux estimated from the inverse solution with the radial position are presented in Fig. 5.4. When the jet is impinged on the hot surfaces, different modes of boiling heat transfer are observed along the flow propagation. Due to the movement of wetting front after a certain time delay, the heat transfer characteristics are changed rapidly. The heat flux estimated by inverse heat conduction method which represented that the value of heat flux also changed with the radial position.

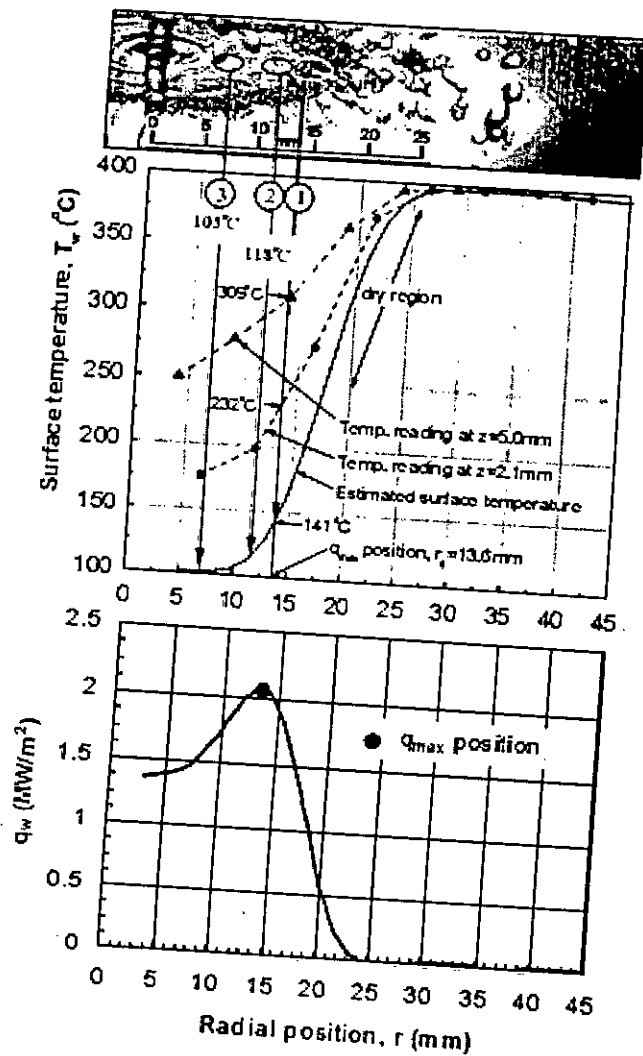


Fig. 5.4 Regimes of boiling and maximum heat flux during wetting front propagation
 $(T_b=400^\circ\text{C}, \Delta T_{sub}=50\text{K}, u=3\text{m/s}, t=4.3\text{ s})$ [18]

From the captured video picture, three distinct regions can be identified: 1) no visible boiling region ($r=0-12\text{mm}$) 2) vigorous boiling region ($r=12-18\text{mm}$) 3) dry region ($18-45\text{mm}$). The no visible boiling region is dominated by the single phase forced convection. Though it is expected that nucleate boiling occurs in this region, no nucleate boiling is observed practically because the bubbles are collapsed very quickly in this region due to its high subcooling. Therefore, in terms of modes of heat transfer the image in Fig. 4.2 can be represented as 1) single phase convection (0-10mm) 2) nucleation boiling (10-14mm) 3) transition boiling (14-18 mm) and 4) single phase convection to vapor phase plus radiation (18-47). The maximum heat flux point in the boiling curve is the borderline between the nucleate boiling and transition boiling region. In Fig. 5.4, the maximum heat flux point appears at a radial position of 13.6 m.

The surface temperatures and heat fluxes estimated from the inverse solution agree with this interpretation. In the single phase convection region, the surface temperature is close to the saturation point and the heat flux is small. The heat flux increases quickly with the wall superheat in the nucleate boiling region and reaches to its maximum value at the wall superheat of 41K. In the dry region, the surface temperature suddenly increases from 250°C to initial block temperature of 400°C and the heat flux becomes very small. Therefore, it is clearly evident that the heated surface experiences different boiling heat transfer modes when the wetting moves outward in the radial direction.

5.5 Surface temperature and surface heat flux distribution

To understand the complex phenomena of quenching process, it is needed to obtain the distribution of surface temperature and surface heat flux with time after the jet impingement. The distribution of these two parameters with spatial position is also needed because they are significantly changed when the wetting front starts to move. By examining these two curves we may expound about the conditions which may contribute to move the wetting front and the factors which may influence the wetting delay period and maximum heat flux propagation.

5.5.1 Surface temperature and surface heat flux distribution with time

The surface temperature and surface heat flux distribution with time is shown in the Fig. 5.5.1.1 and Fig. 5.5.1.2 where the initial block temperature is 400°C , liquid subcooling is 20K and jet velocity is 03 m/s . The temperature falls rapidly near the center of the block within fractions of sec and reaches to 120°C . Then the surface temperature drops at a very slow rate and especially for steel block this rate is too low. It is also evident for this particular situation that the resident time for steel material is very small. The surface heat flux also reaches its maximum value within fractions of sec and then decreases. After few seconds the change of surface heat flux with time is very low and the value of heat flux is very small. It is also observed that the heat transfer rate is higher near the center of the block and then the rate is too slow. Similar characteristics have found for other test conditions as shown in Appendix D.

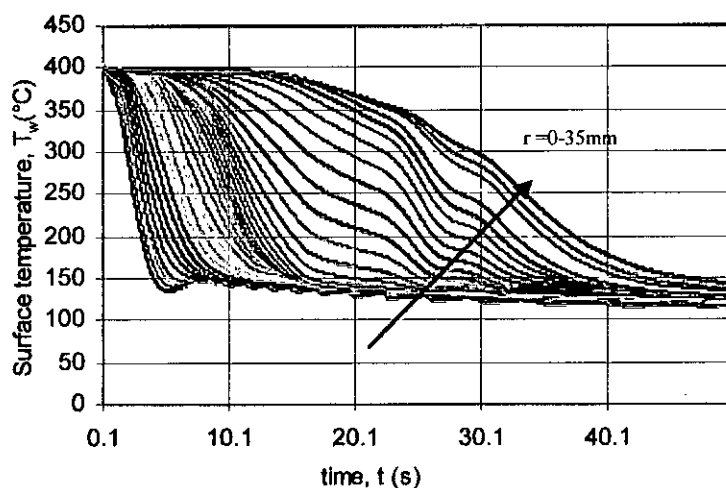


Fig 5.5.1.1 Surface temperature vs. time curve ($T_b=400^{\circ}\text{C}$, $\Delta T_{\text{sub}}=20\text{K}$, $u=03\text{m/s}$)

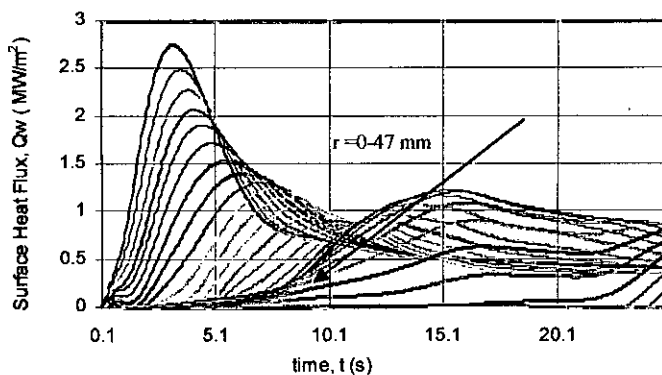


Fig 5.5.1.2 Surface heat flux vs. time curve ($T_b=400^{\circ}\text{C}$, $\Delta T_{\text{sub}}=20\text{K}$, $u=03\text{m/s}$)

5.5.2 Surface temperature and surface heat flux distribution with radial position

It has clearly viewed from the Fig. 5.5.2.1 and Fig. 5.5.2.2 that the surface temperature close to the center of the block drops quickly after the jet strikes. During this time the heat flux rises rapidly and reaches its maximum value. The peak of heat flux moves along the radial position and the value of maximum heat flux also decreases with the radial position which as shown in Fig. 4.4. The rapid drop of maximum heat flux may be the direct result of the sudden drop of surface temperature. The clear understanding of these phenomena can be observed from the video images.

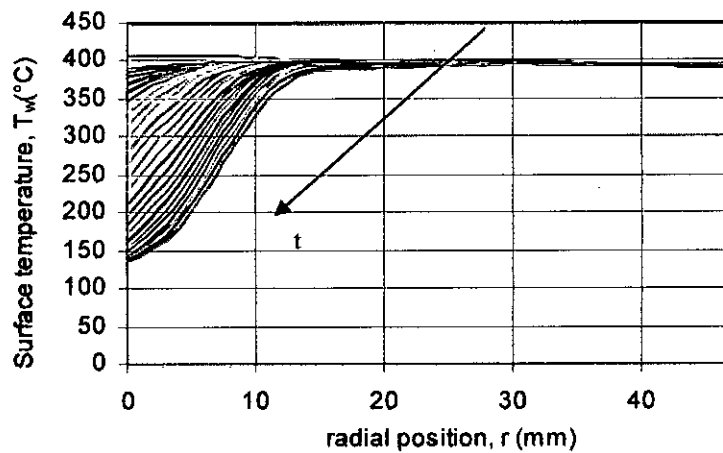


Fig. 5.5.2.1 Variation of surface temperature with radial position
($T_b=400^{\circ}\text{C}$, $\Delta T_{\text{sub}}=20\text{K}$, $u=0.3\text{m/s}$)

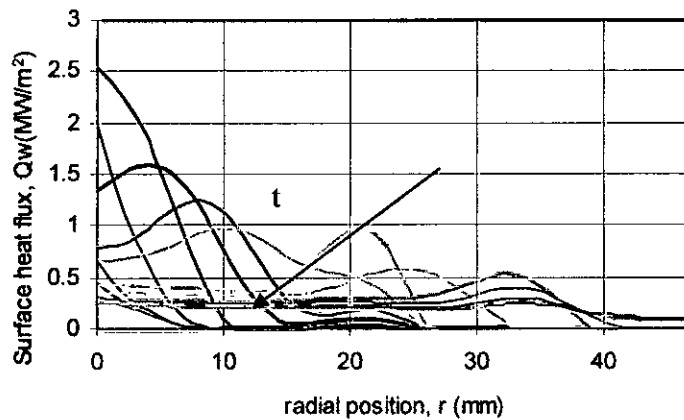


Fig. 5.5.2.2 Surface heat flux distribution with radial position
($T_b=400^{\circ}\text{C}$, $\Delta T_{\text{sub}}=20\text{K}$, $u=0.3\text{m/s}$)

5.6 Visual observations during quenching

The visual and audible observation has done to clarify the boiling phenomena in quenching experiments. The previous study [16] reported that when the jet first struck the surface, the liquid quickly spread over a small central region about to two to four times the jet diameter and it was splashed out from the surface. The size of the solid liquid interaction region stayed relatively fixed for a certain period of time and then the wetting front started to move across the surface. Fig. 5.6 shows two sequences of video image which confirms the wetting front propagation during quenching. This wetting front should not be thought of a single point or single line but it should be considered that the entire transition boiling region will be in the wetting front region.

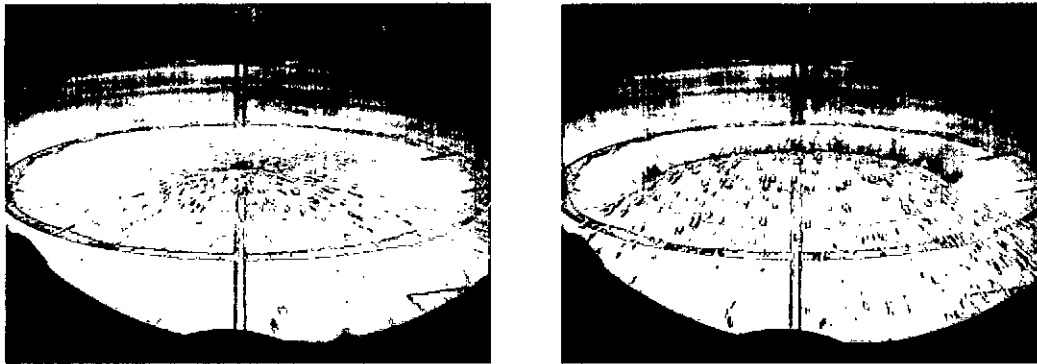


Fig 5.6 Wetting front propagation during quenching

(for $T_b=550C$, $T_{sub}=50K$, $u=05$ m/s)

In the present study, the wetting front is defined as the visible outer edge of the black region though an inner edge of the black region is also visible. A complete thermal and hydrodynamic criterion for the movement of wetting front has not been clarified yet. The video images at least ensure that the time and position of wetting front movement during quenching.

CHAPTER 6

RESULTS AND DISCUSSIONS

6.1 Determination of wetting delay

Surface temperature was plotted against the time for a specific radial position to determine the wetting delay as shown in Fig. 6.1.1. Surface temperature decreased slowly with time just after the jet impingement and after a certain time delay it decreased rapidly. So the resident times are distinguished from other times at the point from which the rapid cooling has started. It was assumed that the region of interaction between the liquid jet and solid was relatively fixed which was around 8 ± 3 mm before movement of the wetting front. The wetting delay has been determined at a radial position of 10 mm in the present study. Fig. 6.1.1 shows the wetting delay for the test condition of initial block temperature of 300°C , liquid subcooling of 50K and jet velocity of 15m/s.

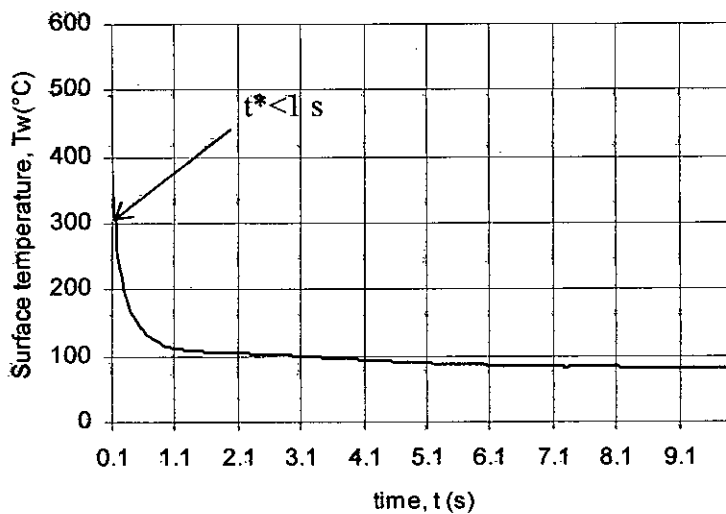


Fig. 6.1.1 Surface temperature vs. time curve (for $T_b=300^\circ\text{C}$ $\Delta T_{\text{sub}}=50\text{K}$, $u=15$ m/s)

The wetting delay has been studied for all conditions of the experiment in the present research work. The previous work [25] also reported the resident time or wetting delay for all conditions of the experiment. It was obtained that the resident time was less than one second for 27 conditions, greater than one second for 10 conditions and not determined for the rest of total 128 conditions. The resident times

could not be determined for a large no. of cases because of difficulties to settle on the sharp changes in the curve. Fig. 6.1.2 shows the temperature distribution with time for one test condition where the wetting delay was 2.4 sec while Fig. 6.1.3 shows another condition of the experiment in which the wetting delay could not be determined. The resident times for all conditions are tabulated in Appendix E.

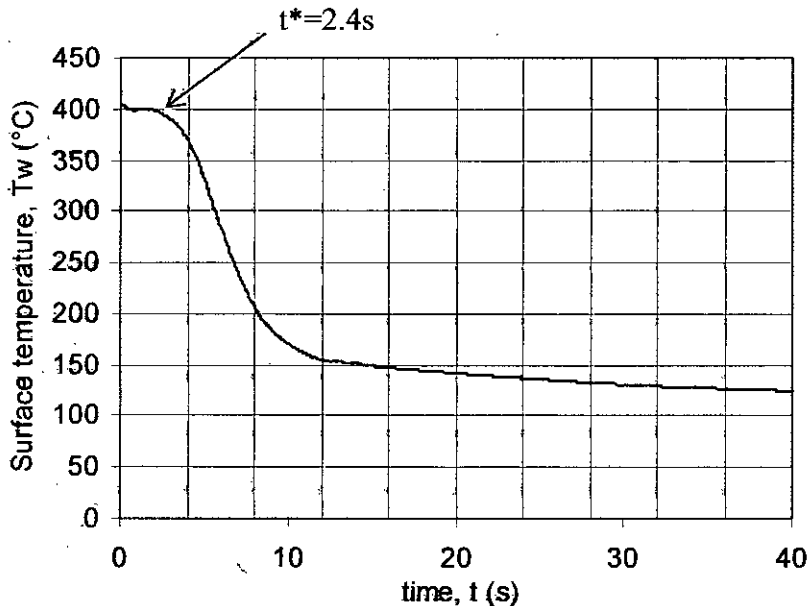


Fig. 6.1.2 Surface temperature vs. time curve (for $T_b=400^\circ\text{C}$ $\Delta T_{\text{sub}}=20\text{K}$, $u=03\text{ m/s}$)

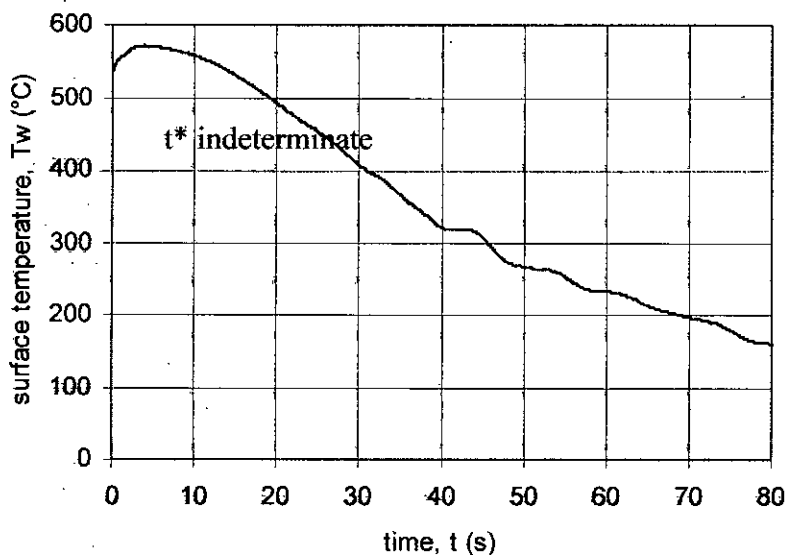


Fig. 6.1.3 Surface temperature vs. time curve (for $T_b=550^\circ\text{C}$ $\Delta T_{\text{sub}}=80\text{K}$, $u=03\text{ m/s}$)

6.2 Effect of different parameters on wetting delay

For the wetting delay of less than one, it is very difficult to distinguish the effects of important parameters on this wetting delay period. In addition, the accuracy of the

surface temperature estimated from the inverse heat conduction solution was not well posed for time less than one sec. That's why the present study has been focused for the resident times of greater than one. But there are only 10 conditions available for understanding the effects of these experimental parameters on the wetting delay of steel block. Therefore, it is very difficult to analyze the behaviors of the parameters as well as to figure out the relationship between them. However, the effects of these parameters are to be pronounced physically which can be summarized below:

6.2.1 Effect of jet velocity

The higher jet velocity will remove the heat quickly from the heated surface and therefore the wetting delay will be less. The direct relationship between the wetting delay and jet velocity did not make out in the experiment because of difficulties to determine the wetting delay for most cases.

6.2.2 Effect of jet subcooling

The higher jet subcooling means the higher temperature gradient between the saturation temperature of water and water jet temperature which indicates the liquid has the higher capacity of extracting heat from the heated block. So the resident time will be less when the jet subcooling will be higher.

6.2.3 Effect of Initial Block Temperature

The block with higher initial temperature will take the more time to become cool. It was also reported [16] that the resident time was longer for higher block initial temperature.

6.3 Effect of parameters on Maximum heat flux

The direct influence of the important parameters on maximum heat flux and its position has described in this section.

6.3.1 Effect of Radial Position on Maximum Heat Flux

The value of maximum heat flux changes with the radial position of the jet impinged point as shown in Fig. 6.3.1. The solid-liquid interaction region remained fixed up to the radial position of 8 ± 3 mm for most of the cases and then the wetting front started to move in the radial direction of the heated surface. The heat flux decreases very

slowly within this region. In this analysis, the variation of maximum heat flux was considered for the regions from where the wetting front started to move. Two distinctive regions are identified: region I (from 10-20 mm) and region II (from 20-35 mm). In the region I, the maximum heat flux decreases slowly with the radial position. In the region II, the maximum heat flux decreases more rapidly with r_q . It was observed that the area of vigorous boiling region increased when the wetting front started to move outward in the radial direction. The available surface area to become cool is increased and the heat carrying capacity of coolant is decreased when it moves outward in the radial direction. This results in decrease of maximum heat flux with increasing radial position.

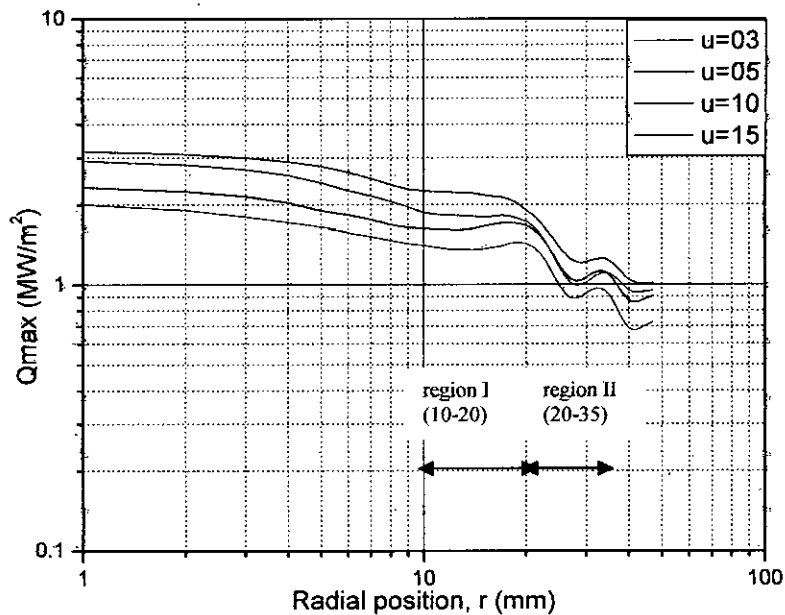


Fig 6.3.1 Variation of maximum surface heat flux with radial position
(for $T_b=300^\circ\text{C}$, $\Delta T_{sub}=20\text{K}$)

6.3.2 Effect of Jet Velocity on maximum heat flux

The effect of jet velocity on maximum heat flux is shown in Fig.6.3.2. Maximum heat flux increases with the jet velocity. Maximum heat flux is higher for a smaller radial position for a particular jet velocity which also indicates the maximum heat decreases with the radial position. The higher jet velocity means the higher flow rate of coolant, supplied to the heated surface which has direct effect on the rate of heat transfer. There is found some discrepancy of this variation for the radial position of 20 mm as shown in Fig. 6.3.2. The effect of jet velocity for other test conditions has shown in Appendix F.

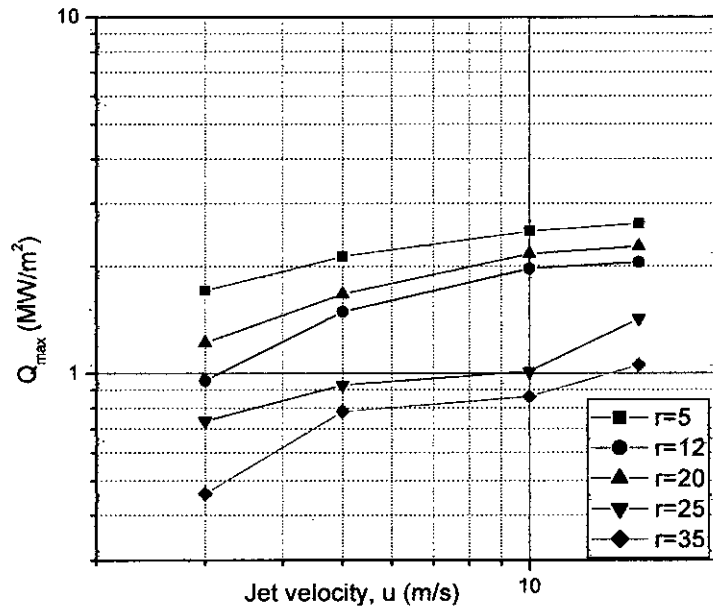


Fig. 6.3.2 Effect of jet velocity on maximum heat flux.
(for $T_b=400^\circ\text{C}$, $\Delta T_{\text{sub}}=20\text{K}$)

6.3.3 Effect of sub-cooling on maximum heat flux

The variation of maximum heat flux with subcooling temperature for different radial position is presented in Fig.6.3.3. Higher subcooling means the higher temperature difference between the saturation temperature and liquid temperature. The lower temperature liquid takes more heat from the heated surface to reach its saturation temperature. Therefore the rate of heat transfer is increased. This observation has been found for all experimental conditions as shown in Appendix F.

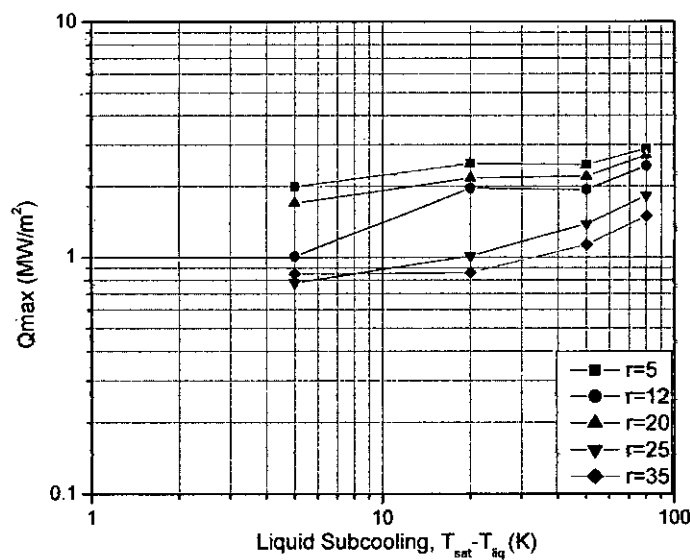


Fig 6.3.3 Variation of Maximum surface heat Flux with liquid subcooling
(for $T_b=400^\circ\text{C}$, $u=10\text{m/s}$)

6.3.4 Effect of initial block temperature on maximum heat flux

Mozumder [16] found that the effect of initial block temperature on maximum heat flux is very small. The largest differences were observed at the smaller radial position where the heat flux was slightly higher for the higher initial temperature. The required time to reach its maximum heat flux point is longer for higher initial temperature. Due to its very small effect it can be considered that maximum heat flux is almost independent of T_b . Fig. 6.3.4 shows the effect of initial temperature on the maximum heat flux for different radial position. In this case, there is very little effect of T_b on the maximum heat flux. Here, some scattering data have been ignored for the initial temperatures of 450-600°C.

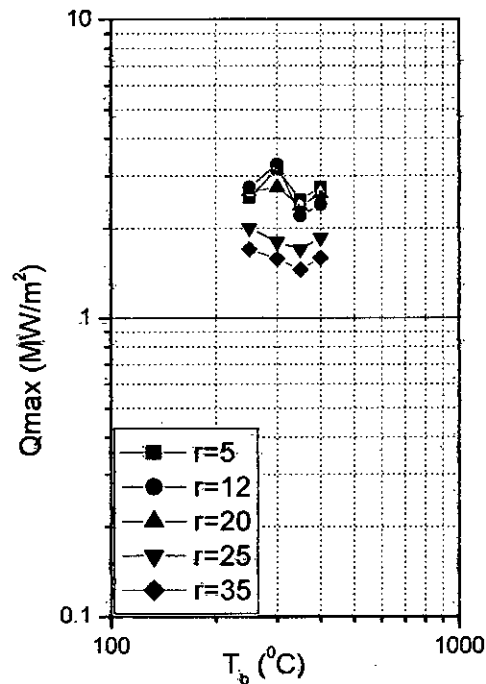


Fig. 6.3.4 Effect of initial block temperature on maximum heat flux

($\Delta T_{sub} = 50K$, $u = 15m/s$)

6.3.5 Effect of block material on maximum heat flux

Generally, it is evident that the block material influences strongly the rate of heat transfer. Mozumder [16] experimented on jet impingement quenching of three different block materials (copper, brass and steel) and reported that the maximum heat flux for copper material is more than two times than steel material. The thermal conductivity of copper, brass and steel are 380 W/mK, 112 W/mK and 37.8 W/mK respectively. Therefore, the thermal conductivity of carbon steel is approximates 1/10 times of copper. The maximum heat flux is strongly affected by the block material. In

case of copper material, the effects of impinged water jet quickly observed on the entire surface. The heat of the quenching area is quickly recovered by the stored heat from the nearer surface area due to its higher thermal conductivity. For steel material, the surface is cooled locally near the surface at which the jet impinged. Because of low thermal conductivity heat is locally removed from the heated surface but the total effect of cooling process does not feel immediately over the entire solid body.

6.3.6 Correlation for maximum heat flux

It is easily perceived that the movement of wetting front is strongly influenced by the some experimental parameters which are discussed in the above section. In the present study, we are concerned to correlate these parameters with the maximum heat flux. Monde et al. [25] proposed a correlation of critical heat flux for sub cooled impinging jets at steady state conditions. Mozumder et al. [18] proposed the correlations of maximum heat flux for copper and brass material for transient heat conditions. They considered that the maximum heat flux would be equal to the critical heat flux when the solid material is of infinite thermal conductivity. They included an important term $\sqrt{\rho c \lambda}$ in their investigation which is the combination of material thermal properties. It plays a dominant role in transient heat transfer when two semi infinite bodies suddenly come into contact. The following correlation was proposed for the radial position of 11 mm to 25 mm.

$$\frac{q_{\max}}{q_c} = 1 - 5.5 \sqrt{\frac{(\rho c \lambda)_l}{(\rho c \lambda)_s}} \quad 6.1$$

Where q_{\max} is maximum heat flux and q_c is critical heat flux.

The above correlation has been initiated from the following correlation of q_c of Monde et al. [25]:

$$\frac{q_{\max}}{q_c} = \frac{1 + \sqrt{1 + 4CJa}}{2} \quad 6.2$$

$$\frac{q_{\infty}}{\rho_s h_x u} = 0.221 \left(\frac{\rho_l}{\rho_g} \right)^{0.645} \left[\frac{2\sigma}{\rho_l u^2 (D-d)} \right]^{0.343} (1 + D/d)^{-0.364}$$

$$C = \frac{0.95(d/D)^2 (1 + D/d)^{0.364}}{\left(\frac{\rho_l}{\rho_g} \right)^{0.645} [2\sigma / \rho_l u^2 (D-d)]^{0.343}}$$

It was found that there was good agreement between the experimental data and the proposed correlation for copper and brass block as shown in Fig. 6.3.6.1. According to their study, the above correlations of maximum heat flux did not fit well with the experimental observations for steel block as shown in Fig. 6.3.6.2. The experimental investigation for quenching of steel block was somewhat different from copper and brass block.

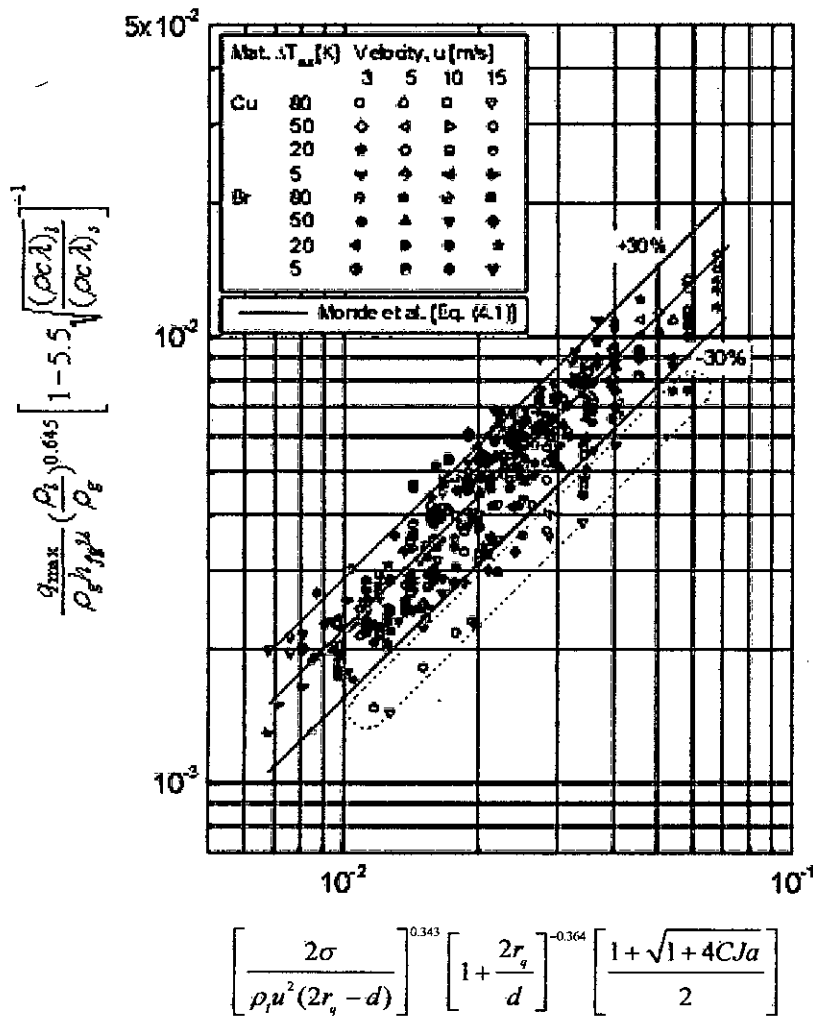


Fig. 6.3.6.1 Comparison of q_{\max} data for copper and brass with the proposed correlation (for region II(11-25 mm)) [18]

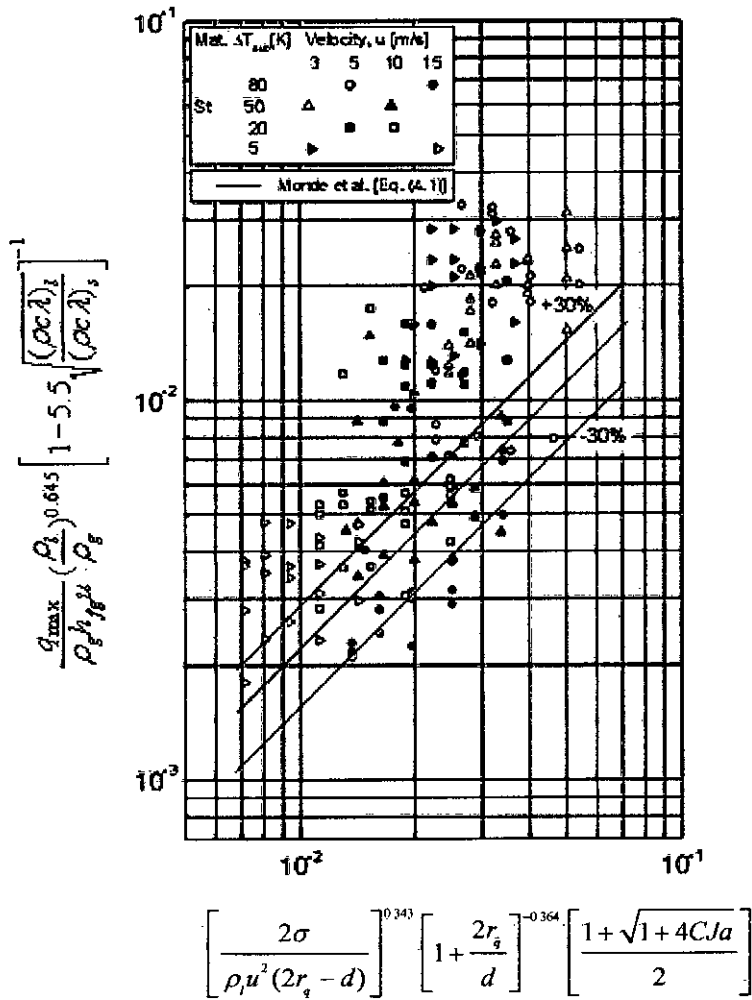


Fig. 6.3.6.2 Comparison of q_{max} data for copper and brass with the proposed correlation (for region II(11-25 mm)) [18]

Therefore, the present investigation includes some important parameters which may have influence on the maximum heat flux. The correlations of maximum heat flux have been developed for the two distinct regions of radial position of 10-20 mm and 20-35 mm in this analysis. It is considered that the wetting front started to move from the radial position of 10 mm. Therefore the maximum heat flux for the radial positions of less than 10 mm has not been included here. The two regions are distinguished according to their heat transfer rate in the radial direction. It is observed that the maximum heat flux gradient with the radial position is higher in the region II.

These correlations have included the terms $\sqrt{(\rho c \lambda)_s / (\rho c \lambda)_l}$, $\frac{\rho_l u^2 (2r_q - d)}{\sigma}$ and $(1 + Ja)$. The term $\sqrt{(\rho c \lambda)_s / (\rho c \lambda)_l}$ indicates the relative effects of solid and

liquid thermal properties. When the wetting front starts to move, the maximum heat flux is influenced by the solid and liquid thermal properties.

Another non-dimensional group $\frac{\rho_l u^2 (2r_q - d)}{\sigma}$ is employed in the proposed correlation. It represents the ratio of inertia force to surface tension force. The relative effects between these two forces can be estimated by this term. This term has sound effect on the maximum heat flux propagation for both regions.

In addition, Jacob number is considered an important non-dimensional number in sub cooled boiling conditions. It is the ratio of the sensible heat for a given volume of liquid to heat through ΔT_{sub} in reaching its saturation temperature, to the latent heat required in evaporating the same volume of vapor.

$$Ja = \frac{\rho_l c_l \Delta T_{sub}}{\rho_g h_{fg}}$$

The lower liquid temperature contributes to the higher sensible heat required for the liquid to reach its saturating condition which indicates the higher heat carrying capacity to remove the heat in quenching. The effects of liquid superheat prior to initiate nucleate boiling can also be realized by this number. The term $(1+Ja)$ has included with the correlation and this term has significant effect for the region I. It indicates the effect of maximum possible heat transfer into the liquid in relative to the heat required to evaporate the same volume of vapor

For the region II, $(1+Ja)$ is found to be negligible because the maximum heat flux tends to decrease when the wetting front moves to the radial direction. The heat removed by the liquid decreases with the radial position due to decrease its temperature gradient along its moving direction. It is found that the effects of $(1+Ja)$ is not dominating in the region II.

Finally, the following two correlations have been developed for the initial temperatures of 250-400°C for the two distinct regions:

For region I (radial position of 10-20mm)

$$\frac{Q_{max}}{\rho_g h_{fg} u} = 55.119 \left(\frac{(\rho c \lambda)_l}{\sqrt{(\rho c \lambda)_s}} \right)^{0.674} \left(\frac{\rho_l u^2 (2r_q - d)}{\sigma} \right)^{-0.295} (1 + Ja)^{0.136} \quad 6.3$$

For region II (radial position of 20-35mm)

$$\frac{Q_{\max}}{\rho_{\infty} h_{\infty} u} = 1.106 \left(\frac{(\rho c \lambda)_{\infty}}{\sqrt{(\rho c \lambda)_{\infty}}} \right)^{-1.291} \left(\frac{\rho_1 u^2 (2r_s - d)}{\sigma} \right)^{-0.287} \quad 6.4$$

The coefficients of these two correlations have been determined by using least square method from the experimental data of maximum heat flux.

Experimental data is then compared with these proposed correlations for the two regions as shown in Fig. 6.3.6.3 and Fig. 6.3.6.4. The experimental data is within the $\pm 25\%$ and $\pm 30\%$ of the proposed correlations respectively

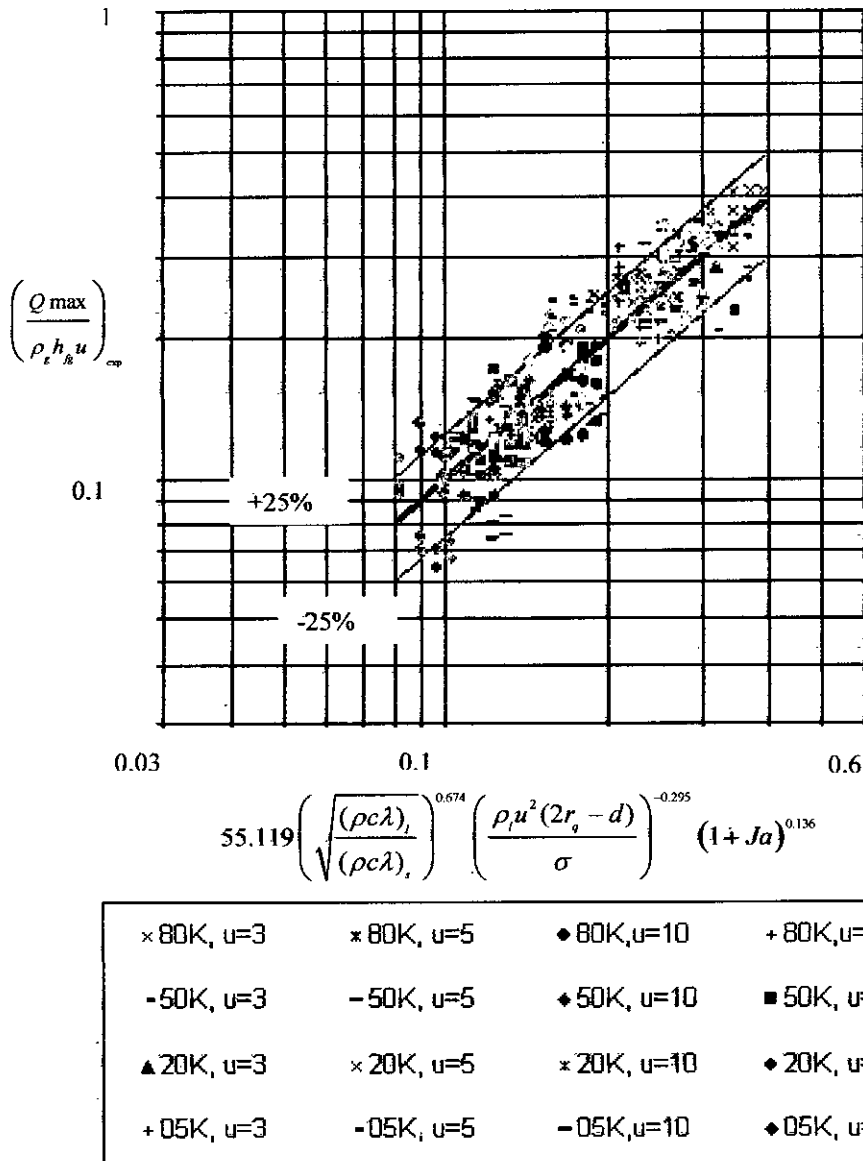


Fig 6.3.6.3 Comparison of experimental data of Q_{\max} for initial temperature of 250-400°C with the proposed correlation (for region I)

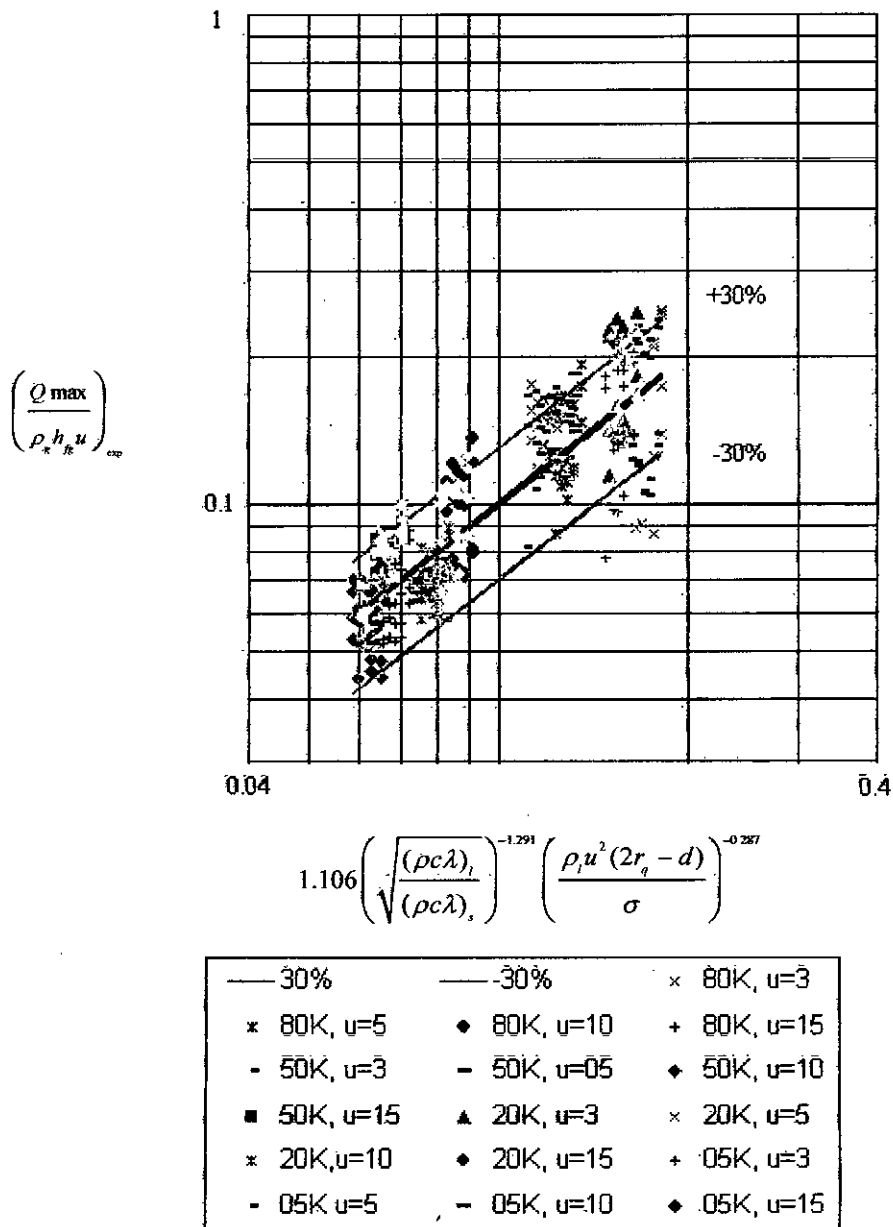


Fig 6.3.6.4 Comparison of experimental data of Qmax for initial temperature of 250-400°C with the proposed correlation (for region II)

These correlations are not well predicted for the initial block temperatures of 450-600°C as shown in Fig. 6.3.6.5 and Fig. 6.3.6.6 because there were some discrepancies of experimental data within this range. A new heated block was placed for the same experiment and the experiment was done for the initial temperatures of 450-600°C with this set up. The above correlations also have applied for this temperature range but most of the data is out of $\pm 30\%$ of the proposed correlation. The experiment may have itself some problems. Most of the data within this range is scattered. This scattering is so high; as a result these correlations are not valid for this temperature range.

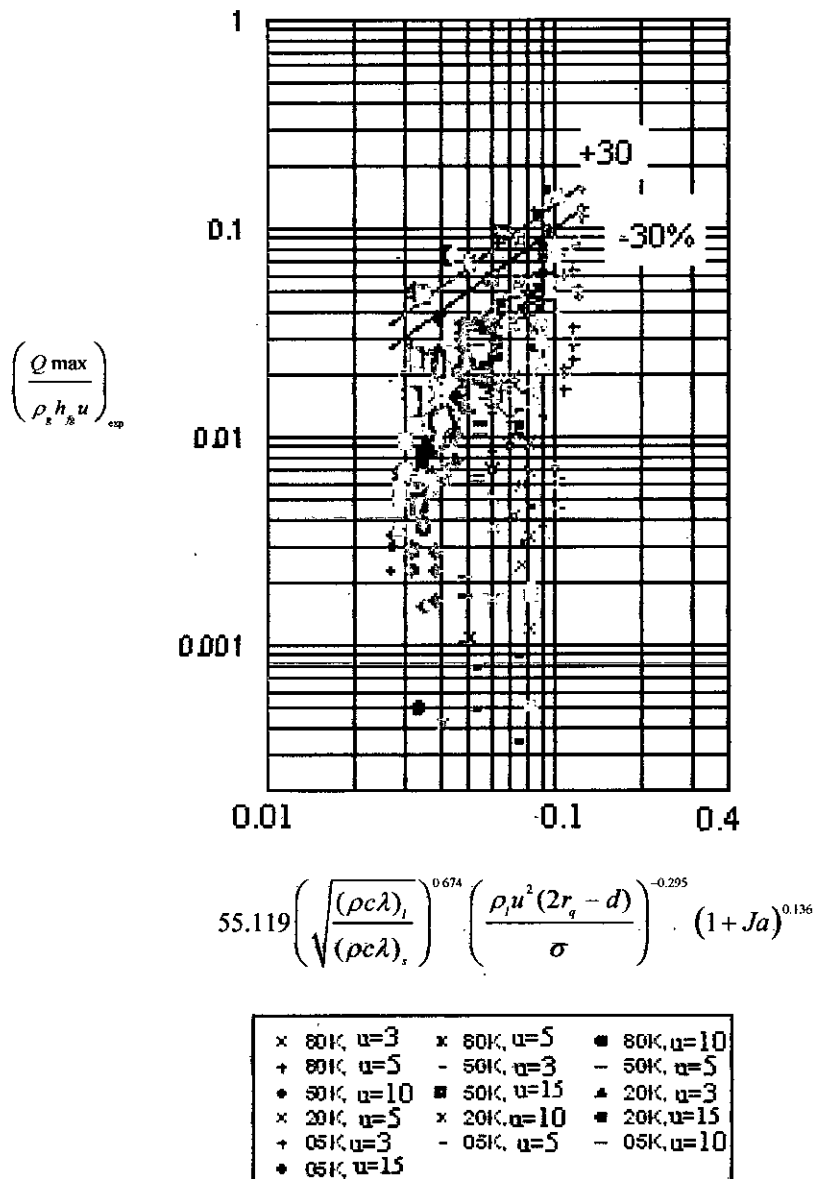
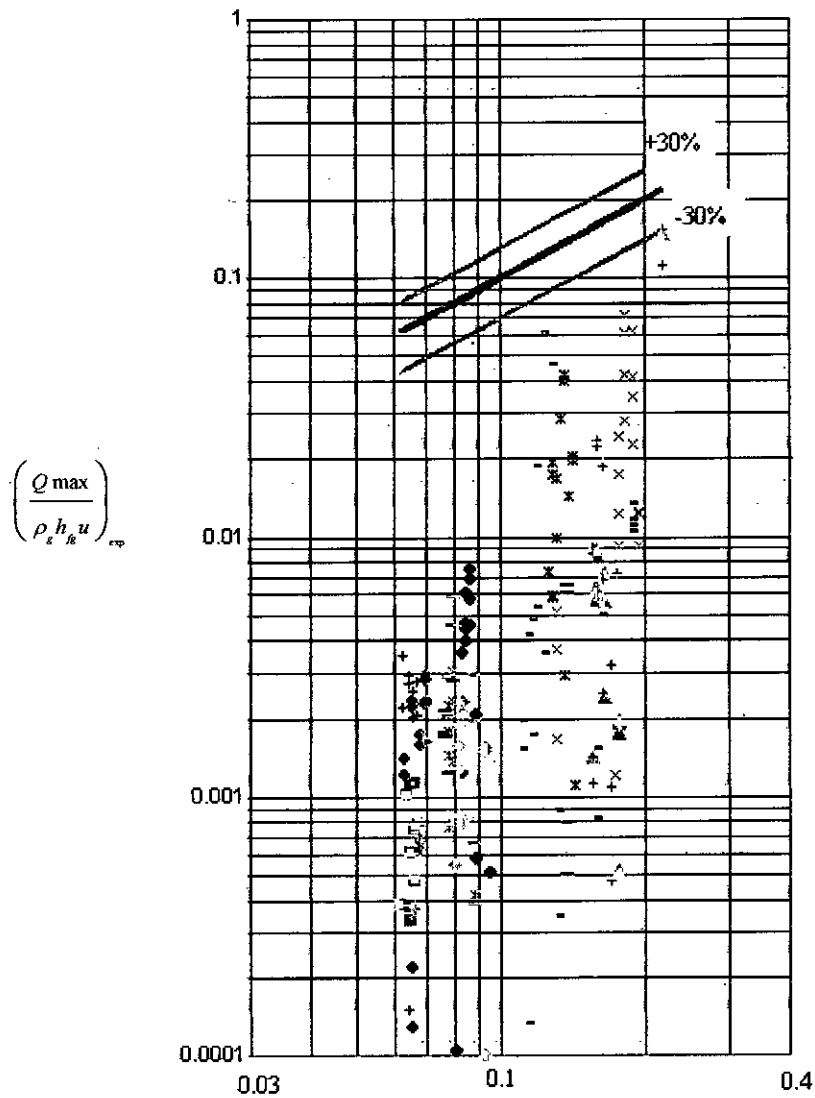


Fig 6.3.6.5 Comparison of experimental data of Q_{max} for initial temperature of 450-600°C with the proposed correlation (for region II)



$$1.106 \left(\frac{(\rho c \lambda)_s}{\sqrt{(\rho c \lambda)_s}} \right)^{-1.291} \left(\frac{\rho_s u^2 (2r_s - d)}{\sigma} \right)^{-0.287}$$

× 80K, u=3	× 80K, u=5	◆ 80K, u=10	+ 80K, u=15
- 50K, u=3	- 50K, u=5	◆ 50K, u=10	■ 50K, u=15
▲ 20K, u=3	× 20K, u=5	× 20K, u=10	◆ 20K, u=15
+ 05K, u=3	- 05K, u=5	- 05K, u=10	◆ 05K, u=15

Fig 6.3.6.6 Comparison of experimental data of Q_{max} for initial temperature of 450-600°C with the proposed correlation (for region II)

CHAPTER 7

CONCLUSIONS

AND RECOMMENDATIONS

7.1 Conclusions

The present study has focused on the wetting delay and maximum heat flux during jet impingement quenching of steel block. These two parameters are very important in investigating the underlying mechanisms of quenching process. The experiment has been actually carried out by Mozumder [16]. In this research work, the effects of dominating experimental parameters on the wetting delay and maximum heat flux phenomena during quenching of carbon steel block have been investigated by analyzing the experimental data from the experiment [16].

The following conclusions can be drawn from the present investigation:

1. The maximum heat flux always occurs during the movement of the wetting front. During this movement the position of the maximum heat flux also moves from the center towards the circumference.
2. Effect of experimental parameters on maximum heat flux has been analyzed. The maximum heat flux is reported to a strong function of jet sub-cooling, jet velocity and material property although, it is almost independent of block initial temperature.
3. The correlations between the maximum heat flux and some important non dimensional groups have been proposed of the steel block for the two regions: region I (10-20mm) and region II (20-35mm).
4. The maximum heat flux for the initial temperatures range of 250-400°C is well predicted within an accuracy of $\pm 25\%$ and $\pm 30\%$ for two regions respectively by comparing it with the proposed correlation of maximum heat flux.
5. The wetting delay for carbon steel block was significantly very smaller than that of copper and brass for some cases while for most cases the wetting delay could not clearly identified. However, it was clearly observed that the wetting

front did not immediately move over the heated surface rather than it stayed fixed for a certain period of time.

6. Due to low thermal conductivity of steel the liquid jet removed heat locally from the heated surface as a result the entire body did not feel immediately the quenching effect. Because, the removed heat did not cover up quickly from the adjacent heated area.

7.2 Recommendations for future works

In the present study the wetting delay for most of the experimental conditions could not be determined. Therefore the correlation for the wetting delay could not be possible to develop. More extensive analysis may be needed to find out the reasons for such behaviors of carbon steel block.

The experiment had itself some discrepancies for the initial block temperatures of 450-600°C. Therefore more reliable data is required for more accurate correlation. In that case, the proposed correlation can be more generalized for a greater temperature range.

Wetting delay and maximum heat flux phenomena was observed for the carbon steel block. Due to low thermal conductivity of steel, the whole block didn't immediately feel the effect of cooling operation by water jet impingement. During cooling of nuclear reactor, though it may have assumed that the element has cooled down but the hot core has remained hot that may cause severe accident. This is also certainly very dangerous for other industries and steel manufacturing industries. Therefore research on effective cooling agents may be required for quenching of steel materials or products with lower thermal conductivity.

REFERENCES

- [1] Wolf, D. H., Incropera, F. P. and Viskanta, R., "Jet Impingement Boiling", In *Advances in Heat Transfer* (Edited by J. P. Hartnett et al.), Vol. 23, pp. 1-132. Academic Press, New York, 1993.
- [2] Nelson, R. A., "Mechanism of Quenching Surfaces", in N. P. Cheremisinoff (ed.), *Hand-book of Heat and Mass Transfer*, Vol. 1, Heat Transfer Operations, Gulf Publishing Co., Houston, TX, pp. 1103-1153, 1986.
- [3] Ueda, T., Tsunenari, S. and Koyanagi, M., "An Investigation of Critical Heat Flux and Surface Rewet in Flow Boiling Systems, *International Journal of Heat Mass Transfer* 26 pp.1189-1198 , 1983.
- [4] Dua, S. S. and Tien, C. L., "An Experimental Investigation of Falling-Film Rewetting", *Int. J. Heat Mass Transfer*, Vol. 21, pp. 955- 965, 1978.
- [5] Chan, A. M. C. and Banerjee, S., "Refilling and Rewetting of a Hot Horizontal Tube, Part I: Experiments", *Trans. ASME, Journal of Heat Transfer*, Vol. 103, pp. 281-286, 1981.
- [6] Iloeje, O. C., Plummer, D. N., Rohsenow, W. M. and Griffith, P., "Effect of Mass Flux, Flow Quality, Thermal and Surface Properties of Materials on Rewet of Dispersed Flow Film Boiling", *Trans. ASME, Journal of Heat Transfer*, Vol. 104, pp. 304-308, 1982.
- [7] Carbajo, J. J., "A Study on the Rewetting Temperature", *Nuclear Engineering and Design*, Vol. 84, pp. 21-52, 1985.
- [8] Ueda, T. and Inoue, M., "Rewetting of a Hot Surface by a Falling Liquid Film-Effects of Liquid Subcooling", *International Journal of Heat Mass Transfer* 27 pp. 999 -1005, 1984.
- [9] Mitsutake, Y. and Monde, M., "Heat Transfer during Cooling of High Temperature Surface with an Impinging Jet", *Heat and Mass Transfer* 37 pp. 321- 328, 2001.
- [10] Bernardin, J.D., Stebbins, C.J. and Mudawar, I., "Mapping of impact and heat transfer regimes of water drops impinging on a polished surface", *Int. J. Heat Mass Transfer* 40 (2) pp. 247-267, 1997.

- [11] Hall, D. E., Incropera, F. P. and Viskanta, R., "Jet Impingement Boiling from a Circular Free-Surface Jet During Quenching: Part 1-Single-Phase Jet", *Trans. ASME, Journal of Heat Transfer*, Vol.123, pp. 901-910, 2001.
- [12] Hall, D.E., Incropera, F.P. and Viskanta, R., "Jet impingement boiling from a circular free-surface jet during quenching: Part 2-two-phase jet", *ASME J. Heat Transfer* 123 (4) pp. 911–917, 2001.
- [13] Woodfield, P.L., Monde, M. and Mozumder, A.K., Observations of high temperature impinging-jet boiling phenomena, *Int. J. Heat Mass Transfer* 48 pp. 2032–2041, 2005.
- [14] Kumagai, S., Suzuki, S., Sano, Y. and Kawazoe, M., "Transient cooling of a hot metal slab by an impingement jet with boiling heat transfer", *ASME/JSME Thermal Eng. Conf. 2*, 1995.
- [15] Hammad, J., "Characteristics of heat transfer and wetting front during quenching high temperature surface by jet impingement", PhD thesis, graduate school of science and engineering, Saga University, Japan, 2004
- [16] Mozumder, A. K., "Thermal and Hydrodynamic Characteristics of Jet Impingement Quenching for high temperature surface", Ph.D thesis, Graduate School of Science and Engineering, Saga University, Japan, 2006.
- [17] Mozumder, A. K., Monde, M. and Woodfield, P.L., "Delay of wetting propagation during jet impingement quenching for a high temperature surface", *Int. J. of Heat and Mass Transfer* 48 pp. 2877-2888, 2005.
- [18] Mozumder, A. K., Monde, M., Woodfield, P. I. and Islam, M. A., "Maximum heat flux in relation to quenching of a high temperature surface with liquid jet impingement", *Int. J. of Heat and Mass Transfer* 49 pp. 2877-2888, 2006.
- [19] Filipovic, J., Incropera, F. P., and Viskanta, R., "Quenching Phenomena Associated with a Water Wall Jet: I. Transient Hydrodynamic and Thermal Conditions", *Experimental Heat Transfer* 8 pp. 97-117, 1995.
- [20] Ochi, T., Nakanishi, S., Kaji, M. and Ishigai, S., "Cooling of a hot plate with an impinging circular water jet", *Multiphase-Phase Flow and Heat Transfer III, Part A:*

Fundamentals (Editors: T. Nejat Veziroglu and Arthur E. Bergles), Elsevier, Amsterdam pp. 671-681, 1984.

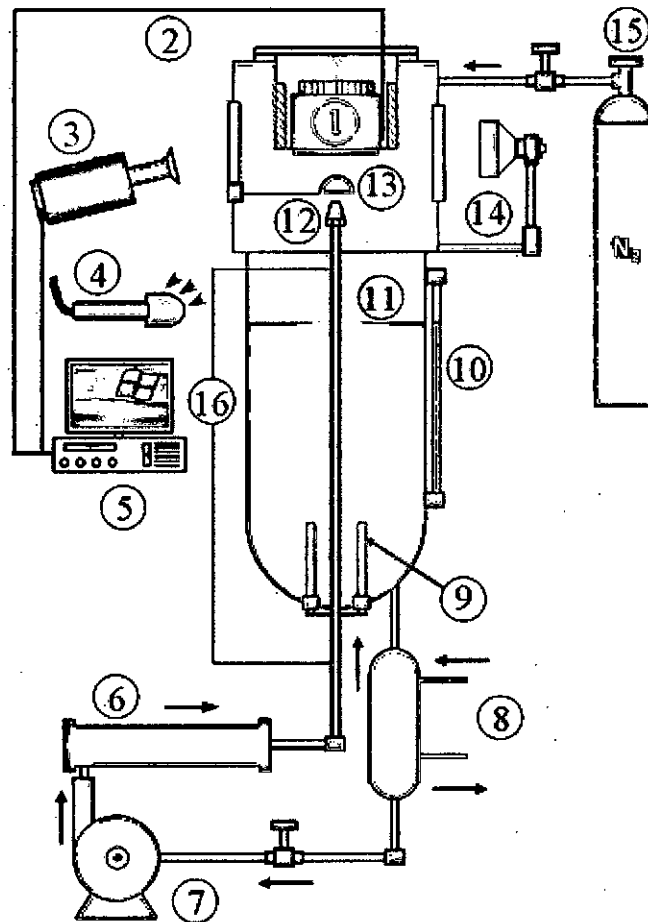
- [21] Monde, M., Arima, H., Liu, W., Mitsutake, Y. and Hammad, J.A., An analytical solution for two-dimensional inverse heat conduction problems using Laplace transform, *Int. J. Heat Mass Transfer* 46, pp. 2135–2148, 2003.
- [22] Hammad, J., Monde, M., Mitsutake, Y. and Arima, H., “Determination of surface temperature and heat flux using inverse solution for two dimensional heat conduction”, *Thermal Science & Engineering* 10 (No. 2) pp.17-26, 2002.
- [23] Woodfield, P. L., Monde, M. and Mitsutake, Y., “Implementation of an analytical two-dimensional inverse heat conduction technique to practical problems”, *International Journal of Heat and Mass Transfer* 49 pp.187-197, 2006.
- [24] Hammad, J., Mitsutake, Y., and Monde, M., “Movement of maximum heat flux and wetting front during quenching of hot cylindrical block”, *International Journal of Thermal Science* 43 pp.743-752, 2004.
- [25] Dutta, Joydip and Hossainy, G.A., “ Study of resident time and maximum heat flux for carbon steel during jet impingement quenching” Undergraduate thesis, Dept. of Mechanical Engineering, BUET, Dhaka, 2008.
- [26] Monde, M., Kitajima, K., Inoue, T., Mitsutake, Y., “Critical heat flux in a forced convection subcooled boiling with an impinging jet”, *Heat Transfer* 7 pp. 515-520, 1994.

APPENDIX A

Experimental set up and procedures

A.1 Experimental Set-up

The main components of the experimental set up are a heated cylindrical block, a fluid flow system, a data acquisition system, a high speed video camera and a sound measuring unit.



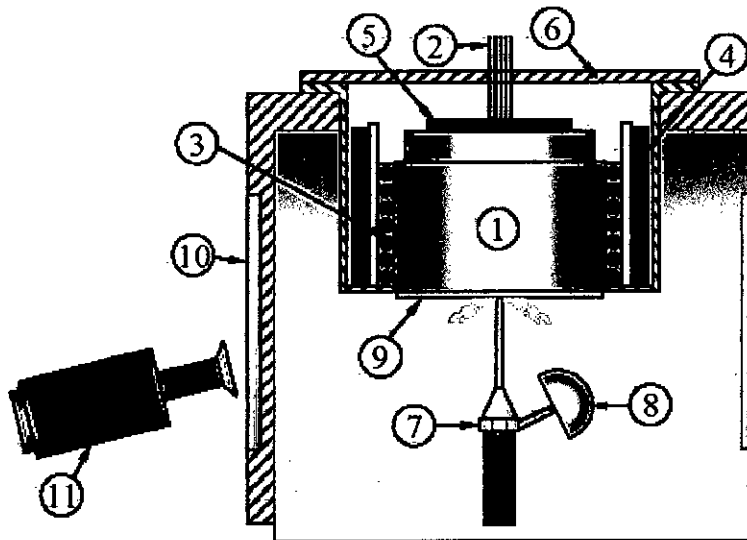
1. Tested block, 2. Thermocouple wire, 3. High-speed video camera, 4. Microphone, 5. Data acquisition system, 6. Auxiliary heater, 7 Pump, 8. Cooler, 9. Main heater, 10. Level gauge, 11. Liquid tank, 12. Nozzle, 13. Rotary shutter, 14. Spot light, 15. Nitrogen cylinder 16. dynamic strain meter (for measuring jet velocity)

Fig. A.1 Schematic diagram of the experimental set-up

A.1.1 Heated Block

The heated block was of cylindrical shape with 94 mm diameter and 59 mm height as shown in Fig. 2.2. Sixteen thermocouples (CA-type, 1 mm sheath diameter and 0.1 mm wire diameter) were located at two different depths, 2.1 mm and 5 mm from the surface as shown in Fig 2.3. At each depth, eight thermocouples were inserted along the r-axis. To protect the heated test surface from oxidation, it was plated with a thin layer of gold, 16 μm , which has an excellent oxidation resistance and also a good thermal conductivity; $\lambda = 317 \text{ W/mK}$. The surface roughness of the tested block was 0.2~ 0.4 μm . The block was heated by an electrical sheath heater with a capacity of 0.94 kW that was coiled around the block circumference. Two auxiliary heaters were used to insulate the block and to keep a uniform heat flux at the surfaces; one of them was placed around the block circumference with capacity of 0.65kW and another one placed on the upper part of the block with capacity of 0.5kW.

A new block was placed instead of old one for the initial block temperatures of 450-600°C for the same experiment. This block has same dimensions as of the old block. The main difference is that there is no cut for inserting the thermocouples. The thermocouple spacing was about 5 mm for the old block and was 6 mm for the new block.



1. Tested block, 2. Thermocouple wires, 3. Sheath heater, 4. Band type heater, 5. Plate heater, 6. Block holder, 7. Nozzle, 8. Rotary shutter, 9. Test surface, 10. Glass window, 11. High speed video camera.

Fig. A.1.1.1 Schematic diagram of the test section and heating element

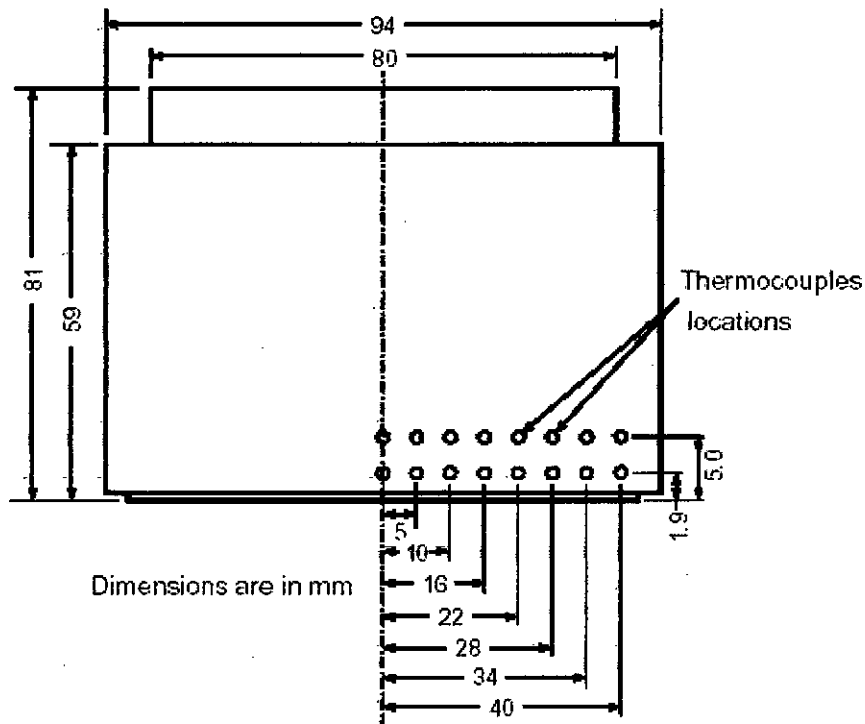


Fig. A.1.1.2 Thermocouple locations in the test block

A.1.2 Data Acquisition System

The thermocouples were scanned sequentially at 0.05 second intervals, with 8.0 ms needed to read all of the thermocouples using 16-bit resolution with an analog-digital converter. The duration of the total data acquisition period was adjusted to suit the experimental conditions so that in all cases the experiment continued until the quench was completed. The uncertainty in the temperature measurements was ± 0.46 °C, while the uncertainty in the placement of the thermocouples was ± 0.1 mm. The time lag for the response of the thermocouples was less than 0.1 sec.

A.1.3 Visual Observation

A high speed video camera was used to capture the fluid flow movement over the heated surface during quenching. The captured picture was with a maximum resolution of $1,280 \times 1,024$ pixels and a maximum rate of 10,000 frame/s.

A.1.4 Audible Observation

A microphone was simultaneously connected to record the sound after the jet impact. The recorded sound signal (electrical voltage) was then normalized against the peak voltage giving a representation of noise level before and after the wetting front propagation.

A.2 Experimental Procedure

The experiment was started at first to fill up the water container with distilled water up to a certain level. A water jet was produced by pumping water through a nozzle of 2mm diameter, which was placed centrally 44 mm from the test surface. A shutter was mounted in front of the nozzle to prevent water from striking the block prematurely and to maintain a constant water temperature by forcing it to run within a closed loop system. The desired temperature of the water was obtained by controlling the main heater, auxiliary heater or by adding cooling water to the cooler. The block was heated to the desired initial temperature by heating it with an electrical heater mounted around the block. A dynamic strain meter was attached at two points of the flow line before the nozzle for measuring differential pressure from which jet velocity was calculated. The whole experiment was done in a nitrogen atmosphere to prevent oxidization of the test surface. One atmospheric pressure was maintained during the experiment. After setting up the all desired initial conditions of the experiment, the shutter was opened for allowing the water jet to strike at the center of the flat surface of the heated block. The high speed video camera was employed to record the flow pattern over the heated block surface and at the same time, the sixteen thermocouples measured the temperatures inside the heated block. Sound has been also recorded by the microphone for some conditions.

APPENDIX B

Inverse Solution

Monde et. al. [21] and Hammad et al. [22] have developed an analytical solution for two dimensional inverse heat conduction problem by using the Laplace transform technique to estimate the surface heat flux and surface temperature. This well established and reliable method is adopted during this research work. For each specific depth, the temperatures were recorded at eight different locations inside the test surface. The previous work [23] recommended to consider 28-30 Eigen values in order to get the better spatial resolution of measured temperatures. Extra points were added by interpolating the measured data points considering data trends with time and space. The interpolation has been done by using the smooth spline method so as to increase the no. of reference points from 8 to 29. Some improvements to implementation of the inverse calculation procedure suggested by Woodfield et al. [23] were incorporated also.

The following approximate equation was proposed for predicting temperature response at each distance:

$$f(\tau, \gamma, \xi_n) = \sum_{j=0}^{N_j} J_0(m_j \gamma) \cdot \sum_{k=0}^N \frac{P_{j,k}^{(n)} \cdot (\tau - \tau_n^*)^{k/2}}{\Gamma(k/2 + 1)} \quad \text{at } n=1,2 \quad (\text{B.1})$$

where $f(\tau, \gamma, \xi_n)$ is temperature variation function on plane $\xi = \xi_n$ beneath the surface. The coefficients $P_{j,k}^{(n)}$ of were determined from the measured temperatures by using the least mean square method. Then the verification of the applicability of coefficients in Eq. (B.1) has done by comparing it with the original measured distributions. The unsteady heat conduction equation and Eq. (B.1) are transformed to the Laplace domain and then solved. The solutions for the surface temperature and heat flux are obtained explicitly using an approximate inverse Laplace transform technique which are given below:

$$\theta_w(\tau, \gamma) = \sum_{j=0}^{N_j} \sum_{l=1}^N G_{j,l}^{(1,2)} \cdot \frac{(\tau - \tau_1^*)^{l/2}}{\Gamma(l/2 + 1)} J_0(m_j \gamma) - \sum_{j=0}^{N_j} \sum_{l=1}^N G_{j,l}^{(2,1)} \cdot \frac{(\tau - \tau_2^*)^{l/2}}{\Gamma(l/2 + 1)} J_0(m_j \gamma) \quad (\text{B.2})$$

$$\begin{aligned}
\Phi_w(\tau, \gamma) = & \sum_{j=0}^{N_j} \sum_{l=-1}^N H_{j,l}^{(1,2)} \cdot \frac{(\tau - \tau_1^*)^{l/2}}{\Gamma(l/2 + 1)} \cdot J_0(m_j \gamma) \\
& - \sum_{j=0}^{N_j} \sum_{l=-1}^N H_{j,l}^{(2,1)} \cdot \frac{(\tau - \tau_2^*)^{l/2}}{\Gamma(l/2 + 1)} \cdot J_0(m_j \gamma)
\end{aligned} \tag{B.3}$$

where J_0 is Bessel function, τ is non dimensional time, ξ is non-dimensional distance in radial direction of the block and m_j is eigen value. The mathematical derivation of this inverse program and the method to determine the coefficients of $G_{j,l}^{(m,n)}$ and $H_{j,l}^{(m,n)}$ in Eq. (B.2) and Eq. (B.3) have been discussed in details in [21] and [22].

APPENDIX C

Thermo-physical properties of materials

Thermo-physical properties of water and tested block of steel material are tabulated below for different experiment conditions:

Table C.1 Thermo-physical properties of water

T_{liq} (°C)	Density (kg/m ³)	Specific heat (J/kg.K)	Conductivity (W/mK)	Diffusivity (m ² /s)	Viscosity (m ² /s)	Prandtl number
20	997.755	4183.65	0.59909	1.44×10^{-7}	1.03×10^{-6}	7.2077
50	987.830	4178.50	0.64000	1.55×10^{-7}	5.44×10^{-7}	3.5086
80	971.635	4199.35	0.64684	1.64×10^{-7}	3.62×10^{-7}	2.2054
95	961.123	4214.00	0.67848	1.67×10^{-7}	3.05×10^{-7}	1.8253

Table C.2 Thermo-physical properties of steel material

Temp. (°C)	Density, ρ (kg/m ³)	Sp. heat, c (kJ/kg.K)	Conductivity, λ (W/mK)	Diffusivity, a (m ² /s)	$\sqrt{\rho c \lambda}$ (kJ/m ² K ^{1/2} s ^{1/2})
100	7833	0.485	52	1.368×10^{-5}	14.06
200	7806	0.509	48	1.208×10^{-5}	13.81
300	7775	0.545	45	1.061×10^{-5}	13.81
400	7741	0.589	42	9.211×10^{-6}	13.84

APPENDIX D

Surface temperature and Surface heat flux distribution

D.1 Surface temperature distribution with time

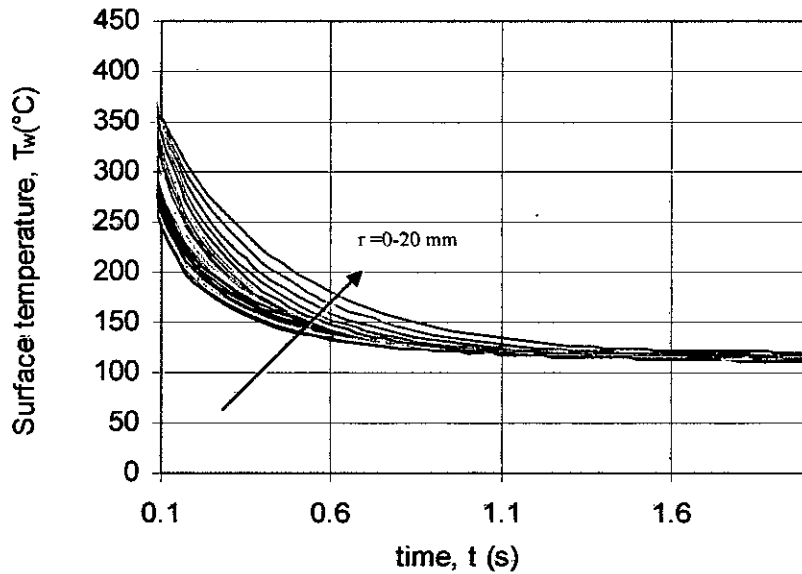


Fig. D.1.1 Surface temperature vs. time curve

($T_b=250^\circ\text{C}$, $\Delta T_{\text{sub}}=50\text{K}$, $u=5\text{m/s}$)

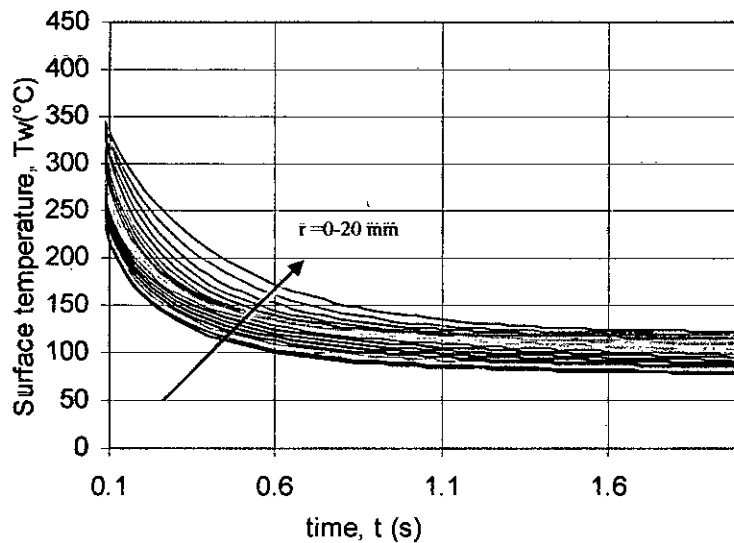


Fig. D.1.2 Surface temperature vs. time curve

($T_b=250^\circ\text{C}$, $\Delta T_{\text{sub}}=80\text{K}$, $u=10\text{m/s}$)

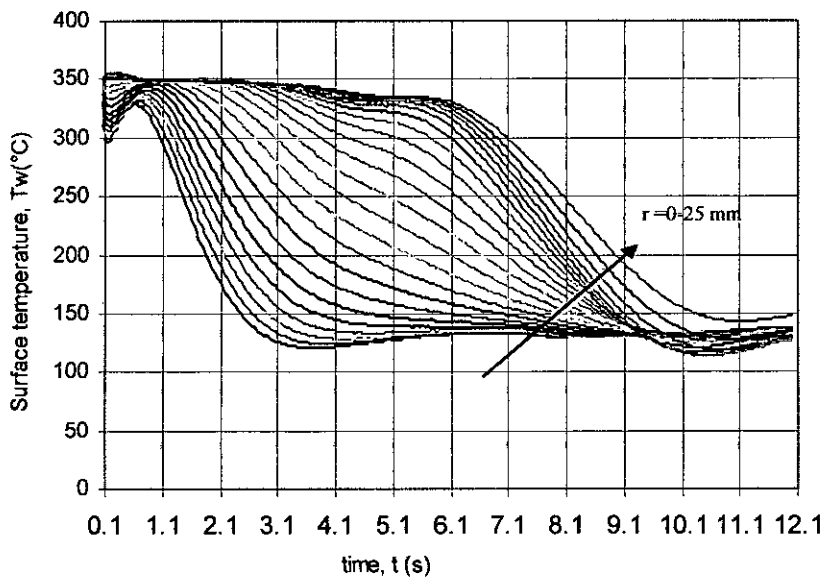


Fig. D.1.3 Surface temperature vs. time curve
 ($T_b=350^\circ\text{C}$, $\Delta T_{sub}=05\text{K}$, $u=05\text{m/s}$)

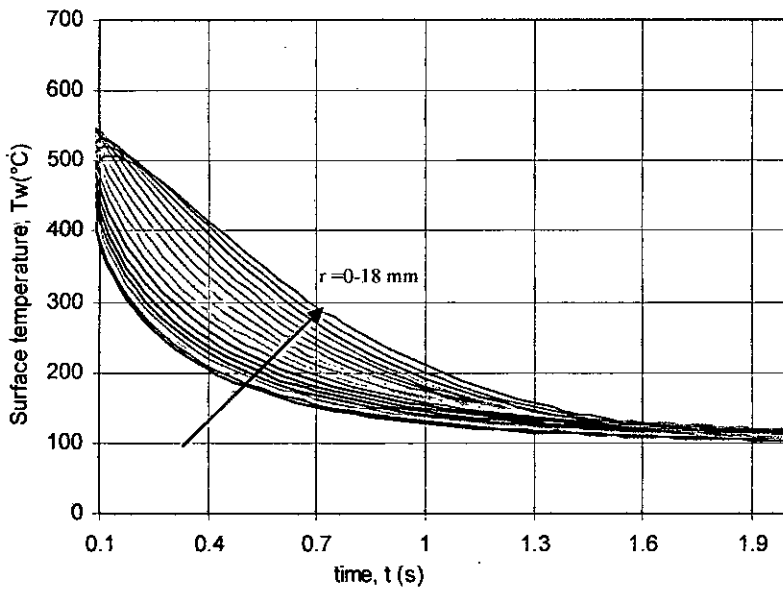


Fig. D.1.4 Surface temperature vs. time curve
 ($T_b=350^\circ\text{C}$, $\Delta T_{sub}=80\text{K}$, $u=10\text{m/s}$)

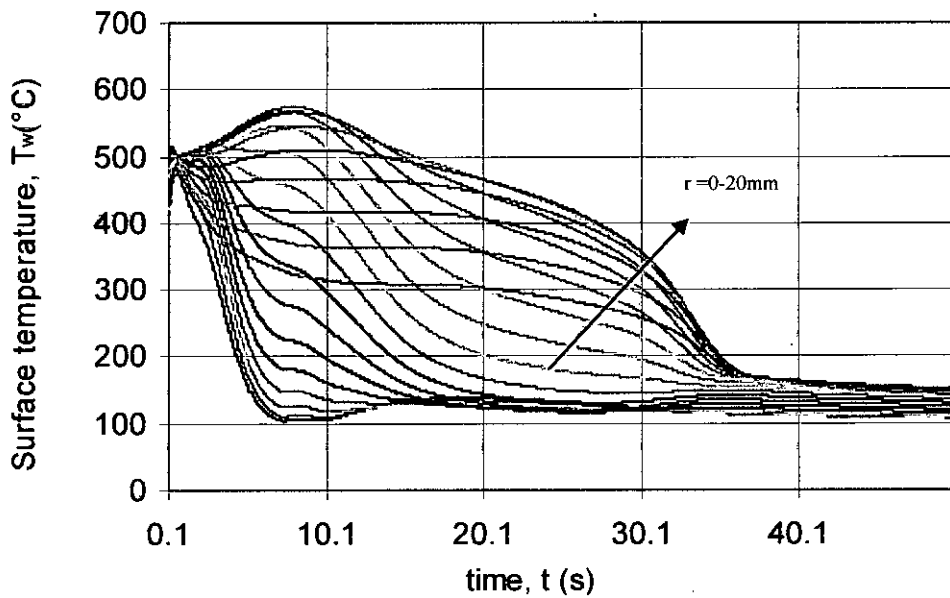


Fig. D.1.5 Surface temperature vs. time curve
 $(T_b=500^\circ\text{C}, \Delta T_{\text{sub}}=50\text{K}, u=0.5\text{m/s})$

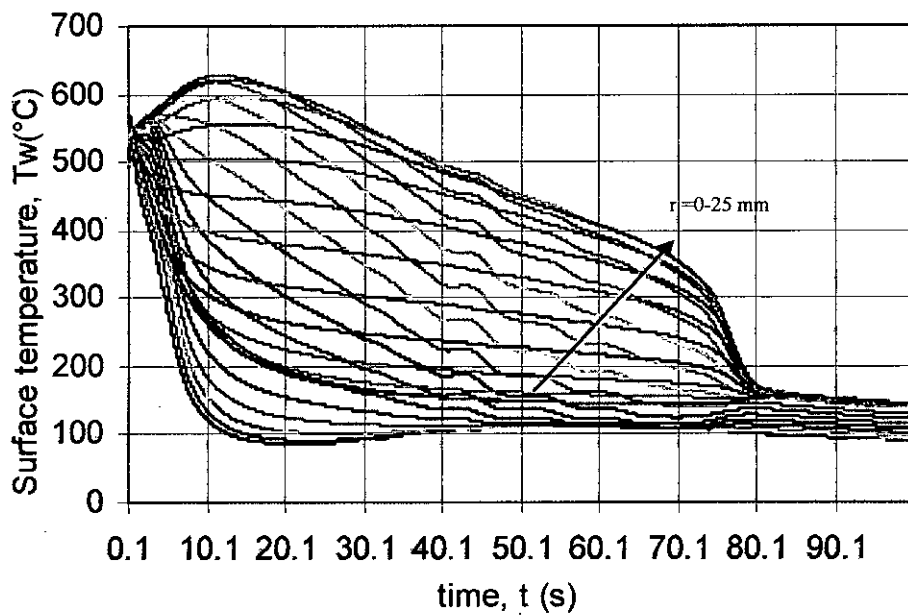


Fig. D.1.6 Surface temperature vs. time curve
 $(T_b=550^\circ\text{C}, \Delta T_{\text{sub}}=80\text{K}, u=0.3\text{m/s})$

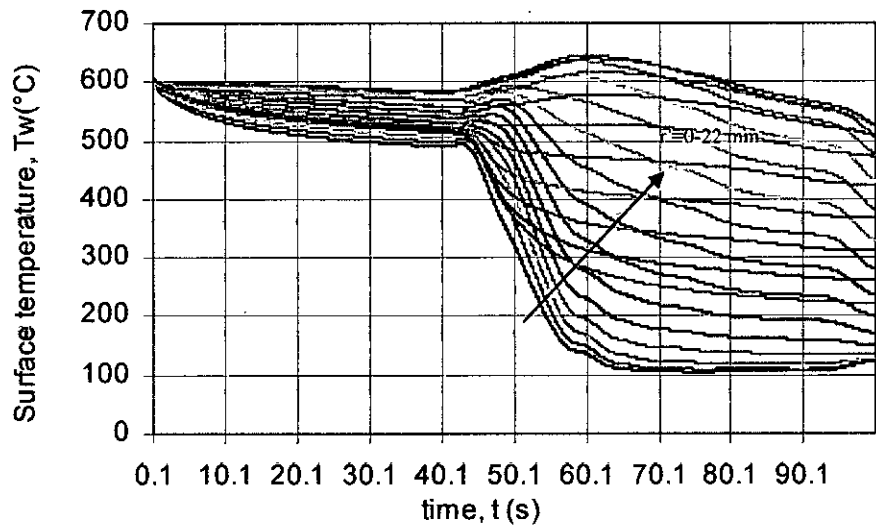


Fig. D.1.7 Surface temperature vs. time curve

($T_b=600^\circ\text{C}$, $\Delta T_{\text{sub}}=05\text{K}$, $u=05\text{m/s}$)

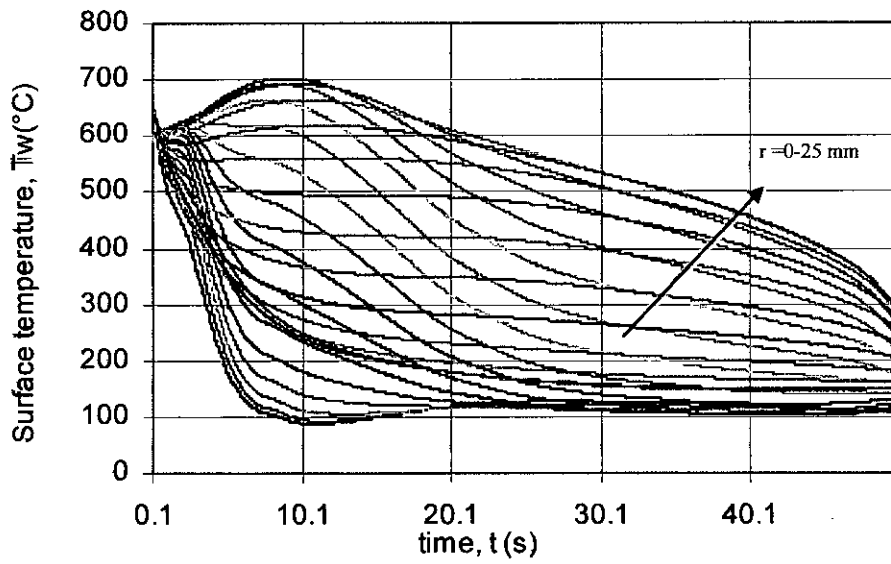


Fig. D.1.8 Surface temperature vs. time curve

($T_b=600^\circ\text{C}$, $\Delta T_{\text{sub}}=80\text{K}$, $u=05\text{m/s}$)

D.2 Surface temperature distribution with radial position

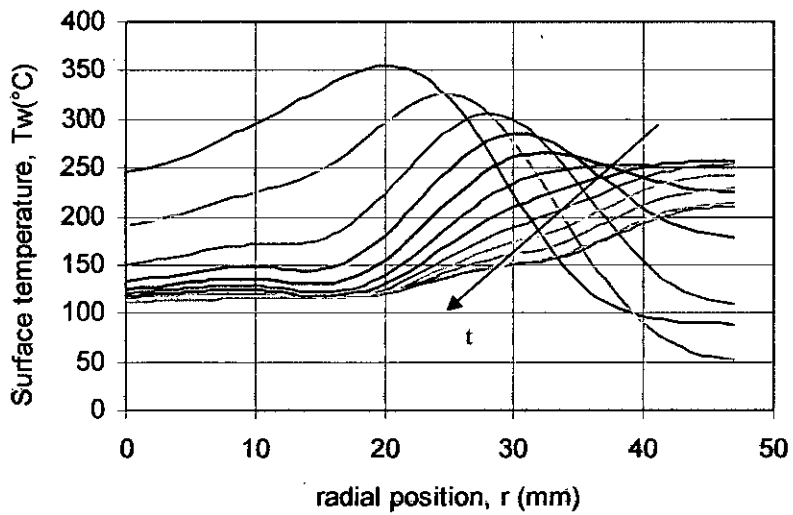


Fig. D.2.1 Variation of surface temperature with radial position
($T_b=250^\circ\text{C}$, $\Delta T_{\text{sub}}=50\text{K}$, $u=5\text{m/s}$)

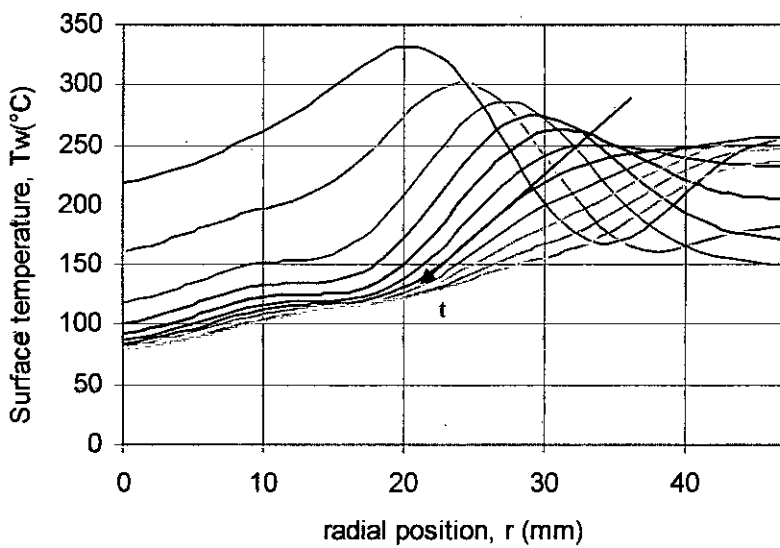


Fig. D.2.2 Variation of surface temperature with radial position
($T_b=250^\circ\text{C}$, $\Delta T_{\text{sub}}=80\text{K}$, $u=10\text{m/s}$)

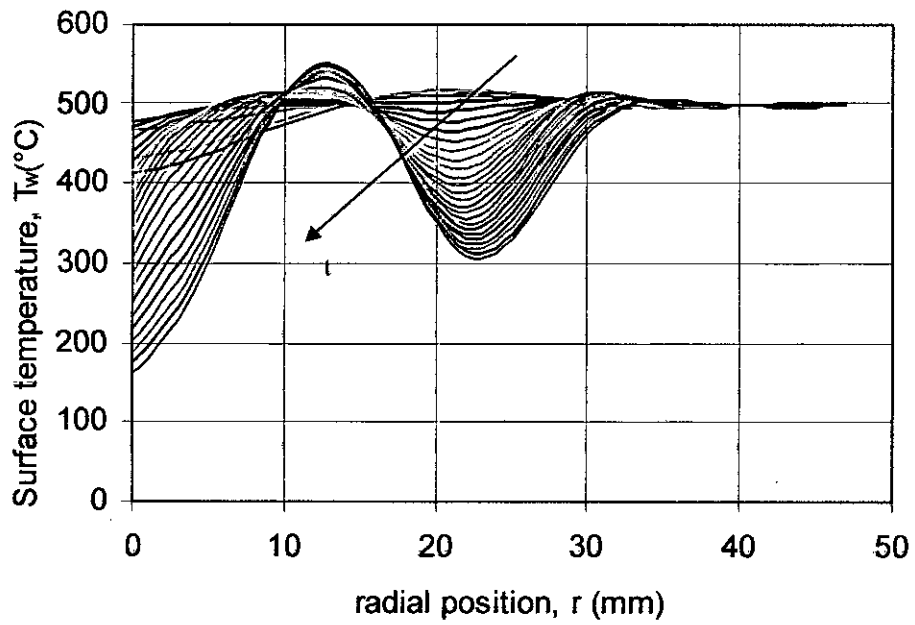


Fig. D.2.3 Variation of surface temperature with radial position
 ($T_b=500^\circ\text{C}$, $\Delta T_{\text{sub}}=50\text{K}$, $u=0.5\text{m/s}$)

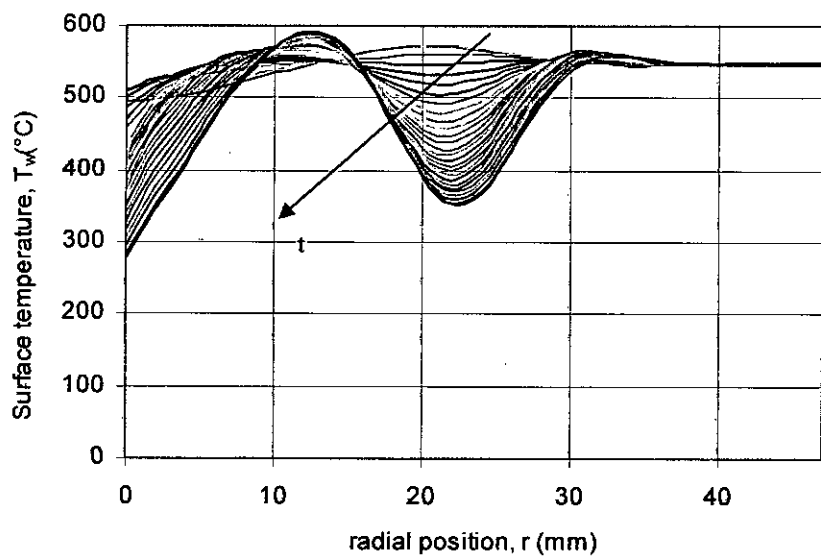


Fig. D.2.4 Variation of surface temperature with radial position
 ($T_b=550^\circ\text{C}$, $\Delta T_{\text{sub}}=80\text{K}$, $u=0.3\text{m/s}$)

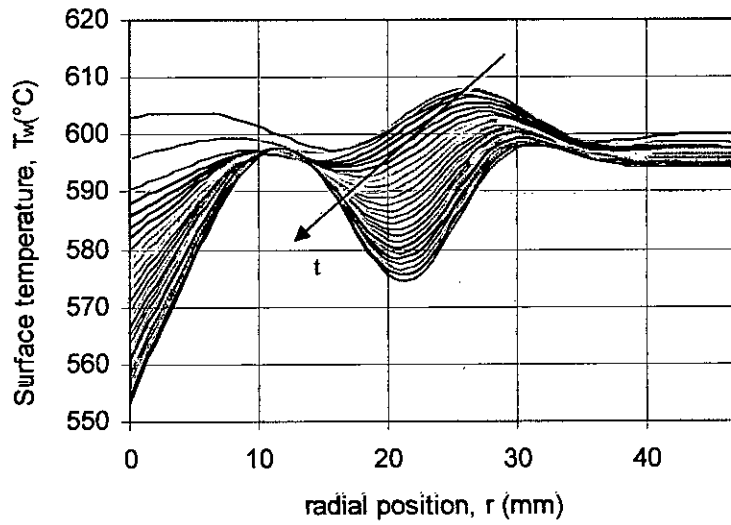


Fig. D.2.5 Variation of surface temperature with radial position
 $(T_b=600^\circ\text{C}, \Delta T_{\text{sub}}=05\text{K}, u=05\text{m/s})$

D.3 Surface heat flux distribution with time

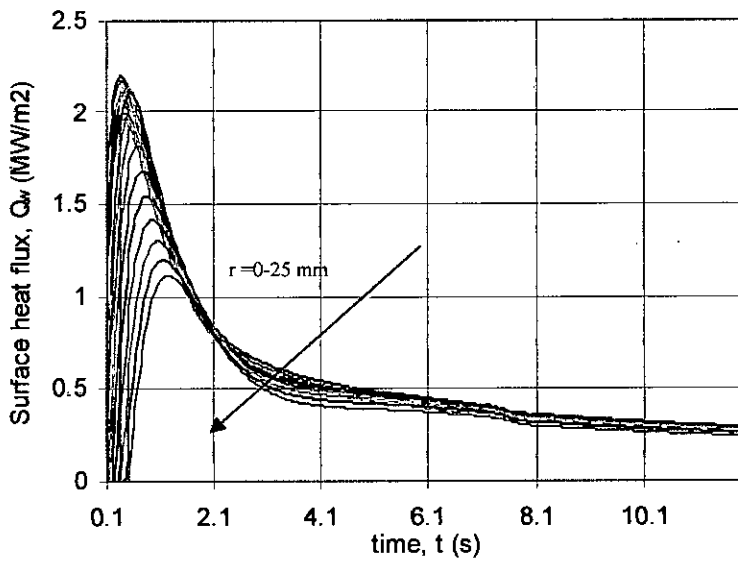


Fig. D.3.1 Surface heat flux vs. time curve
 $(T_b=250^\circ\text{C}, \Delta T_{\text{sub}}=50\text{K}, u=05\text{m/s})$

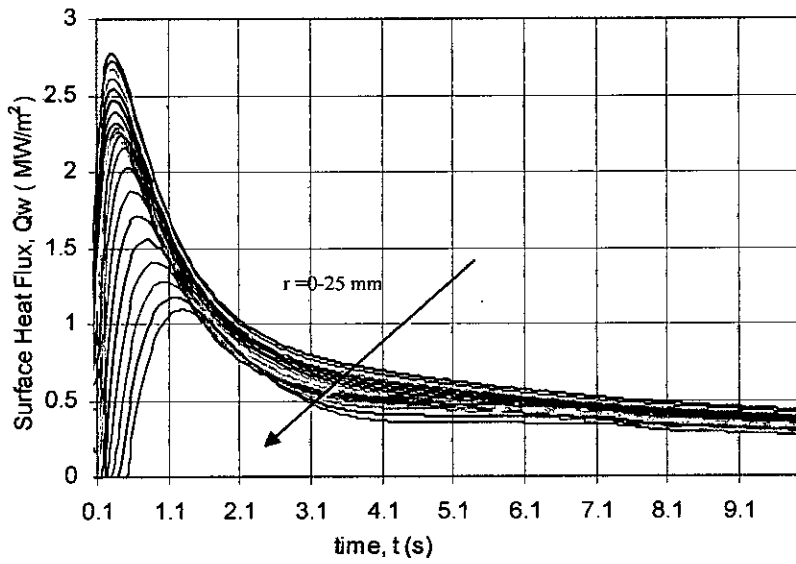


Fig. D.3.2 Surface heat flux vs. time curve
 ($T_b=250^\circ\text{C}$, $\Delta T_{\text{sub}}=80\text{K}$, $u=10\text{m/s}$)

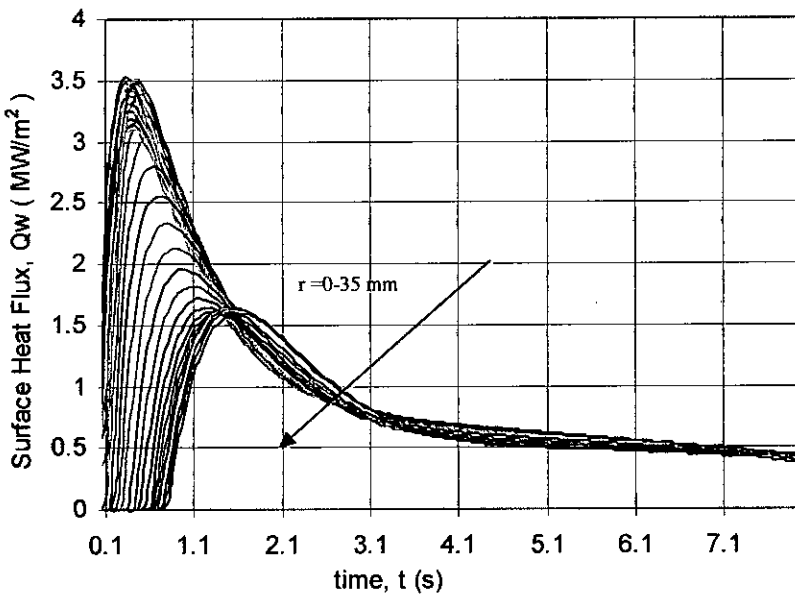


Fig. D.3.3 Surface heat flux vs. time curve
 ($T_b=300^\circ\text{C}$, $\Delta T_{\text{sub}}=50\text{K}$, $u=15\text{m/s}$)

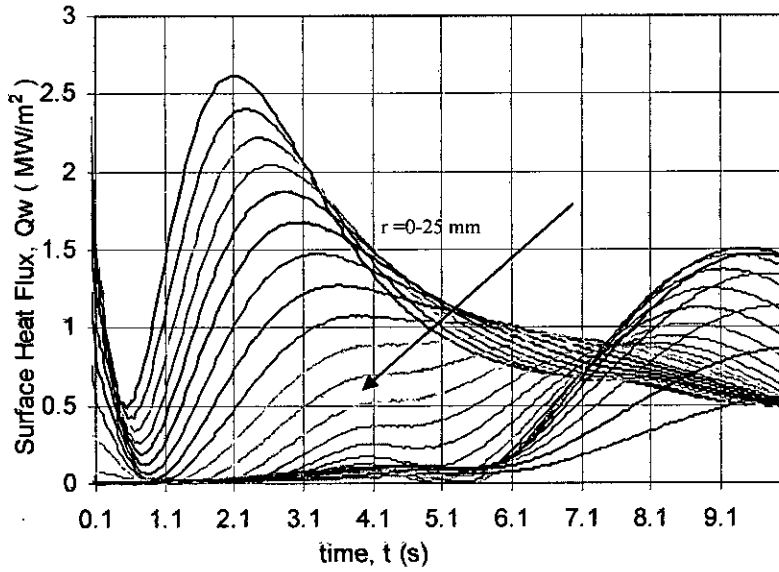


Fig. D.3.4 Surface heat flux vs. time curve
 ($T_b=350^\circ\text{C}$, $\Delta T_{\text{sub}}=05\text{K}$, $u=05\text{m/s}$)

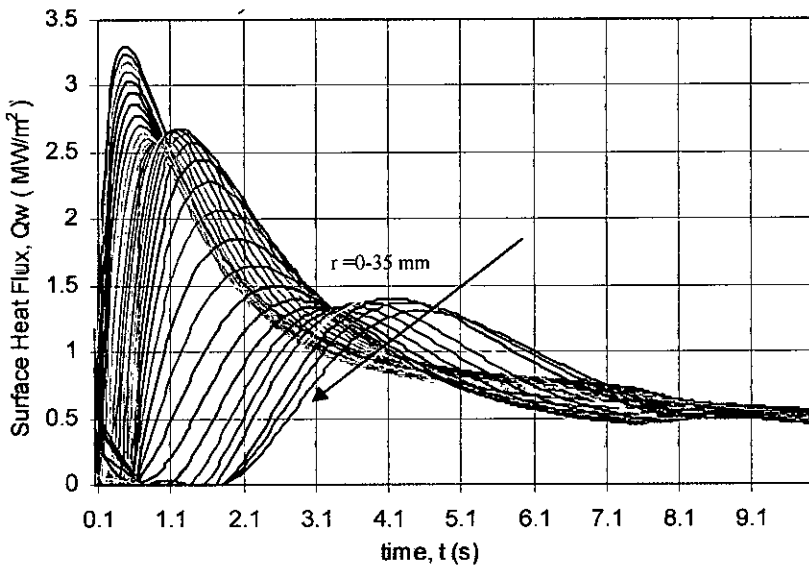


Fig. D.3.5 Surface heat flux vs. time curve
 ($T_b=350^\circ\text{C}$, $\Delta T_{\text{sub}}=80\text{K}$, $u=10\text{m/s}$)

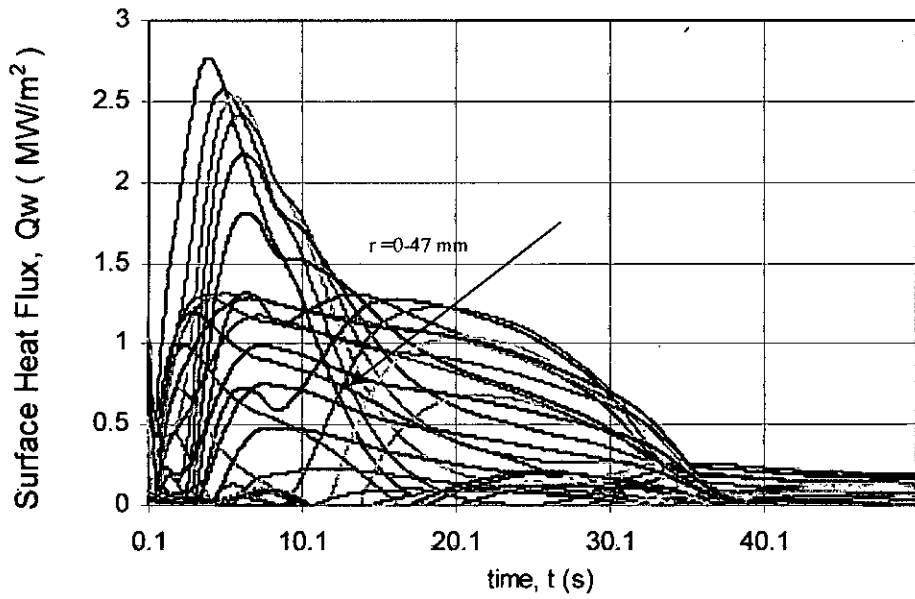


Fig. D.3.6 Surface heat flux vs. time curve
 $(T_b=500^\circ\text{C}, \Delta T_{\text{sub}}=50\text{K}, u=05\text{m/s})$

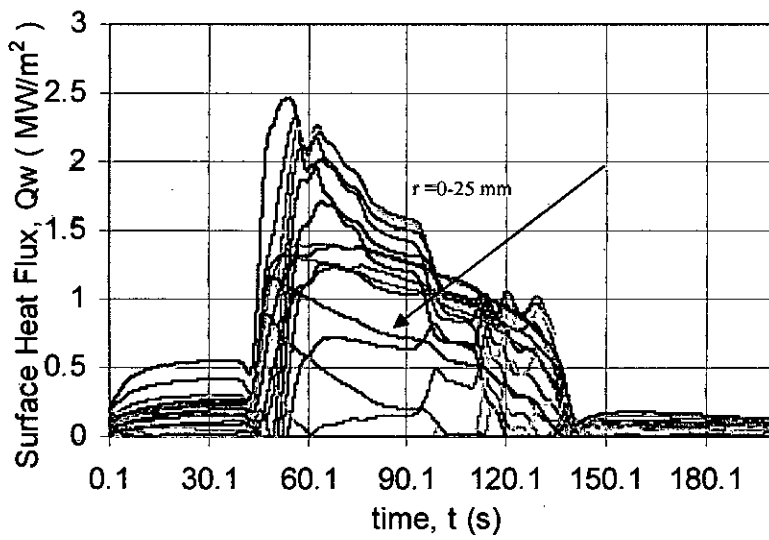


Fig. D.3.7 Surface heat flux vs. time curve
 $(T_b=600^\circ\text{C}, \Delta T_{\text{sub}}=05\text{K}, u=05\text{m/s})$

D.4 Surface heat flux distribution with radial position

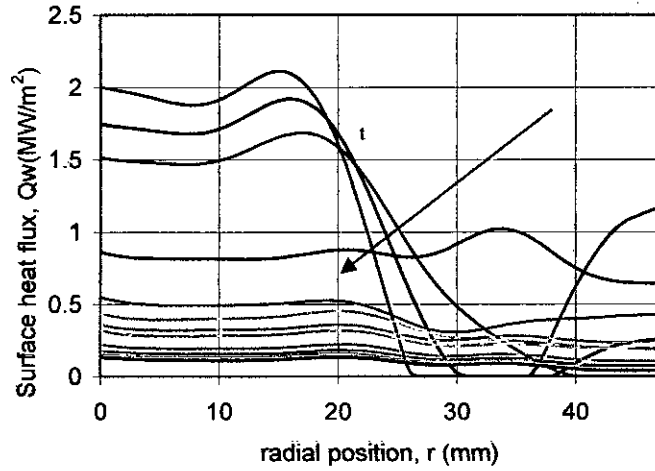


Fig. D.4.1 Surface heat flux distribution with radial position
($T_b=250^\circ\text{C}$, $\Delta T_{\text{sub}}=50\text{K}$, $u=5\text{m/s}$)

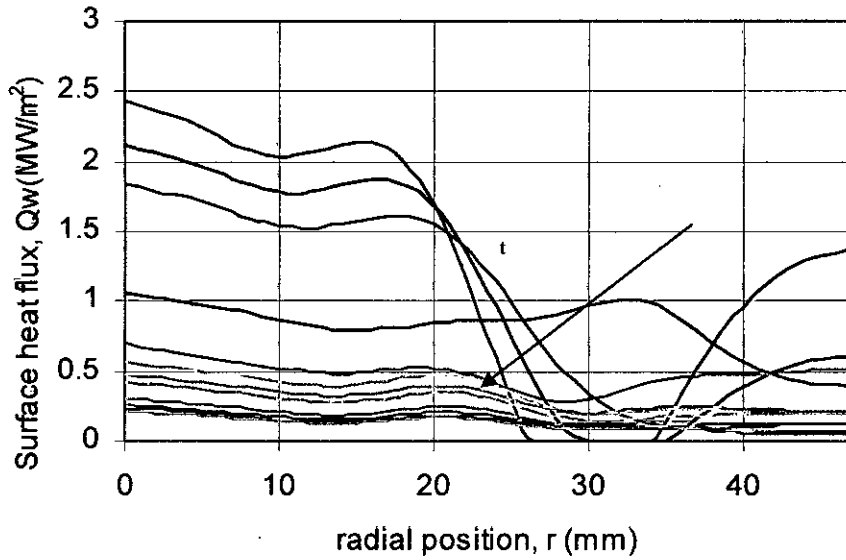


Fig. D.4.2 Surface heat flux distribution with radial position
($T_b=250^\circ\text{C}$, $\Delta T_{\text{sub}}=80\text{K}$, $u=10\text{m/s}$)

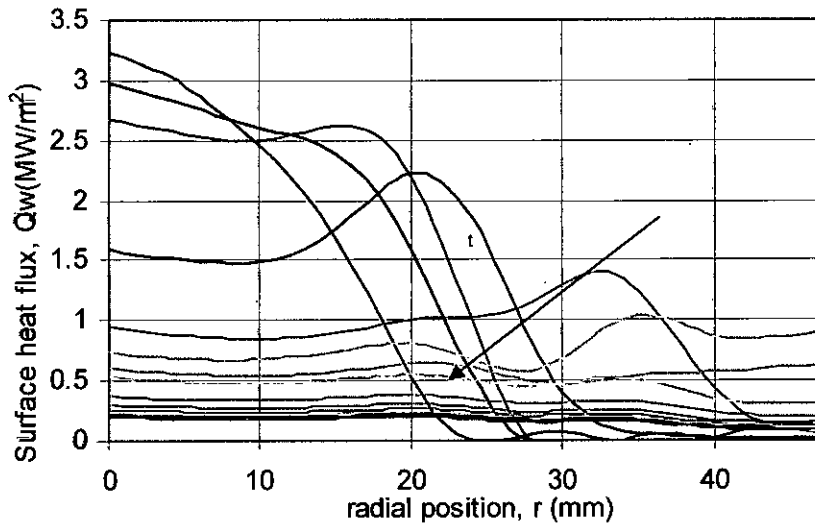


Fig. D.4.3 Surface heat flux distribution with radial position
 ($T_b=350^\circ\text{C}$, $\Delta T_{\text{sub}}=80\text{K}$, $u=10\text{m/s}$)

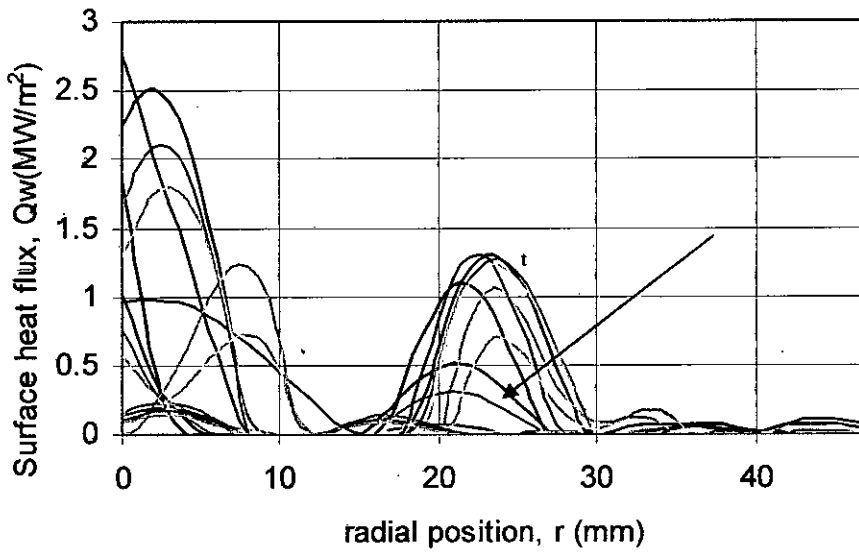


Fig. D.4.4 Surface heat flux distribution with radial position
 ($T_b=500^\circ\text{C}$, $\Delta T_{\text{sub}}=50\text{K}$, $u=05\text{m/s}$)

APPENDIX E

Determination of wetting delay in different test conditions

Table E.1 Resident time or wetting delay for all experimental conditions

Condition	Resident time (sec)	Condition	Resident time (sec)	Condition	Resident time (sec)
S250 20 03	<1	S300 20 03	X	S350 20 03	X
S250 20 05	<1	S300 20 05	<1	S350 20 05	X
S250 20 10	<1	S300 20 10	<1	S350 20 10	<1
S250 20 15	<1	S300 20 15	<1	S350 20 15	X
S250 50 03	<1	S300 50 03	X	S350 50 03	X
S250 50 05	<1	S300 50 05	<1	S350 50 05	X
S250 50 10	<1	S300 50 10	<1	S350 50 10	X
S250 50 15	<1	S300 50 15	<1	S350 50 15	X
S250 80 03	<1	S300 80 03	X	S350 80 03	X
S250 80 05	<1	S300 80 05	X	S350 80 05	X
S250 80 10	<1	S300 80 10	<1	S350 80 10	X
S250 80 15	<1	S300 80 15	<1	S350 80 15	X
S250 95 03	X	S300 95 03	X	S350 95 03	X
S250 95 05	<1	S300 95 05	X	S350 95 05	X
S250 95 10	<1	S300 95 10	X	S350 95 10	X
S250 95 15	<1	S300 95 15	<1	S350 95 15	X

Condition	Resident time (sec)	Condition	Resident time (sec)	Condition	Resident time (sec)
S400 20 03	X	S450 20 03	X	S500 20 03	X
S400 20 05	X	S450 20 05	X	S500 20 05	X
S400 20 10	X	S450 20 10	X	S500 20 10	X
S400 20 15	<1	S450 20 15	X	S500 20 15	X
S400 50 03	1.9	S450 50 03	X	S500 50 03	X
S400 50 05	X	S450 50 05	X	S500 50 05	X
S400 50 10	X	S450 50 10	X	S500 50 10	X
S400 50 15	X	S450 50 15	X	S500 50 15	X
S400 80 03	2.4	S450 80 03	X	S500 80 03	X
S400 80 05	X	S450 80 05	X	S500 80 05	X
S400 80 10	X	S450 80 10	X	S500 80 10	X
S400 80 15	X	S450 80 15	X	S500 80 15	X
S400 95 03	4.9	S450 95 03	X	S500 95 03	59.1
S400 95 05	2.6	S450 95 05	X	S500 95 05	X
S400 95 10	X	S450 95 10	X	S500 95 10	X
S400 95 15	X	S450 95 15	X	S500 95 15	X

Condition	Resident time (sec)	Condition	Resident time (sec)
S550 20 03	X	S600 20 03	X
S550 20 05	X	S600 20 05	X
S550 20 10	X	S600 20 10	X
S550 20 15	X	S600 20 15	X
S550 50 03	X	S600 50 03	91.6
S550 50 05	X	S600 50 05	X
S550 50 10	X	S600 50 10	X
S550 50 15	X	S600 50 15	X
S550 80 03	X	S600 80 03	X
S550 80 05	X	S600 80 05	X
S550 80 10	X	S600 80 10	X
S550 80 15	X	S600 80 15	X
S550 95 03	508	S600 95 03	580
S550 95 05	56.8	S600 95 05	111.8
S550 95 10	X	S600 95 10	X
S550 95 15	X	S600 95 15	X

APPENDIX F

Effect of different parameters on maximum surface heat flux

F.1 Maximum heat flux with radial position

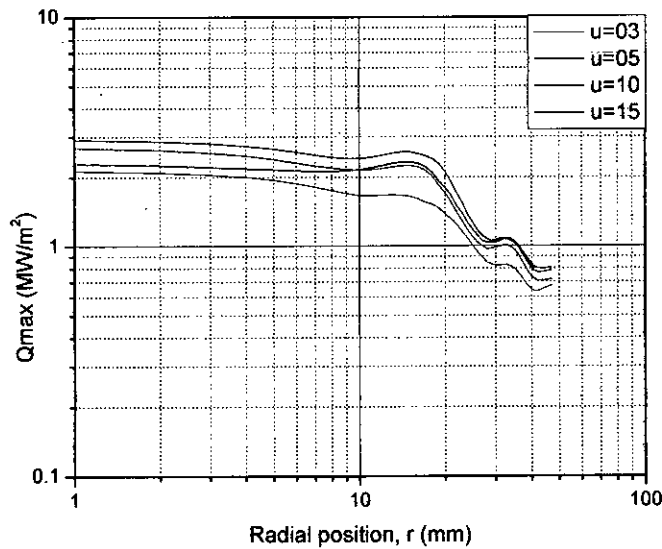


Fig F.1.1 Variation of maximum surface heat flux with radial position
(for $T_b=250^\circ\text{C}$, $\Delta T_{sub}=80\text{K}$)

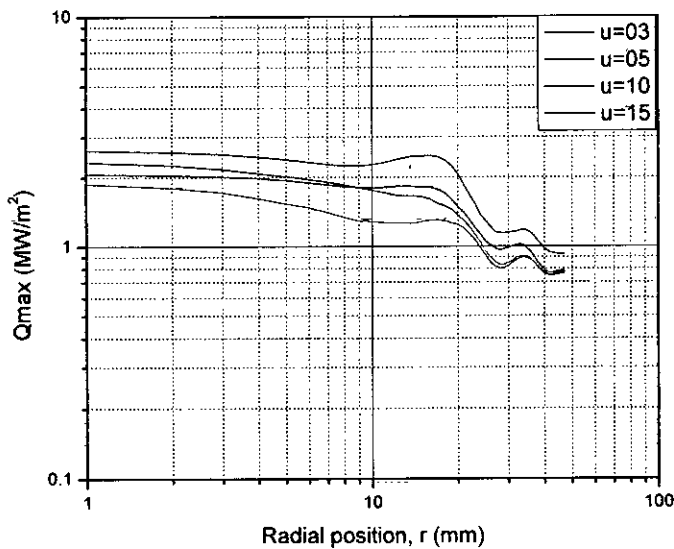


Fig. F.1.2 Variation of maximum surface heat flux with radial position
(for $T_b=250^\circ\text{C}$, $\Delta T_{sub}=20\text{K}$)

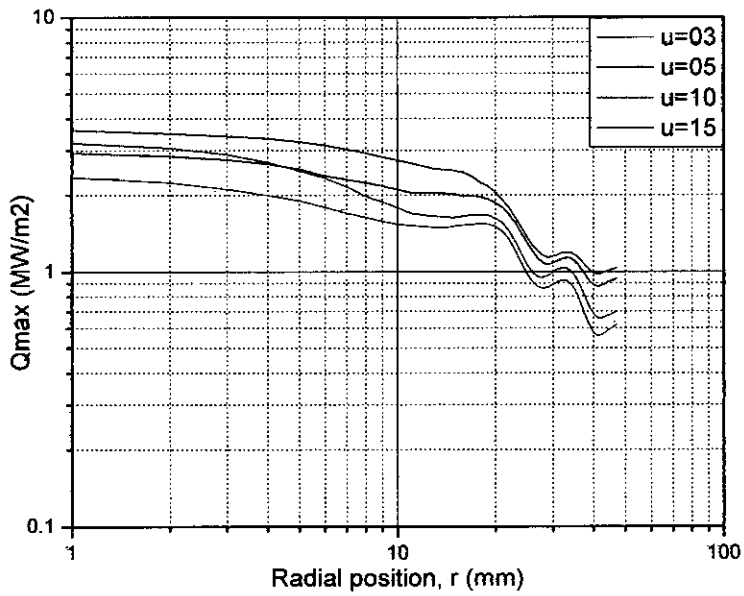


Fig. F.1.3 Variation of maximum surface heat flux with radial position
(for $T_b=300^\circ\text{C}$, $\Delta T_{sub}=80\text{K}$)

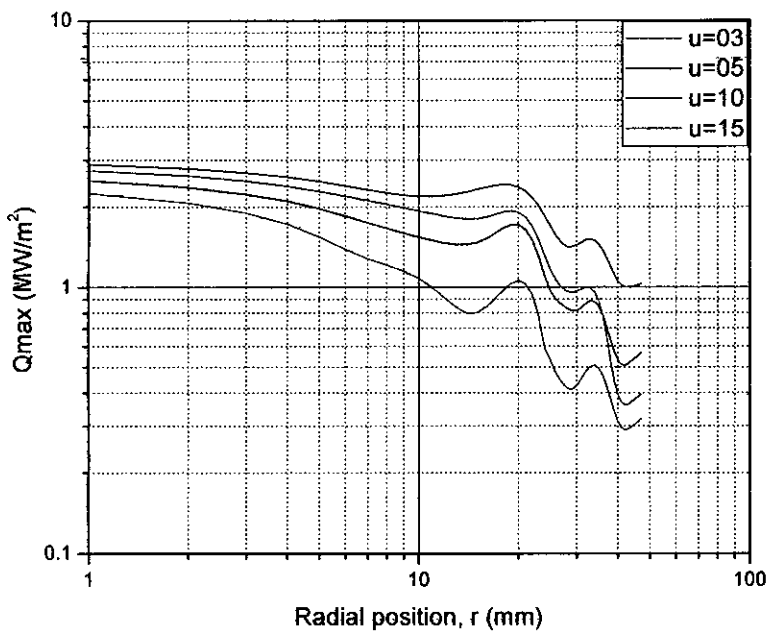


Fig. F.1.4 Variation of maximum surface heat flux with radial position
(for $T_b=350^\circ\text{C}$, $\Delta T_{sub}=50\text{K}$)

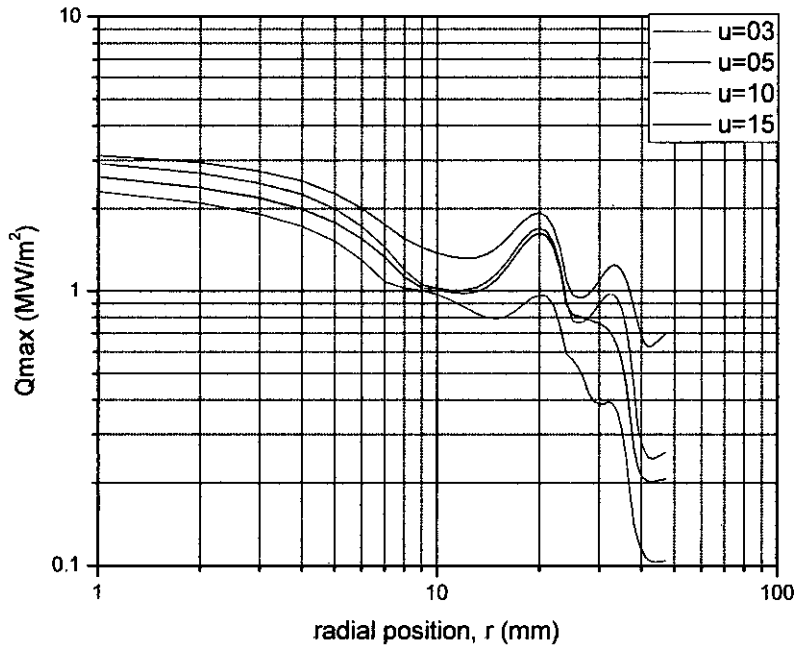


Fig. F.1.5 Variation of maximum surface heat flux with radial position
(for $T_b=400^\circ\text{C}$, $\Delta T_{\text{sub}}=05\text{K}$)

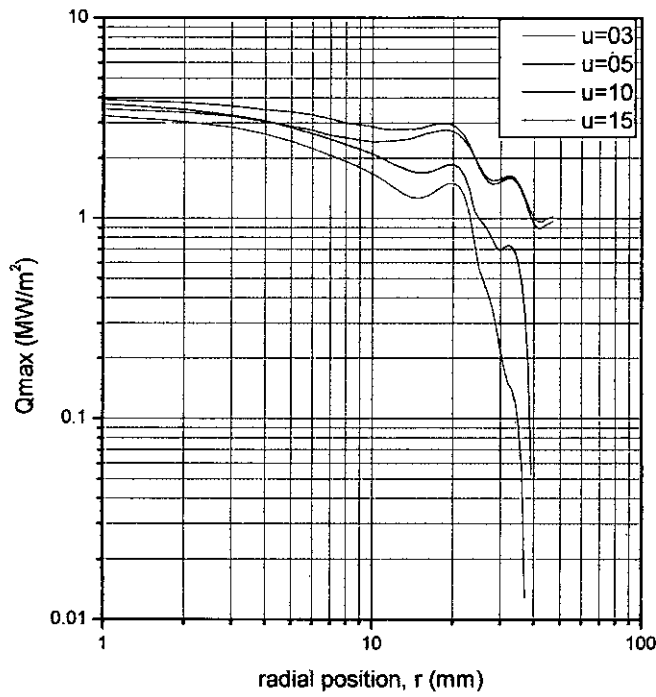


Fig F.1.6 Variation of maximum surface heat flux with radial position
(for $T_b=400^\circ\text{C}$, $\Delta T_{\text{sub}}=80\text{K}$)

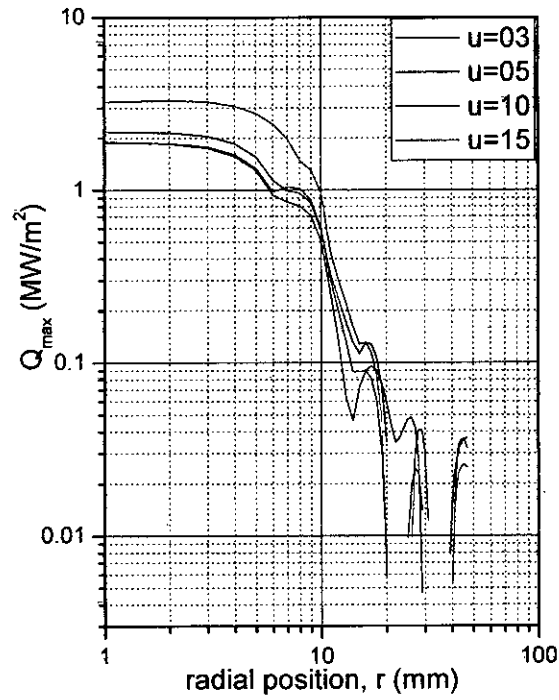


Fig. F.1.7 Variation of maximum surface heat flux with radial position
(for $T_b=450^\circ\text{C}$, $\Delta T_{sub}=20\text{K}$)

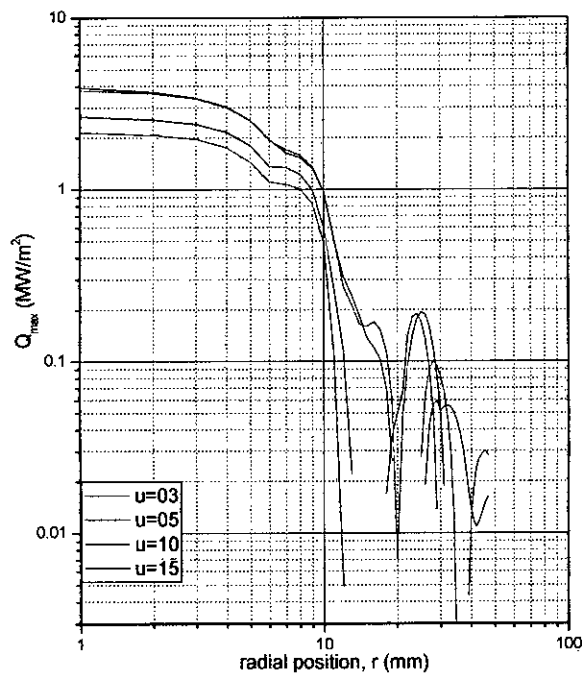


Fig. F.1.8 Variation of maximum surface heat flux with radial position
(for $T_b=450^\circ\text{C}$, $\Delta T_{sub}=80\text{K}$)

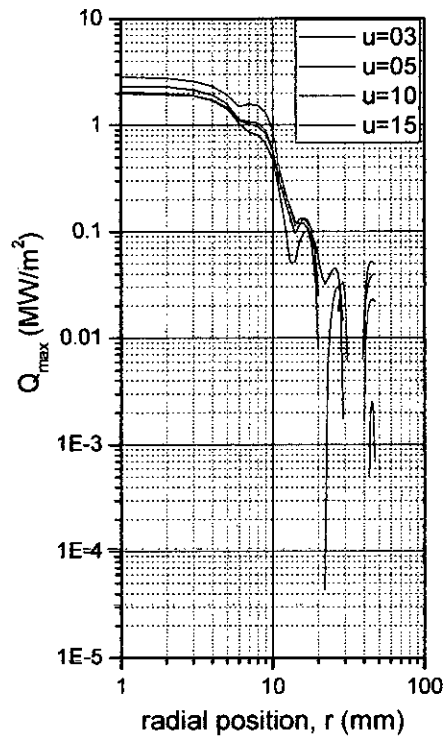


Fig. F.1.9 Variation of maximum surface heat flux with radial position
(for $T_b=500^\circ\text{C}$, $\Delta T_{\text{sub}}=20\text{K}$)

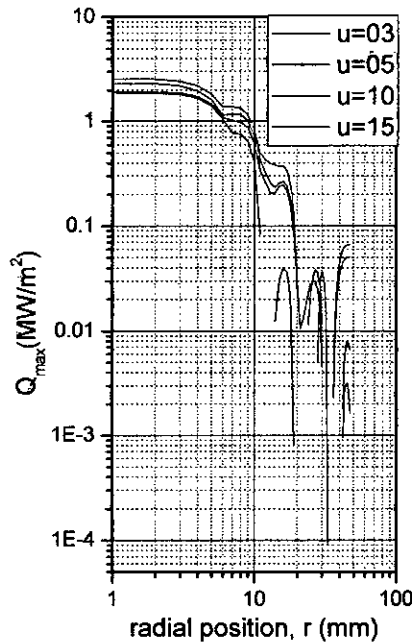


Fig. F.1.10 Variation of maximum surface heat flux with radial position
(for $T_b=500^\circ\text{C}$, $\Delta T_{\text{sub}}=05\text{K}$)

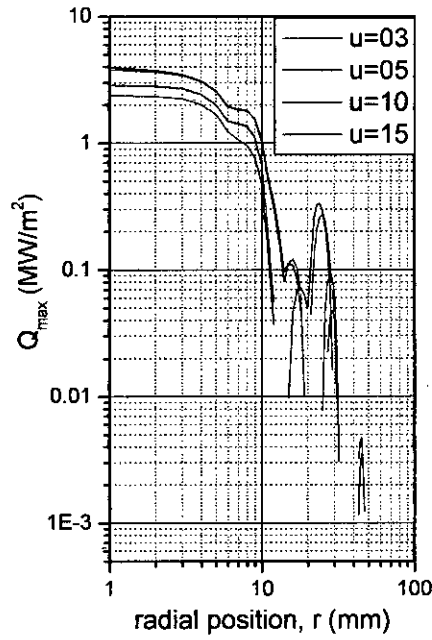


Fig. F.1.11 Variation of maximum surface heat flux with radial position
(for $T_b=550^\circ\text{C}$, $\Delta T_{sub}=80\text{K}$)

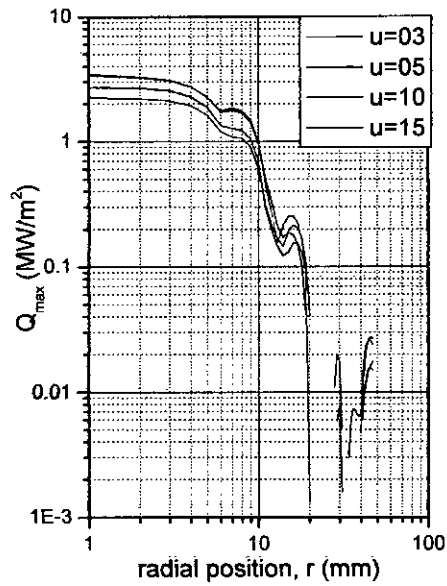


Fig. F.1.12 Variation of maximum surface heat flux with radial position
(for $T_b=550^\circ\text{C}$, $\Delta T_{sub}=50\text{K}$)

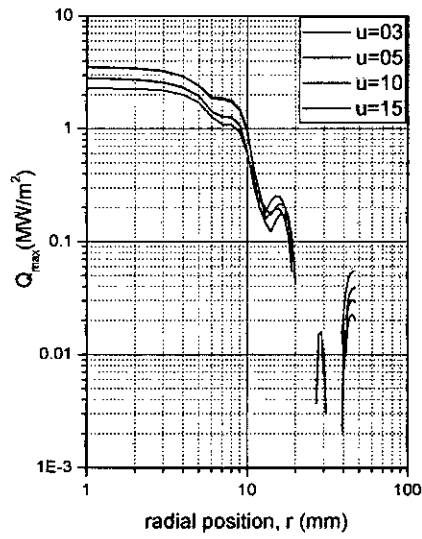


Fig. F.1.13 Variation of maximum surface heat flux with radial position
(for $T_b=600^\circ\text{C}$, $\Delta T_{sub}=50\text{K}$)

F.2 Effect of jet velocity on maximum heat flux

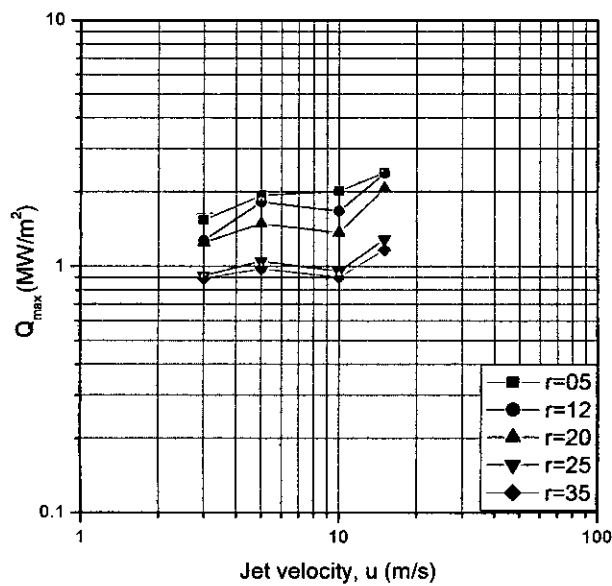


Fig. F.2.1 Variation of maximum heat flux with jet velocity
(for $T_b=250^\circ\text{C}$, $\Delta T_{sub}=20\text{K}$)

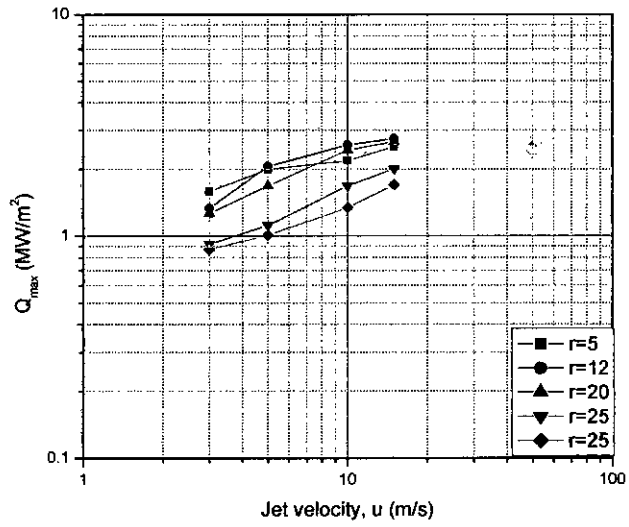


Fig. F.2.2 Variation of maximum heat flux with jet velocity
(for $T_b=250^\circ\text{C}$, $\Delta T_{\text{sub}}=50\text{K}$)

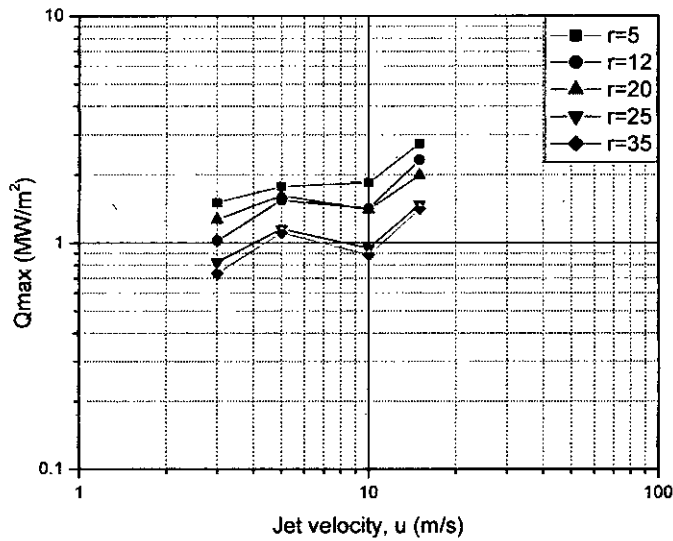


Fig. F.2.3 Variation of maximum heat flux with jet velocity
(for $T_b=300^\circ\text{C}$, $\Delta T_{\text{sub}}=05\text{K}$)

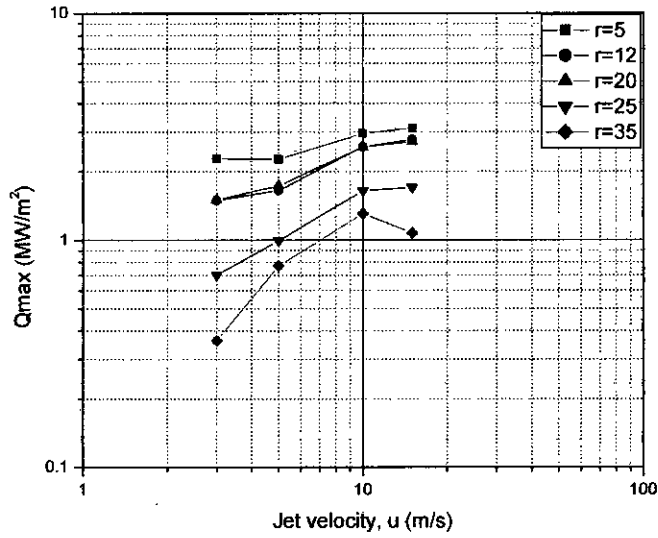


Fig. F.2.4 Variation of maximum heat flux with jet velocity
(for $T_b=350^\circ\text{C}$, $\Delta T_{\text{sub}}=80\text{K}$)

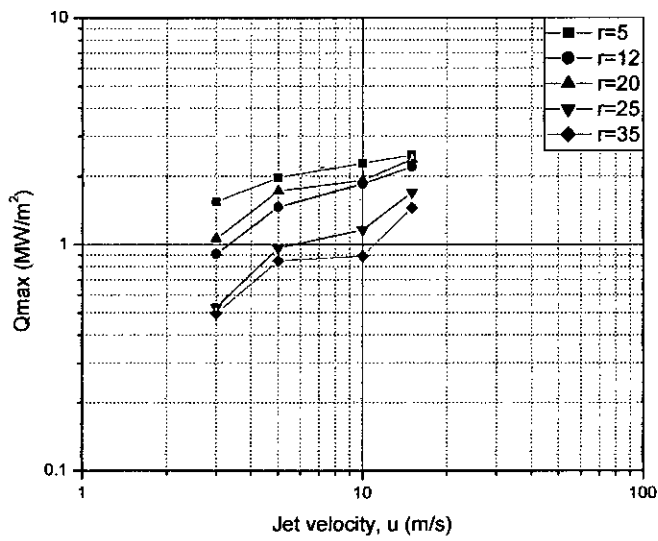


Fig. F.2.5 Variation of maximum heat flux with jet velocity
(for $T_b=350^\circ\text{C}$, $\Delta T_{\text{sub}}=50\text{K}$)

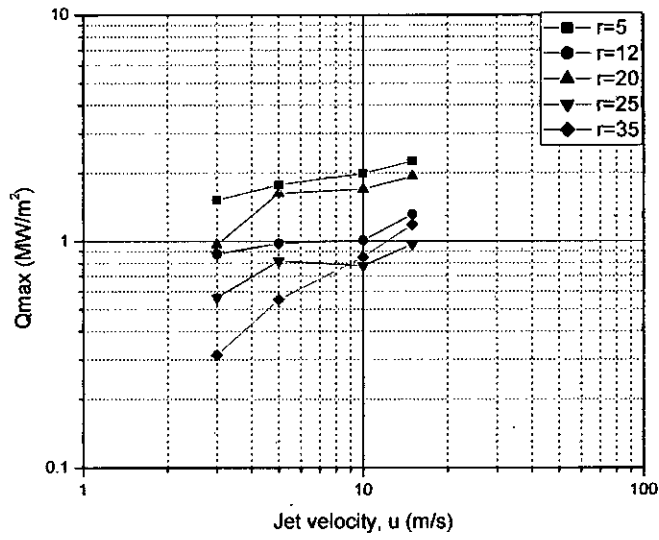


Fig. F.2.6 Variation of maximum heat flux with jet velocity
(for $T_b=400^\circ\text{C}$, $\Delta T_{\text{sub}}=05\text{K}$)

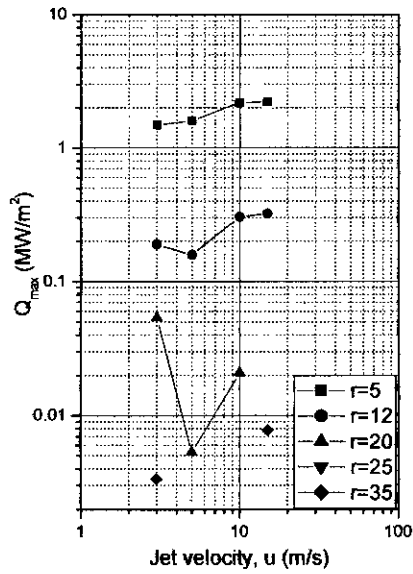


Fig. F.2.7 Variation of maximum heat flux with jet velocity
(for $T_b=450^\circ\text{C}$, $\Delta T_{\text{sub}}=50\text{K}$)

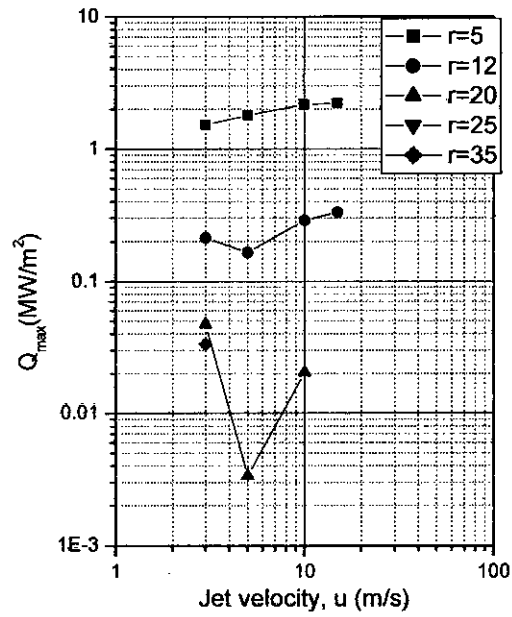


Fig. F.2.8 Variation of maximum heat flux with jet velocity
(for $T_b=500^\circ\text{C}$, $\Delta T_{\text{sub}}=50\text{K}$)

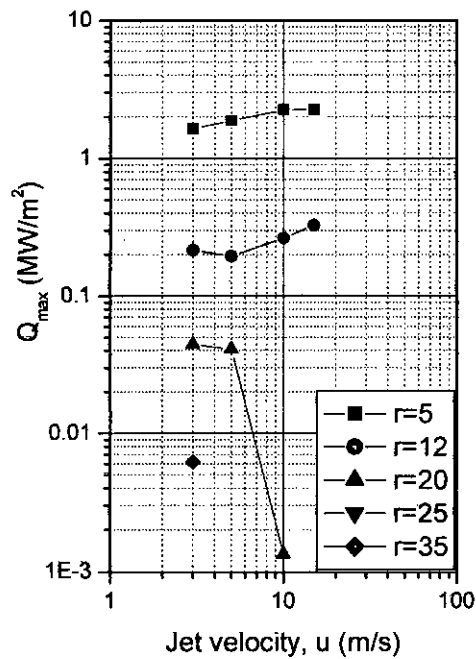


Fig. F.2.9 Variation of maximum heat flux with jet velocity
(for $T_b=550^\circ\text{C}$, $\Delta T_{\text{sub}}=50\text{K}$)

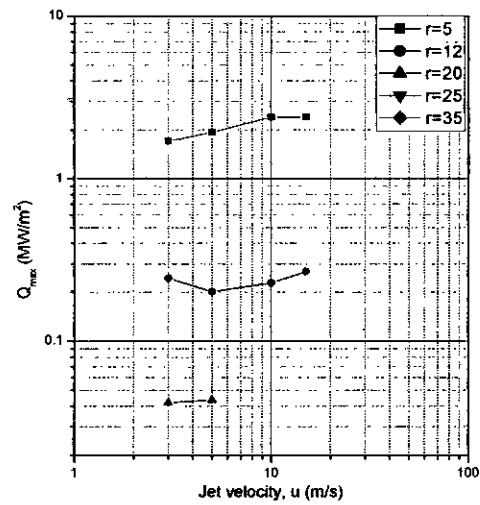


Fig. F.2.10 Variation of maximum heat flux with jet velocity
(for $T_b=600^\circ\text{C}$, $\Delta T_{sub}=50\text{K}$)

F.3 Maximum heat flux with liquid subcooling

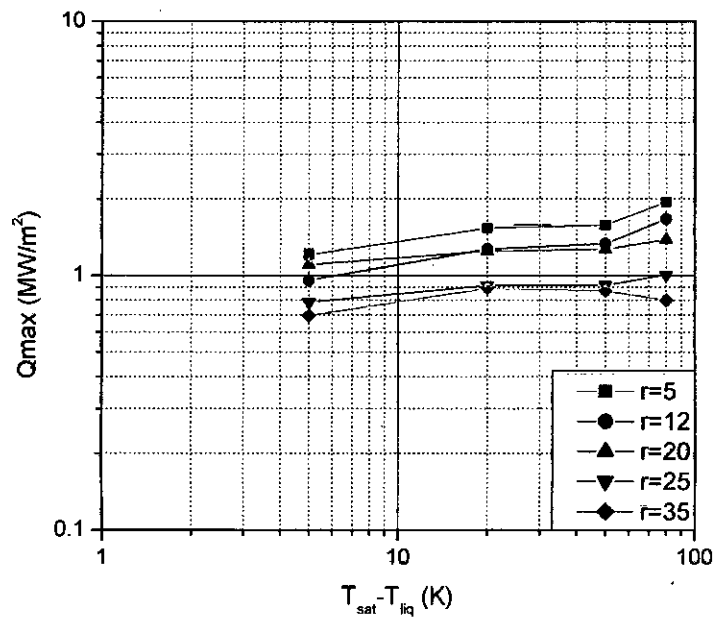


Fig. F.3.1 Variation of Maximum surface heat Flux with liquid subcooling
(for $T_b=250^\circ\text{C}$, $u=0.3$ m/s)

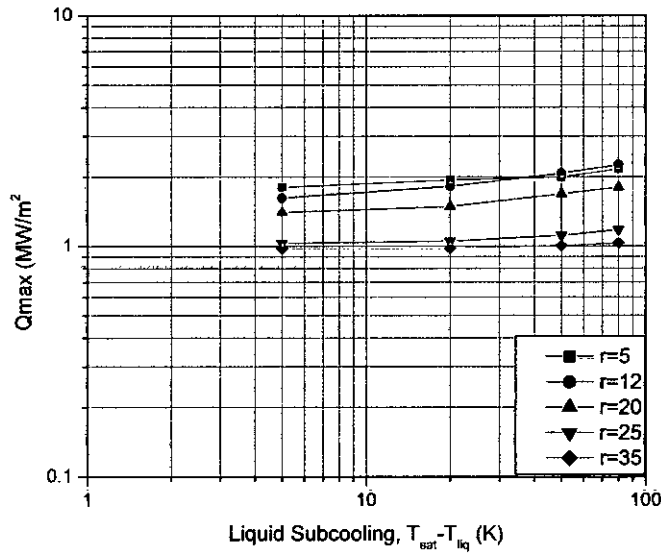


Fig. F.3.2 Variation of Maximum surface heat Flux with liquid subcooling
(for $T_b=250^\circ\text{C}$, $u=05\text{ m/s}$)

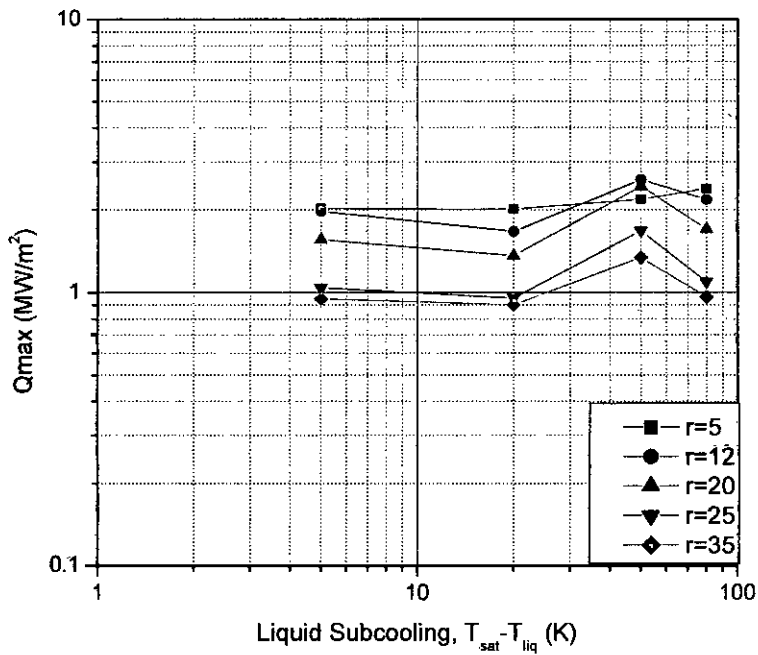


Fig. F.3.3 Variation of Maximum surface heat Flux with liquid subcooling
(for $T_b=250^\circ\text{C}$, $u=10\text{m/s}$)

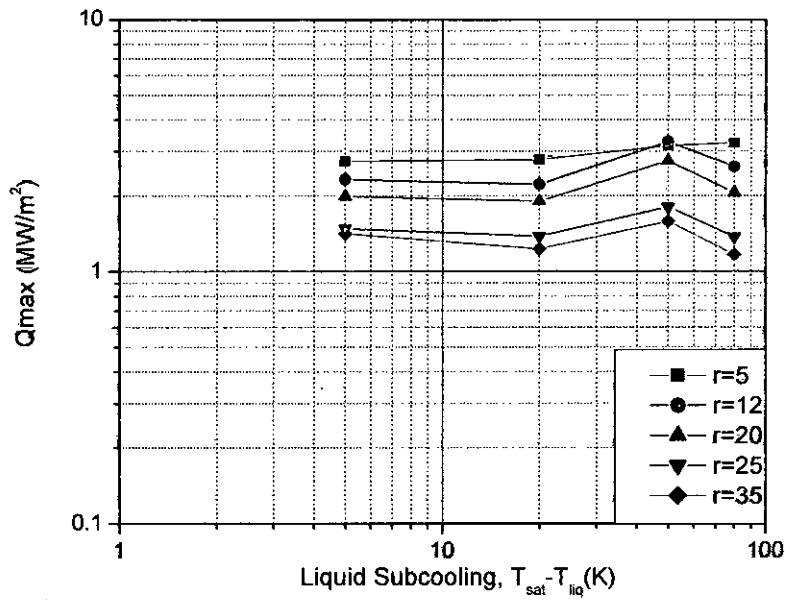


Fig. F.3.4 Variation of Maximum surface heat Flux with liquid subcooling
(for $T_b=300^\circ\text{C}$, $u=15\text{m/s}$)

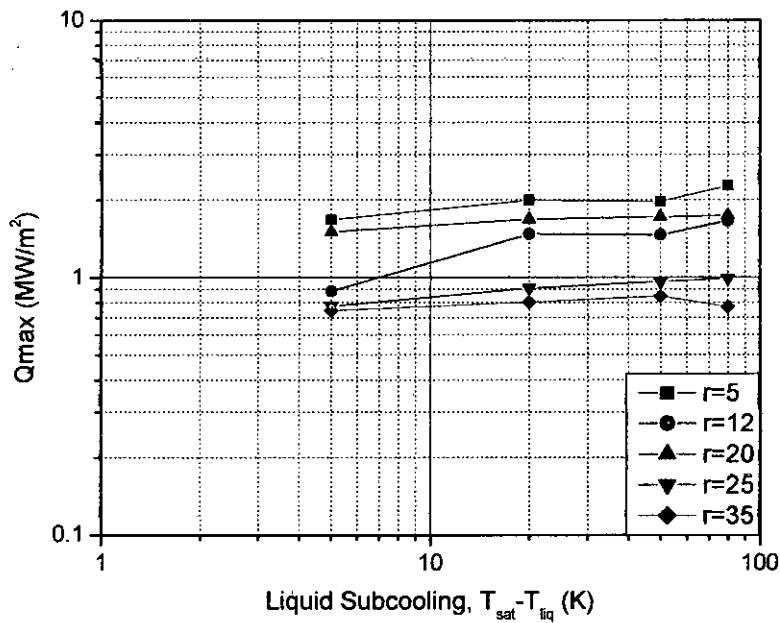


Fig. F.3.5 Variation of Maximum surface heat Flux with liquid subcooling
(for $T_b=350^\circ\text{C}$, $u=05\text{m/s}$)

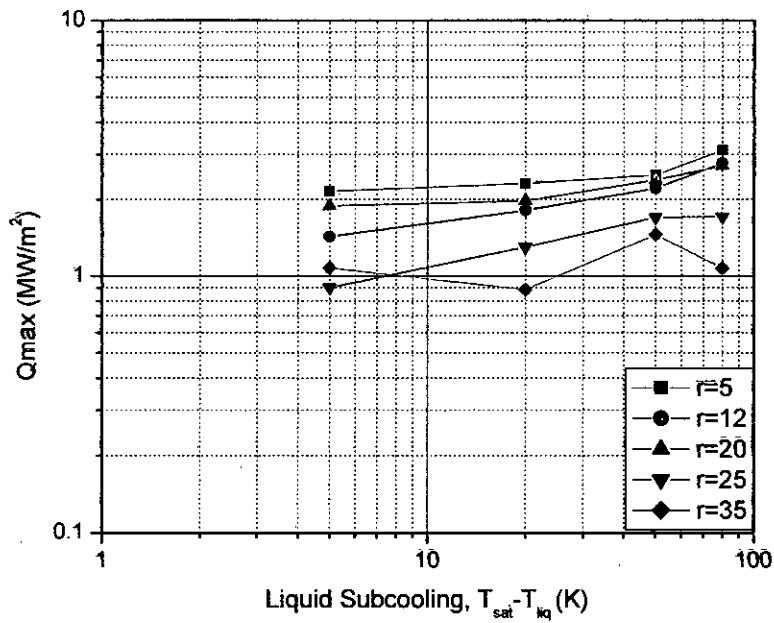


Fig. F.3.6 Variation of Maximum surface heat Flux with liquid subcooling (for $T_b=350^\circ\text{C}$, $u=15\text{m/s}$)

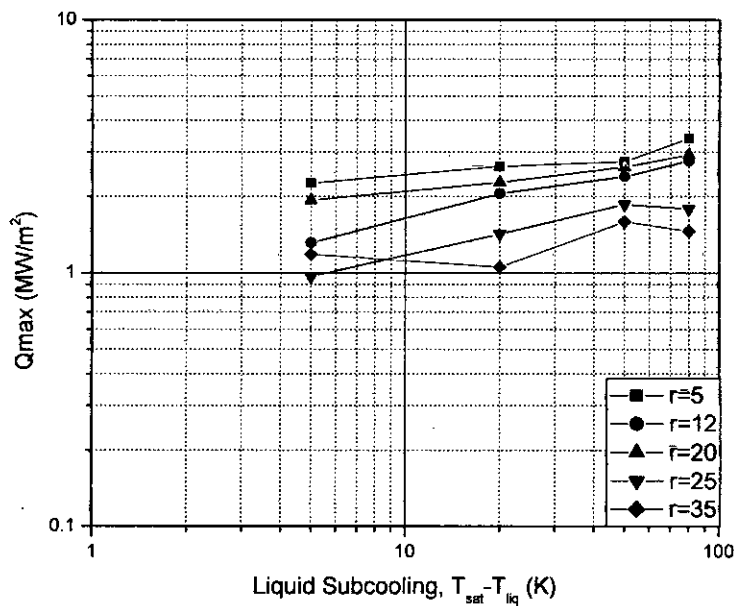


Fig. F.3.7 Variation of Maximum surface heat Flux with liquid subcooling (for $T_b=400^\circ\text{C}$, $u=15\text{m/s}$)

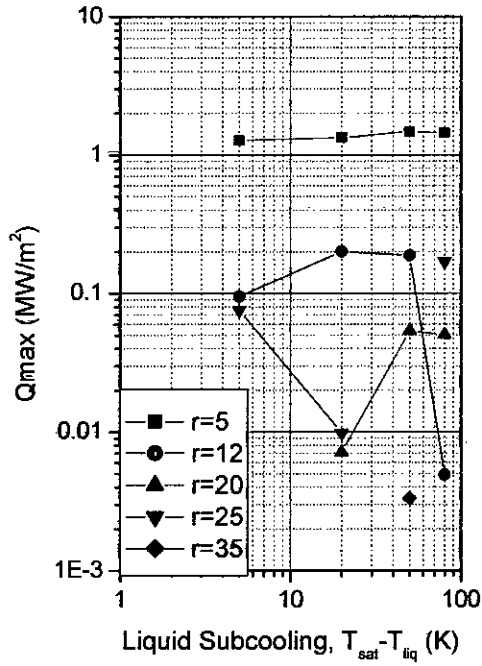


Fig. F.3.8 Variation of Maximum surface heat Flux with liquid subcooling
(for $T_b=450^\circ\text{C}$, $u=0.03\text{m/s}$)

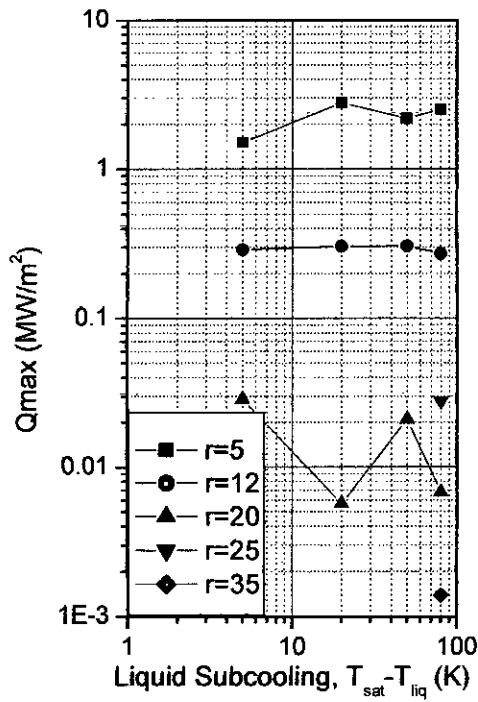


Fig. F.3.9 Variation of Maximum surface heat Flux with liquid subcooling
(for $T_b=450^\circ\text{C}$, $u=0.10\text{m/s}$)

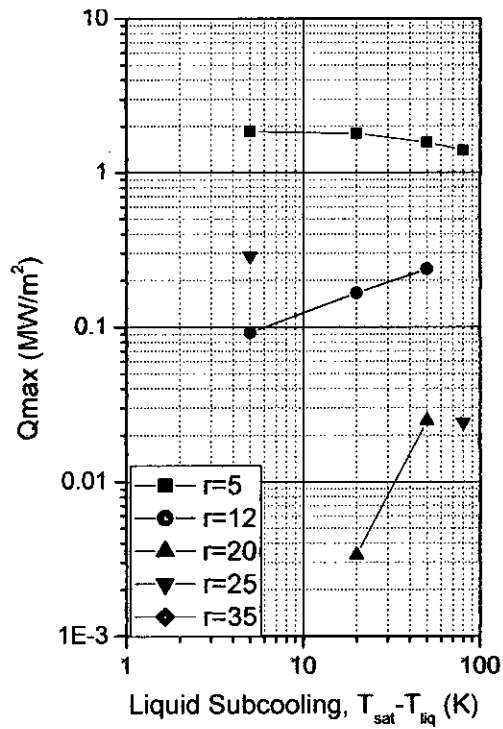


Fig. F.3.10 Variation of Maximum surface heat Flux with liquid subcooling
(for $T_b=500^\circ\text{C}$, $u=0.05\text{m/s}$)

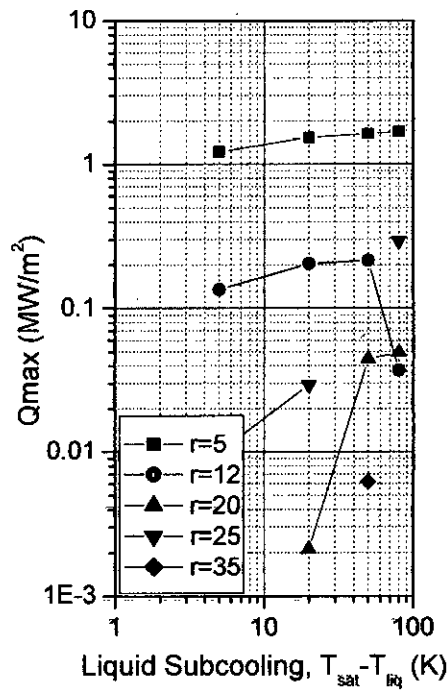


Fig. F.3.11 Variation of Maximum surface heat Flux with liquid subcooling
(for $T_b=550^\circ\text{C}$, $u=0.03\text{ m/s}$)

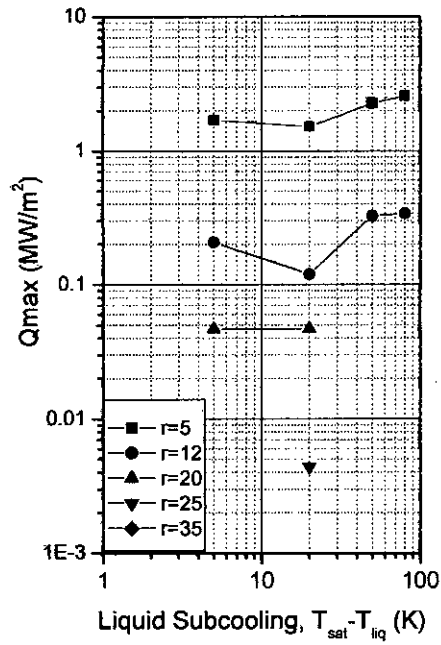


Fig. F.3.12 Variation of Maximum surface heat Flux with liquid subcooling
(for $T_b=550^\circ\text{C}$, $u=15$ m/s)

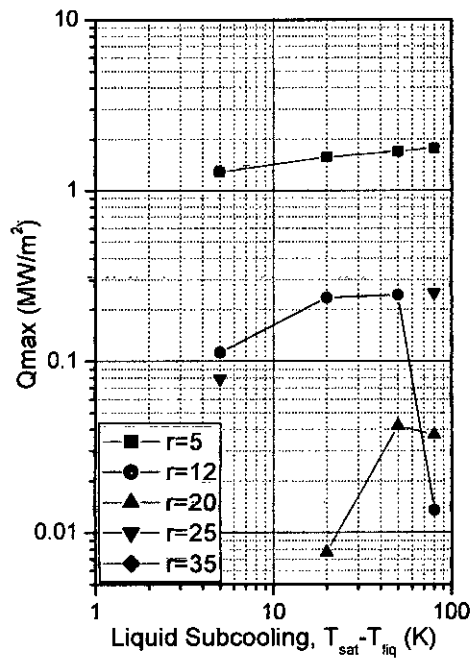


Fig. F.3.13 Variation of Maximum surface heat Flux with liquid subcooling
(for $T_b=600^\circ\text{C}$, $u=0.3$ m/s)